

Physics Beyond Colliders

QCD Working Group Report

A. Dainese¹, M. Diehl^{2,*}, P. Di Nezza³, J. Friedrich⁴, M. Gaździcki^{5,6}, G. Graziani⁷,
C. Hadjidakis⁸, J. Jäckel⁹, J. P. Lansberg⁸, A. Magnon¹⁰, G. Mallot¹⁰,
F. Martinez Vidal¹¹, L. M. Massacrier⁸, L. Nemenov¹², N. Neri¹³, J. M. Pawłowski^{9,*},
S. M. Puławski¹⁴, J. Schacher¹⁵, G. Schnell^{16,*}, A. Stocchi¹⁷, G. L. Usai¹⁸, C. Vallée¹⁹,
G. Venanzoni²⁰

Abstract: This report summarises the main findings of the QCD Working Group in the CERN Physics Beyond Colliders Study.

¹ INFN, Sezione di Padova, Padova, Italy

² Deutsches Elektronen-Synchrotron DESY, 20603 Hamburg, Germany

³ INFN, Laboratori Nazionali di Frascati, Frascati, Italy

⁴ Technische Universität München, Physik Dept., 85748 Garching, Germany

⁵ University of Frankfurt, Frankfurt, Germany

⁶ Jan Kochanowski University in Kielce, Poland

⁷ INFN, Sezione di Firenze, Firenze, Italy

⁸ IPNO, CNRS-IN2P3, Univ. Paris-Sud, Université Paris-Saclay, 91406 Orsay Cedex, France

⁹ Institut für Theoretische Physik, Universität Heidelberg, Philosophenweg 16, 69120 Heidelberg, Germany

¹⁰ CERN, 1211 Geneva 23, Switzerland

¹¹ IFIC, Universitat de València-CSIC, Valencia, Spain

¹² JINR Dubna, Russia

¹³ INFN, Sezione di Milano and Università di Milano, Milan, Italy

¹⁴ University of Silesia, Katowice, Poland

¹⁵ Albert Einstein Center for Fundamental Physics, Laboratory of High Energy Physics, Bern, Switzerland

¹⁶ Department of Theoretical Physics, University of the Basque Country UPV/ EHU, 48080 Bilbao, Spain and IKERBASQUE, Basque Foundation for Science, 48013 Bilbao, Spain

¹⁷ LAL, CNRS-IN2P3, Univ. Paris-Sud, Université Paris-Saclay, 91440 Orsay Cedex, France

¹⁸ Dipartimento di Fisica dell'Università and Sezione INFN, Cagliari, Italy

¹⁹ CPPM, CNRS-IN2P3 and Aix-Marseille University, Marseille, France

²⁰ INFN, Sezione di Pisa, Pisa, Italy

*Working group conveners and editors of this summary report

Contents

1 Overview	3
1.1 Proposals and physics topics	4
2 Proposals	10
2.1 LHC Fixed Target	10
2.1.1 Physics motivation	10
2.1.2 LHCb-FT	16
2.1.3 LHCSpin	19
2.1.4 ALICE-FT	21
2.2 LHC-FT: crystals	22
2.3 COMPASS++	25
2.3.1 μp elastic scattering and the proton charge radius	26
2.3.2 Pion PDFs from Drell-Yan production	31
2.3.3 Kaon polarisability from the Primakov reaction	33
2.3.4 Strange meson spectroscopy with kaon beams	35
2.3.5 Selected other COMPASS++ measurements and summary	37
2.4 MUonE	37
2.5 NA60++	42
2.6 NA61++	46
2.7 DIRAC++	49
3 Summary of heavy-ion measurements	52
4 Measurements for cosmic-ray physics and for neutrino experiments	53
5 Compatibility of COMPASS++ and MUonE at the M2 beam line	60
6 Conclusions	68
List of Figures	70
List of Tables	73
References	74

1 Overview

Quantum chromodynamics (QCD) is a well-established part of the Standard Model, but at the same time remains an area of active research, with many aspects we would like to understand better. Among these are for instance the mechanism of confinement, the quark-gluon structure of hadrons, and the nature of the QCD phase diagram. Furthermore, an increasingly precise description of QCD processes is required in several other fields. Perhaps most prominent among these is the description of pp collisions at LHC, but QCD cross sections are also required as an input for describing air showers induced by cosmic rays and for neutrino oscillation experiments.

The CERN Physics Beyond Colliders (PBC) study, summarised in [1], included a physics working group dedicated to QCD, in which a wide range of proposals was discussed. These proposals concern future measurements at the CERN SPS as well as fixed-target installations at the LHC. Before presenting them, let us briefly mention other major facilities worldwide at which the investigation of QCD dynamics is a major goal.

Facilities in operation:

- All four **LHC** experiments have a vigorous programme of measurements related to QCD. Prominent examples are the determination of parton densities, the dynamics of QCD radiation in hadronic jets, and heavy ion physics.
- The experiments PHENIX and STAR at the **RHIC** collider at BNL pursue both measurements in heavy-ion physics and, using the only polarised high-energy proton beams available so far, in proton spin physics. Significant upgrades are foreseen to turn the PHENIX detector into sPHENIX, which is foreseen to start operation in the beginning of the 2020s.
- Jefferson Lab has successfully completed the upgrade of its electron beam facility (called **JLab 12** in the following). It now operates fixed-target experiments with polarised electron beams at 11 GeV in Halls A, B, C, and with a 12 GeV photon beam in Hall D. Whilst the focus of Hall D is on spectroscopy, the other three halls have a varied programme of investigations of the structure of the nucleon and of light nuclei.
- The **J-PARC** complex in Japan operates a wide range of experiments based on its high-intensity primary proton beam, which currently has a maximum energy of 30 GeV. In the hadron hall, a variety of secondary beams are used for experiments in hadron and nuclear physics. An extension of this hall is under discussion, as well as a heavy ion programme with $\sqrt{s_{NN}} = 1.9 - 6.2$ GeV (foreseen 2025).

Facilities under construction:

- The **NICA** facility at JINR (Dubna) will pursue a broad range of measurements in heavy ion physics, hadron structure and spin physics, both in collider and in fixed target mode. The collider mode works at collision energies of $\sqrt{s_{NN}} = 4 - 11$ GeV. Commissioning is foreseen for 2020.

- The **FAIR** facility at GSI will pursue measurements in heavy ion physics at the **CBM** experiment, with **SIS 100** at collision energies of $\sqrt{s_{NN}} = 2.7 - 4.9$ GeV. The experiment will investigate the phase structure at high densities, chiral symmetry and the equation of state at neutron star densities. Commissioning is planned for 2025. Parts of the detector will be used in the RHIC beam energy scan (BES-II) in 2019/2020.

The **PANDA** experiment will use an anti-proton beam from SIS 100 with momenta 1.5 -15 GeV/ c for experiments on hadron spectroscopy, in medium effects of hadrons, nucleon structure and hypernuclei. Commissioning is planned for 2025.

Proposed facilities:

- The Electron-Ion Collider (**EIC**) is a facility planned in the US that would collide polarised electrons with polarised protons or with light to heavy ions in the range $\sqrt{s} = 20$ to 100 GeV in its initial stage. With its high luminosity (10^{33} to 10^{34} $\text{cm}^{-2} \text{s}^{-1}$ for ep) it is designed for in-depth studies of proton and nuclear structure in the regime dominated by gluons and sea quarks [2]. It has been identified as “the highest priority for new facility construction following the completion of FRIB” in the 2015 Long-Range Plan for U.S. nuclear science, and both BNL and JLab are actively working towards its realisation. Provided a successful outcome of various stages of reviews and of appropriate funding, an EIC could start operation around 2030 [3].
- The **LHeC** would collide the LHC proton or ion beam with 60 GeV electrons, aiming at luminosities in the range 10^{33} to 10^{34} $\text{cm}^{-2} \text{s}^{-1}$ for ep . Its primary physics motivation is the search of physics beyond the Standard Model, but – similarly to the LHC – it would also permit detailed studies of QCD at high energy and/or high resolution scale, with precise determinations of PDFs and of α_s being among the highlights. From a technical point of view, an LHeC could start operation in LHC run 5 [4].
- In the context of planning future hadron colliders at the energy frontier, the possibilities of electron-proton collisions are also being discussed, for example for an eh option at an FCC. Such facilities would extend the possibilities described for the LHeC to yet higher scales.

This list is not meant to be comprehensive; measurements at other facilities that are relevant in the context of PBC proposals will be mentioned in the appropriate sections.

1.1 Proposals and physics topics

The following proposals were discussed in the PBC QCD working group and will be presented in this summary:

LHC-FT gas A number of studies were performed for using one of the LHC beams in fixed-target mode. A viable solution is a gaseous target internal to the LHC ring. Corresponding studies were presented by members of ALICE, one by LHCb with a focus on the improvement of the already existing SMOG programme, one by members

of LHCb on the possibilities to install a polarised gas target for the investigation of proton spin phenomena (labelled “LHCSpin” in the following), and a study by the AFTER@LHC group. A comprehensive review by the latter has recently appeared in [5]. Studies for similar measurement campaigns, but with solid targets and beam extraction using bent crystals are ongoing [5, 6].

LHC-FT crystals This proposal studies the possibility to use a setup with bent crystals at LHCb in order to measure the magnetic dipole moments of short-lived baryons such as the Λ_c [7, 8]. The measurement of their electric dipole moment was investigated in the same proposal and – given its main physics motivation – was discussed in the PBC BSM working group [9]. The prospect to measure the magnetic moment of the τ lepton in this setup was just recently discussed in [10].

COMPASS++ A diverse programme of QCD measurements, using major upgrades of the COMPASS detector at the M2 beamline of the SPS, is being proposed in the LoI [11]. For the purpose of this summary, this proposal is termed COMPASS++. The first group of proposed measurements can be realised with the existing muon or hadron beams at M2, whereas a second group requires RF separated high-intensity kaon or antiproton beams. The technical feasibility of the latter was studied in the PBC Conventional Beams working group [12].

MUonE This proposal aims at extracting the hadronic vacuum polarisation at very small spacelike momentum transfers t from elastic scattering of muons on the shell electrons of a target. Via a sum rule one could then evaluate the contribution of hadronic vacuum polarisation to the anomalous magnetic moment $(g - 2)_\mu$ of the muon. The location of this measurement would be the M2 beamline of the SPS.

NA61++ The NA61/SHINE collaboration has presented its plans for running after LS2 as proposal addenda to the SPSC [13, 14]. The proposed measurements range from charm hadron production in Pb Pb collisions for heavy ion physics to nuclear fragmentation cross sections for cosmic ray physics and hadron production in hadron-induced reactions for neutrino physics.

NA60++ Pursuing earlier studies by the NA60 experiment, this proposal aims at probing the QCD phase transition in the production of low energy lepton pairs in Pb Pb collisions. In addition, comparison of a_1 and ρ meson production at this experiment would offer the possibility to investigate the restoration of chiral symmetry.

DIRAC++ The DIRAC experiment at the CERN proton synchrotron (PS) reported the first observation of π^+K^- and π^-K^+ atoms. With a similar experiment at the SPS, reusing parts of the original DIRAC detector, such atoms could be produced with significantly higher statistics, which would yield precise information on the πK scattering lengths.

Due to the beam intensities required by both the NA60++ and DIRAC++, they would need to be installed in an underground hall. As a consequence, the only possible location

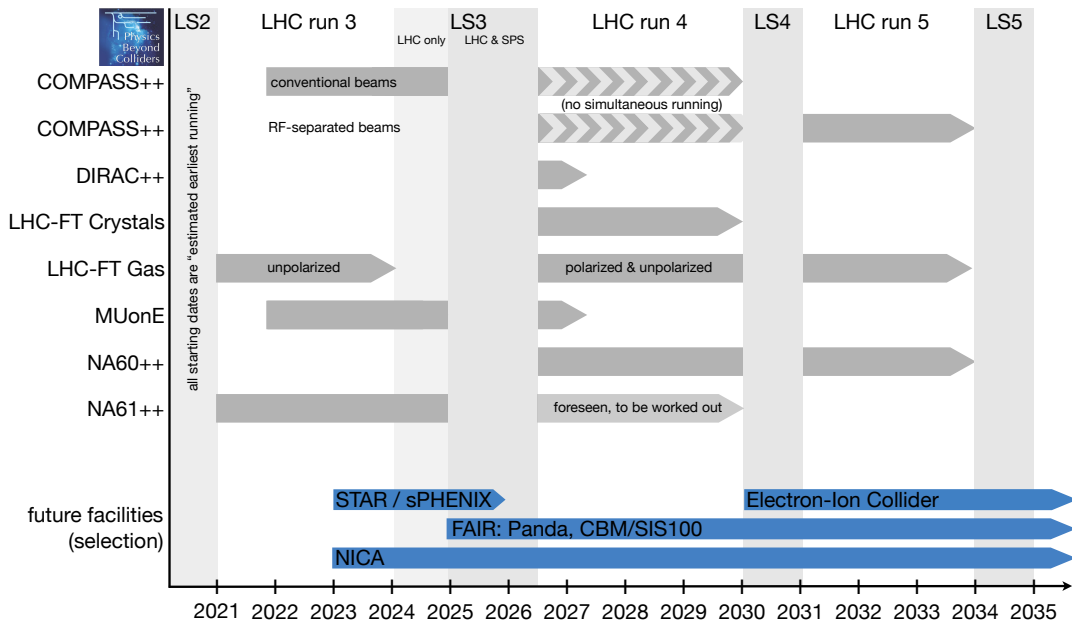


Figure 1. Schematic overview of the proposals discussed in the working group, together with their possible timelines. The beginning of an arrow marks the estimated earliest possible running. Possible timelines of selected other facilities with a focus on QCD studies are shown for comparison.

for both experiments is the ECN3 cavern, where the NA62 experiment is currently installed and running. A study in the PBC Conventional Beams working group found that both experiments would fit together in that cavern, but none of them could be installed in the presence of NA62 [12].

Concerning the M2 beamline, different scenarios for concurrent running of COMPASS++ and MUonE were discussed in the QCD working group. A detailed study of this issue is presented in section 5.

A schematic overview of the different proposals is presented in figure 1. For comparison, possible timelines of other major QCD facilities outside CERN are also given. Not shown are the already running experiments at Jefferson Lab, at BNL (RHIC) and at J-PARC, nor the different options of high-energy colliders (LHeC, FCC, etc.) that are currently under discussion.

We now briefly present the different physics topics addressed in the proposals just listed.

Parton distributions. Parton distribution functions (PDFs) are among the most prominent quantities that describe the structure of hadrons at the quark-gluon level. Measurements with **LHC-FT gas** setups could significantly increase our knowledge of the unpolarised PDFs of the proton (which are a key ingredient for the description of LHC collider data) and PDFs of nuclei (which in particular describe the initial state of heavy-ion collisions). The PDFs of pions and kaons are of special theory interest since these hadrons are the pseudo-Goldstone bosons of QCD. Measurements

proposed by **COMPASS++** could have a substantial impact on better determining their shape. Several intriguing spin effects in QCD are quantified in parton distributions that depend on the transverse parton momentum and on the polarisation of the proton. Polarised Drell-Yan production as envisaged in the **LHC-FT** and the **COMPASS++** proposals is a prime reaction to determine these distributions and would be highly complementary to the spin physics programme of JLab 12 and the EIC.

Heavy-ion physics. The phase structure and physics of QCD at large densities $\mu_B/T \gtrsim 2 - 3$ is not uncovered yet. Neither experimental data from heavy ion collisions nor theoretical investigations have provided conclusive answers so far. The proposed experiments **NA60++** and **NA61++** cover an important part of this density regime with $\sqrt{s_{NN}} \sim 5 - 17$ GeV at the CERN SPS. Major open questions concern the existence and location of a critical end point in the QCD phase diagram, the details of chiral symmetry restoration, as well as the onset of deconfinement. In this context the SPS experiments offer unique opportunities, in particular with the open charm measurements at **NA61++** and the precise determination of the fireball initial temperature at **NA60++**. The energy range covered by the **LHC-FT** experiments is unique and connects the energy range covered by the LHC collider experiments with the lower energy range covered by SPS, RHIC, HADES (GSI) and the planned experiments at NICA and CBM.

Elastic muon scattering. Measurements of elastic μp scattering by **COMPASS++** and of elastic μe scattering by **MUonE** would provide valuable input to two outstanding questions in precision physics.

(i) The extraction of the electromagnetic proton radius from either spectroscopy (on ordinary or muonic hydrogen) or elastic ep scattering leads to a bewildering spread of results that are inconsistent within their quoted uncertainties. Elastic μp scattering at SPS energies would give independent experimental input, with systematic uncertainties that are quite different from those in the ep channel.

(ii) The discrepancy between the theoretical and experimental values of $(g - 2)_\mu$ is a significant problem of the Standard Model. The contribution a_μ^{HVP} from hadronic vacuum polarisation is one of the two dominant sources of theoretical uncertainty on $a_\mu = (g - 2)_\mu/2$. The MUonE proposal aims at extracting a_μ^{HVP} with an accuracy comparable to the one of the currently most precise determination, which is based on data for e^+e^- annihilation into hadrons (supplemented in part by hadronic τ decays).

Low-energy QCD. The behaviour of QCD in the low-energy limit is largely dominated by the dynamics of chiral symmetry breaking. This is described by an effective field theory, chiral perturbation theory (χ PT), which beyond its role in QCD also serves as a blueprint for many extensions of the Standard Model. χ PT in the flavour SU(2) sector of u and d quarks has become precision physics, whilst the inclusion of s quarks to flavour SU(3) remains more challenging. Reasons for this are the larger value of

the s quark mass, which results in a larger expansion parameter of the theory, and the higher number of low-energy constants that need to be determined in order to make the theory predictive at loop level. Information on the πK scattering lengths from **DIRAC++** or from the electromagnetic kaon polarisabilities from **COMPASS++** would be highly valuable, as both quantities can be computed in three-flavour χ PT.

The spectrum of mesons carrying strangeness with masses beyond 1 GeV is known with much less precision than the one of non-strange mesons. **COMPASS++** proposes a comprehensive measurement campaign of the strange meson spectrum with RF separated kaon beams. The data analysis would significantly benefit from the partial wave analysis methods developed by the COMPASS collaboration during its spectroscopy programme with non-strange mesons [15].

Hadrons made from both heavy and light quarks play a particular role in QCD, both for practical reasons (such as the study of the CKM mechanism in b or c quark decays) and because the heavy quark mass opens up the possibility to employ modern field theory methods based on an expansion around the heavy quark limit. The **LHC-FT crystal** proposal discussed here aims at measuring the magnetic moments of baryons containing a c or a b quark.

Measurements for cosmic ray and for neutrino physics. Measurements of hadronic cross sections that are relevant to the propagation of cosmic rays are proposed by **LHC-FT**, **COMPASS++** and **NA61++**. An example is the production cross section for antiprotons or antideuterons. Both LHCb and NA61/SHINE have already published measurements in this area [16, 17]. **NA61++** also proposes to further pursue measurements of hadroproduction cross section that can reduce the uncertainties on neutrino fluxes in neutrino oscillation experiments.

A schematic overview of the different physics topics and the proposals that address them is shown in Table 1.

	LHC FT gas			LHC FT crystals	COMPASS++	MUonE	NA61++	NA60++	DIRAC++
	ALICE	LHCb	LHCSpin						
proton PDFs	×	×		×					
nuclear PDFs	×	×		×	×				
spin physics	×		×	×	×				
meson PDFs	×			×	×				
heavy ion physics	×			×			×		
elast. μ scattering					×	×			
chiral dynamics					×				×
magnet. moments				×					
spectroscopy					×				
measurements for									
cosmic rays and	×	×		×	×		×		
neutrino physics									

Table 1. Schematic overview of the physics topics addressed by the studies presented in the QCD working group.

2 Proposals

In the present section, we discuss the different proposals one by one, with the exception of the proposed measurements for cosmic ray or neutrino physics, which will be reviewed together in section 4.

2.1 LHC Fixed Target

A fixed-target program using the proton and ion beams of the LHC offers highest ever collision energies in the fixed-target mode. It allows for a novel physics program for heavy-ion, hadron, spin, and astroparticle physics with existing (or new set-ups), while at the same time complying with constraints of a parasitic running along with the LHC collider program. The clear advantages of such program can be summarised as [5].

- large luminosities, comparable to those of the LHC and well above those of experiments at similar energies
- wide kinematic coverage with access to backward rapidities in the centre-of-mass
- a variety of target nuclei including polarised ones

The kinematical conditions put such a program in a unique position, with little direct competition in the nearby future. On the other hand the program complements various ongoing and planned programs, and provides important input to studies at the LHC and astroparticle physics. In particular, following highlights can be addressed:

- high- x unpolarized and polarised quark and gluon distributions of the proton, difficult to access at other facilities;
- nuclear parton distributions;
- detailed studies related to heavy-ion physics;
- hadron production (e.g., \bar{p}) as input to interpretation of astroparticle physics data.

The first two points will be further discussed below, while heavy-ion physics will be addressed in section 3, and the cross-links to astroparticle physics will be presented in section 4, due to larger overlap with other proposals.

2.1.1 Physics motivation

The driving physics processes for an LHC Fixed-Target (LHC-FT) program are Drell–Yan and heavy-quark (including $b\bar{b}$ mesons) production, complemented by particle production in nuclear collisions. The large boost of the system in a fixed-target forward-acceptance setup using the LHC beams (cf. figure 2) permits to probe quark and gluon distributions at very high parton momentum fractions, x , and intermediate hard scales, Q^2 , where data with high statistics is unavailable so far and hard to access in the near future at any other facility. Parton distributions are on one side an indispensable tool for the interpretation of proton-induced processes as, e.g., searches at the LHC, and on the other hand interesting

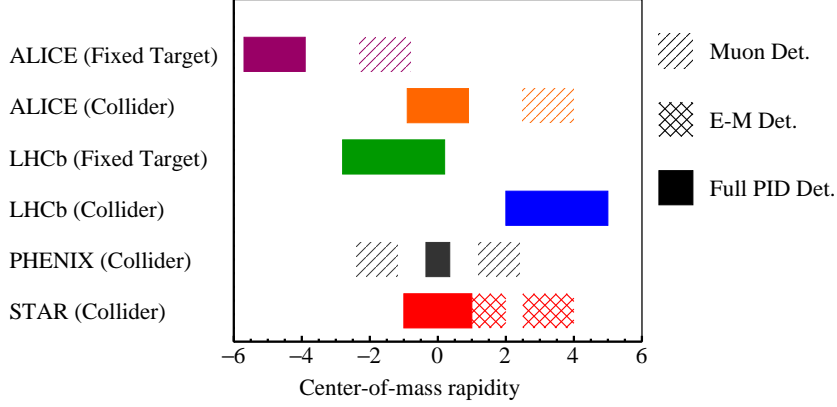


Figure 2. Comparison of the kinematic coverage of the ALICE and LHCb detectors at the LHC and the STAR and PHENIX detectors at RHIC. For ALICE and LHCb, the acceptance is shown in the collider and the fixed-target modes with a target position at the nominal Interaction Point (IP) for a 7 TeV proton beam. The “Full PID Det.” label indicates detector with particle identification capabilities, “E-M Det.” an electromagnetic calorimeter, and “Muon Det.” a muon detector. (Figure taken from [5].)

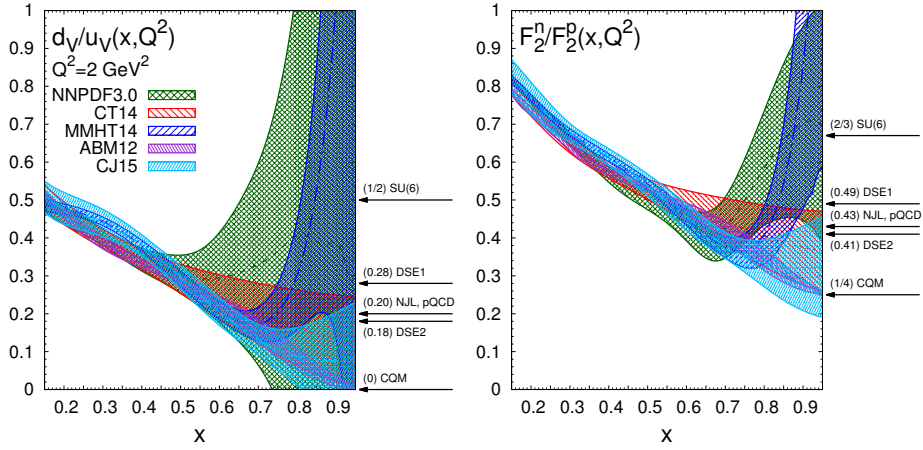


Figure 3. The ratios of the valence down to up distributions (left) and of F_2^n/F_2^p (right) at $Q^2 = 2 \text{ GeV}^2$ for various PDF sets. Indicated as well are the high- x predictions from different nonperturbative models (see Ref. [18] for details). (Figures taken from [18].)

by themselves. They directly touch the foundation of our understanding of the proton in the Standard Model. While parton distributions at low momentum fractions are dominated by QCD-radiative effects and scale evolution can be reliably predicted using perturbative methods, the initial shape including the large- x behaviour of those distributions provide insights into the non-perturbative quark and gluon dynamics, at the moment still out of reach of theoretical calculations. A wide range of predictions exists for the behaviour of quark distributions based on, e.g., counting rules [19], spin-flavor SU(6) symmetry, dominance of scalar valence diquarks etc., resulting in differing predictions for the down-to-up-quark ratio in the limit of $x \rightarrow 1$, where the parton carries practically all the proton

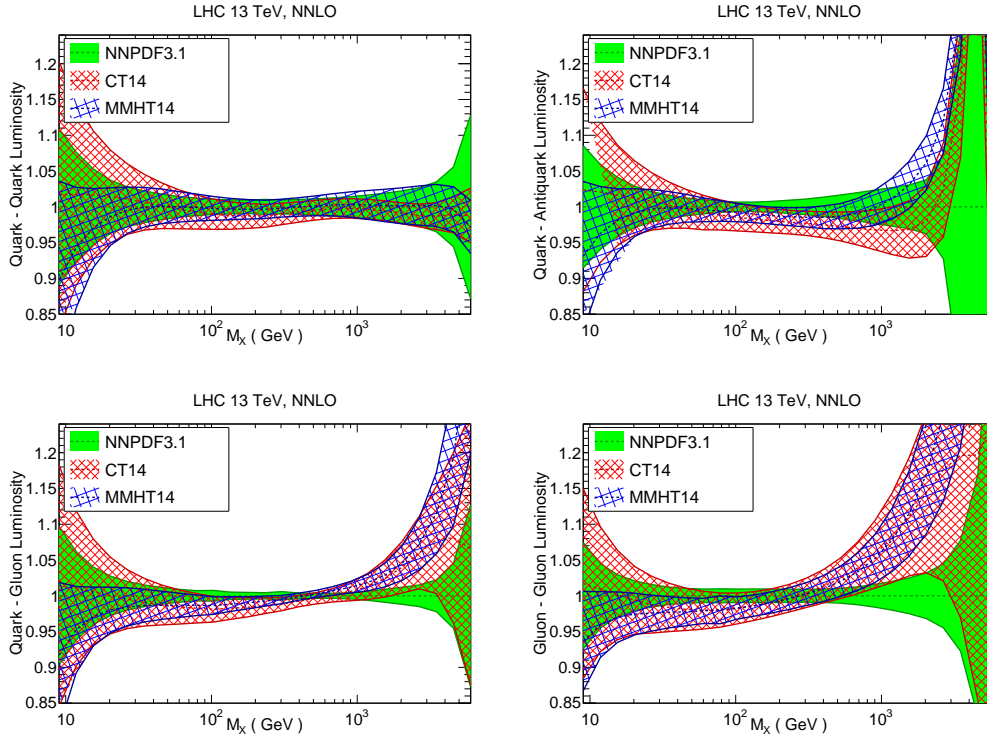


Figure 4. Parton-parton luminosities for 13 TeV proton-proton collisions for quark-quark (top left), quark-antiquark (top right), quark-gluon (bottom left), and gluon-gluon (bottom right) processes for various sets [22–24] of parton distribution functions, as labelled. (Figures taken from [22].)

momentum. That behaviour in the large- x behaviour, in turn, has direct impact on the F_2 structure-function ratio for proton and neutrons (see, e.g., Ref. [20] and references therein). This is illustrated in figure 3, where the ratios of valence-quark distributions and of F_2^n/F_2^p are plotted for various PDF sets and compared to a set of non-perturbative QCD predictions.

It is apparent from figure 3 that present PDF fits cannot discriminate the various predictions and, much more, that the ratios are hardly constrained starting from around $x = 0.6$. A very similar picture emerges for the gluon distribution [21, 22]. This has far-reaching consequences, illustrated in figure 4. High-mass particles at the LHC can only be probed reliably if the high- x parton distributions are known well enough because they determine the parton-parton luminosities and thus cross sections at those masses. In particular the gluon-gluon channel suffers from precision already at masses above 1 TeV.

A similarly elusive parton distribution at high x is that of charm quarks. In the 1980s it was already advocated that besides perturbatively produced $c\bar{c}$ pairs, the proton should possess intrinsic charm [25], which should be probed at high x to isolate it from the perturbative sea (for a recent review see Ref. [26]). In most PDF fits the charm-quark PDFs are set to zero below an energy scale driven by the charm mass of about 1.3 GeV. In contrast, the NNPDF collaboration finds that including charm degrees of freedom the fits favour a non-vanishing intrinsic large- x component, which carries about $0.7 \pm 0.3\%$ of

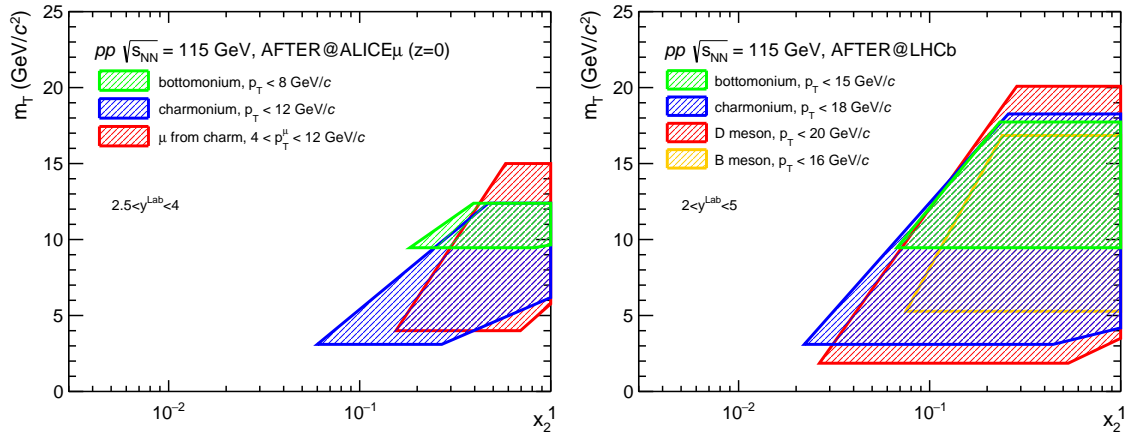


Figure 5. Schematic comparison of kinematical reach for heavy-quark production in pp collision at $\sqrt{s} = 115$ GeV for ALICE-FT (left) and LHCb-FT (right). (Figures from Ref. [5].)

the nucleon momentum at $Q = 1.65$ GeV [27].

Data on the production of mesons containing charm or bottom quarks in LHC-FT kinematics would be valuable both to constrain the gluon distribution at high x and to investigate the presence of intrinsic charm in the nucleon. Figure 5 shows the broad kinematic range for heavy flavor accessible to ALICE and LHCb in fixed-target mode.

It has been known for a long time that parton distributions are modified by the nuclear environment when probed in nuclei. The features observed in the different x regions are shadowing, anti-shadowing, and the "EMC effect". A bulk of the data presently available comes from lepton scattering by a variety of nuclei, which restricts the flavor separation of nuclear PDFs (nPDFs). The Drell–Yan process can provide complementary flavor information, undisturbed by the nuclear environment as the final-state leptons do not interact (strongly) with the nuclear medium, in contrast to semi-inclusive DIS in which the propagation of the struck parton and final-state hadrons might be affected beyond the modification of the parton distribution. Just as proton PDFs, nPDFs are hardly constrained by data at large x . Nuclear PDFs are intriguing by themselves but are also important as input for the description of the initial state of heavy-ion collisions. Furthermore, nuclear targets are often employed, e.g., for the production of neutrinos. A precise description of the neutrino flux depends on the level of understanding of nuclear modifications, especially of the gluon distribution.

Switching to polarised distribution, the three-dimensional mapping of the nucleon structure has become an intense field of research. Spin-dependent transverse-momentum distributions probe in a unique way the gauge structure of the strong interaction. The observation of the Sivers effect [28] in semi-inclusive DIS [29] called immediately for the verification of the fundamental QCD prediction of a sign change when probing the Sivers effect in the Drell–Yan process [30]. By now an extensive data set on the Sivers and other transverse-momentum distributions has been collected at various facilities (see, e.g., Ref. [31] for a review), but a similar data set on polarised Drell–Yan (or the related W and Z boson production) lags behind. Sparse data exist from COMPASS on Drell–Yan [32]

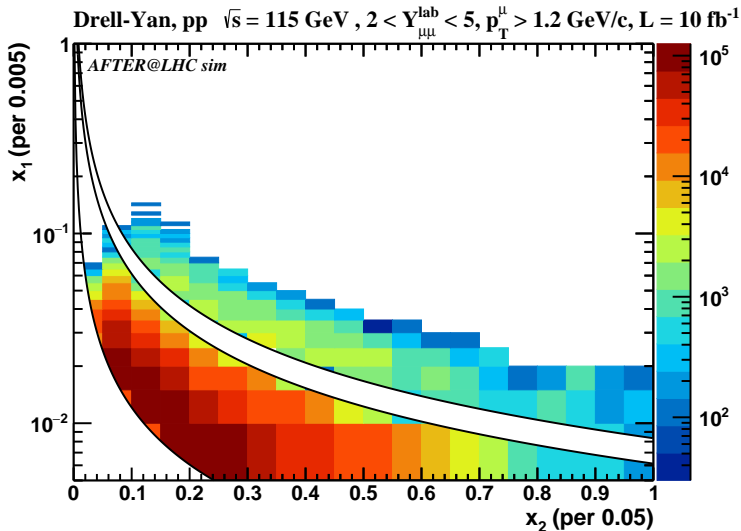


Figure 6. Kinematical reach in beam (x_1) and target (x_2) momentum fractions for Drell–Yan lepton-pair production in pp collisions at $\sqrt{s} = 115$ GeV with an acceptance of $2 < \eta_{\mu}^{\text{lab}} < 5$ and $p_{T,\mu} > 1.2$ GeV. Each coloured cell contains at least 30 events. (Figures taken from [5].)

and STAR on W and Z boson production [33] are not yet conclusive, and while additional data has been taken, a similar precision as in lepton-nucleon scattering is not to be reached in the near future.

Drell–Yan and heavy-quark production in a fixed-target setup using the LHC beam will greatly improve the knowledge of large- x parton distributions. The combination of a forward acceptance and large centre-of-mass energy, \sqrt{s} , samples a phase space of large- x in the target and small enough x in the beam hadron to have copious gluons and sea quarks (cf. figure 6). This allows to study large- x valence-quark (via Drell–Yan) and gluon (via heavy-quark production) distributions.

As an example, figure 7 demonstrates the impact on the proton PDFs using Drell–Yan data in pp collision. Likewise, Figs. 8 and 9 illustrate the improvement in precision on the nuclear modification of quark and gluon distributions, expressed as the nuclear-modification factor $R_{q/g}^A$ of nuclei (A) to proton PDFs, using Drell–Yan and heavy-quark (here D^0 , B^\pm , J/ψ , and $\Upsilon(1S)$) production in pA collision, respectively [5]. Note that for the quark distributions, tungsten was used in above simulation for convenience. Prompt-photon production and W production may provide further constraints on the gluon and anti-quark distributions, respectively, both in protons and nuclei. In above examples, a realisation of a fixed-target experiment using the LHCb detector [35] was assumed (see also Section 2.1.2). Such a program could be pursued with moderate modifications already during LHC run 3.

Figure 10 compares schematically the kinematic reach (here Drell–Yan) for a fixed-target setup using the LHCb detector for both proton (left) and nuclear (right) PDFs with the kinematic coverage of relevant current and future data sets. As highlighted already, LHC-FT can access the large x region with high statistics. Measurements at JLab 12

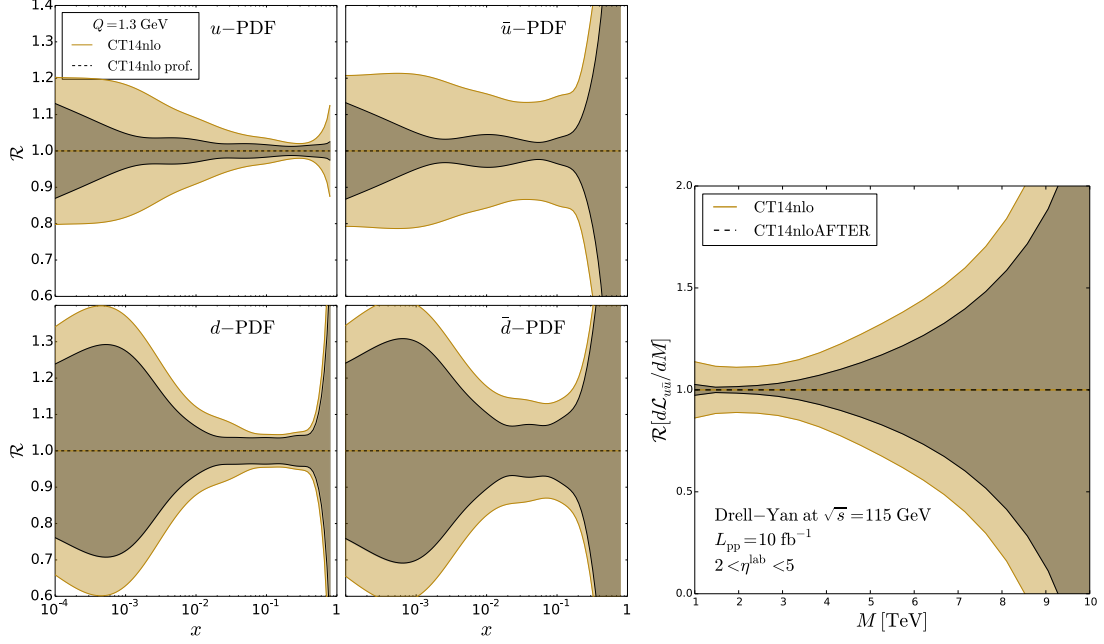


Figure 7. (Left panels) Proton PDF profiling using 10 fb^{-1} of Drell–Yan data in pp collisions for the LHCb fixed-target conditions. The smaller darker band indicates the reduction in the CT14 [21] NLO PDF uncertainty when the pseudo-data are accounted for. (Right) Corresponding improvement of $u\bar{u}$ luminosities. (Left figures taken from [5], right figure from [34].)

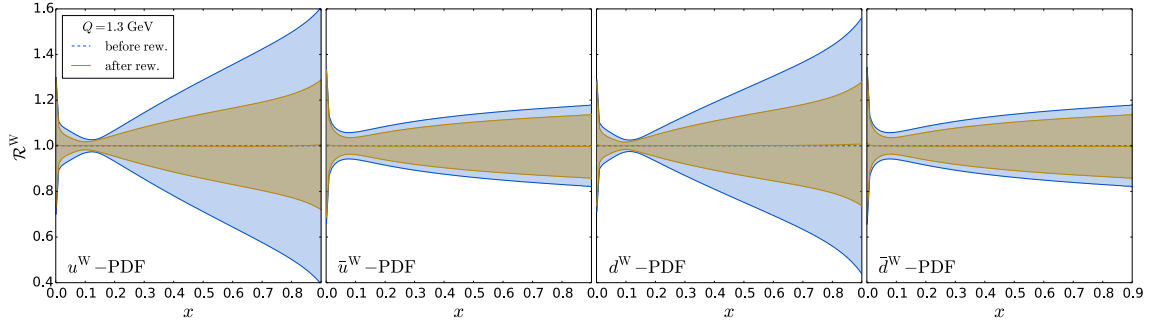


Figure 8. Impact of 10 fb^{-1} of pp and 100 pb^{-1} of $p\text{Xe}$ collisions on nuclear-modification factors R_q^W ($q = u, \bar{u}, d, \text{ and } \bar{d}$) from Drell–Yan data for LHCb fixed-target conditions. (Figures taken from [5].)

are also targeting large x , but at smaller Q^2 , so that the information from the respective data will be complementary in PDF fits. Vigorous PDF studies are foreseen for the HL-LHC [36] and for future lepton-hadron colliders like EIC and LHeC.¹ Given the respective timescales of these programs, the projected performance of LHC-FT measurements is highly competitive.

Measurements with a polarised target will require more substantial modifications and

¹See e.g. the presentations by E. C. Aschenauer and P. Newman at http://www.int.washington.edu/talks/WorkShops/int_18_3.

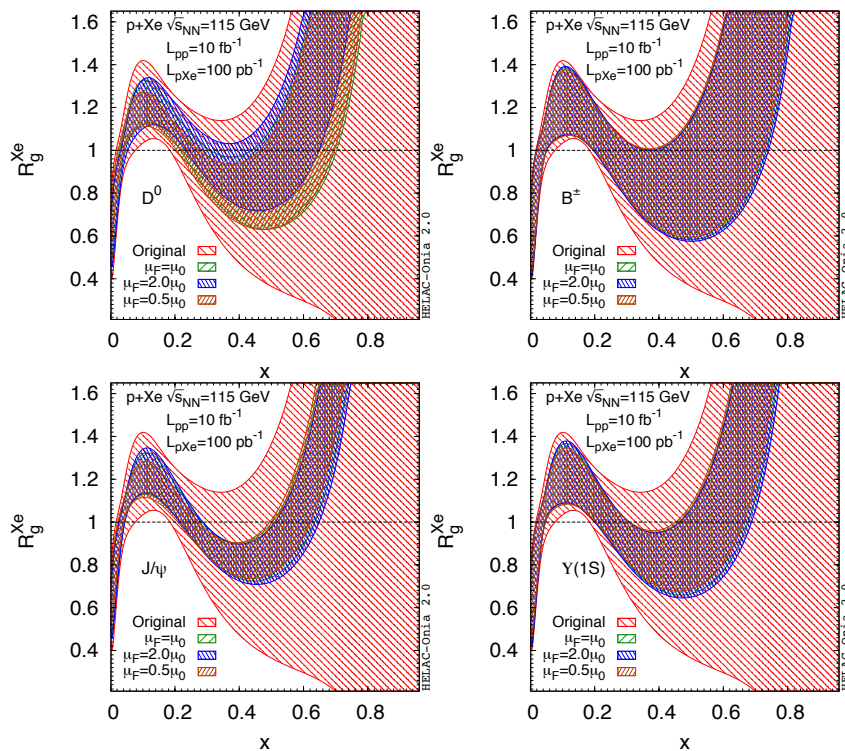


Figure 9. Impact of 10 fb^{-1} of pp and 100 pb^{-1} of $p\text{Xe}$ collisions on nuclear-modification factors R_g^{Xe} through gluon-sensitive probes (D^0 , B^\pm , J/ψ , and $\Upsilon(1S)$ production) for LHCb fixed-target conditions. (Figures taken from [5].)

are thus not expected to commence before LHC run 4. Even then, the physics impact is still expected to be large in view of the world-wide landscape (see, e.g., figure 11). As an example, the expected precision for the Drell–Yan transverse single-spin asymmetry is compared in figure 12 to predictions based on two different phenomenological fits to lepton–nucleon scattering data. Note that for a significant part of the x region probed in such an experiment no data are yet available. This is expected to improve with data to come from the upgraded Jefferson Lab, albeit at relatively low Q^2 . Furthermore, Drell–Yan with polarised beams at RHIC and at an even longer time-scale the Electron-Ion Collider will also contribute.

Beyond Drell–Yan measurements, heavy flavour production can be used to explore the Sivers asymmetry in the gluon sector. Last but not least, a wide range of azimuthal correlations and hadronic final states allow studies of a variety of transverse-momentum distributions and the transversity distribution at large x [5].

2.1.2 LHCb-FT

LHCb is planning to pursue its fixed-target program during Run3 after improving the gas target setup (known currently as SMOG). Its upgrade, SMOG2 [41], aims at containing the injected gas inside a storage cell. Because of that the gas density can be increased by up to two orders of magnitude without changing the impact on the LHC operations.

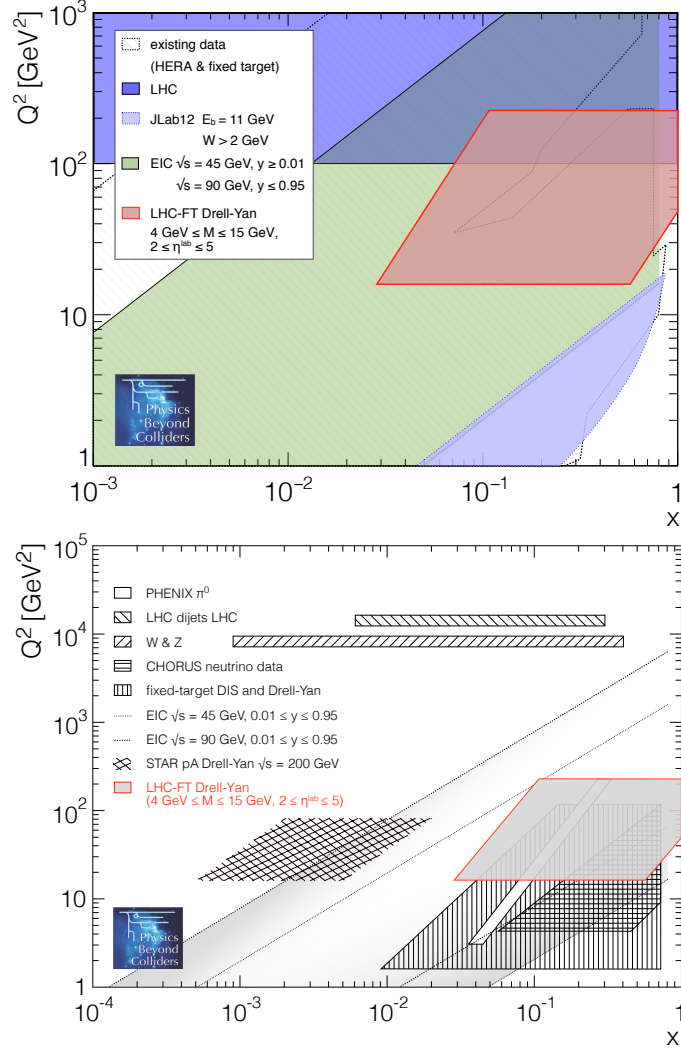


Figure 10. Schematic comparison of kinematical reach in x and Q^2 for Drell-Yan lepton-pair production ($4 \text{ GeV} < M < 15 \text{ GeV}$) in pp and $p\text{Xe}$ collisions at $\sqrt{s} = 115 \text{ GeV}$ with an acceptance of $2 < \eta^{\text{lab}} < 5$ with typical data sets used in proton (top) and nuclear (bottom) PDF fits. (bottom figure inspired by [37].)

This has recently been approved within the Collaboration to be installed during the LHC Long Shutdown II. The goal is also to extend the choice of gas species that can be injected, including notably hydrogen and deuterium. The pp collisions in fixed-target mode would be a reference for all pA collision samples. Moreover, H and D targets would provide additional inputs to the study of cosmic ray propagation in the interstellar medium (cf. section 4) and allow to extend the physics case to the study of the three-dimensional structure of the nucleon through spin-independent observables. Another important advantage of the new target setup is the accurate control of the injected gas density, so that the acquired luminosity can be determined to a better precision with respect to the present setup.

It is clear that the physics reach strongly depends on the achievable integrated lumi-

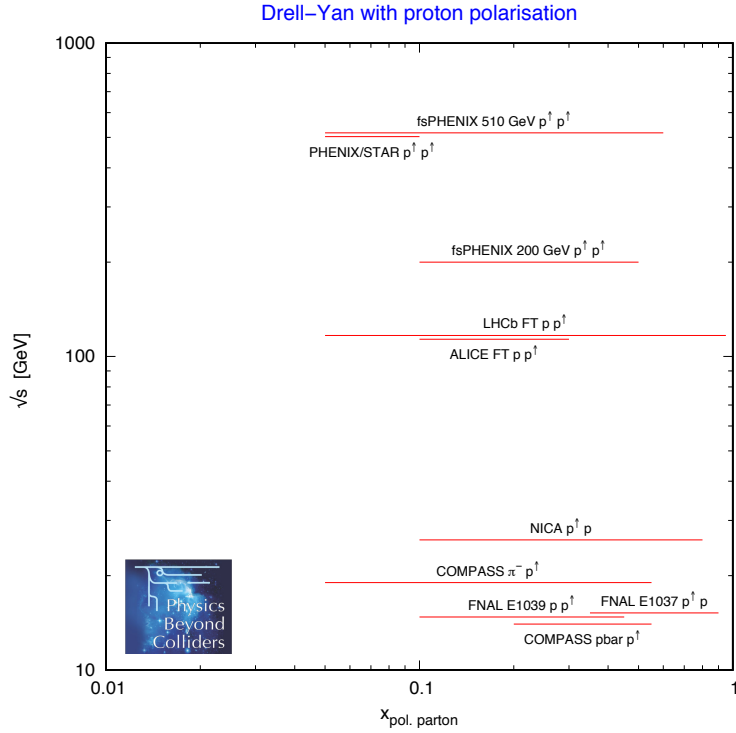


Figure 11. Kinematic reach of future or planned polarised Drell–Yan experiments (from Table 16 in Ref. [5]).

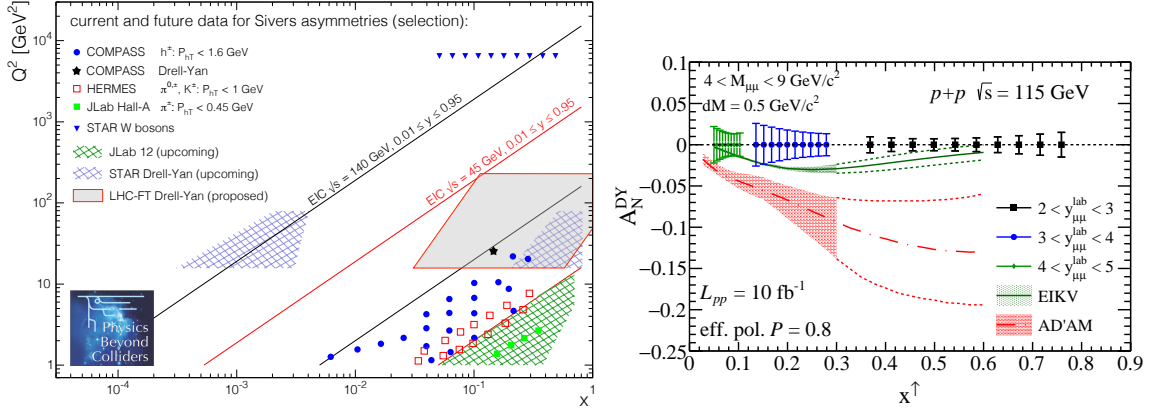


Figure 12. (left) Schematic comparison of kinematical reach in x and Q^2 for Drell–Yan lepton-pair production ($4 \text{ GeV} < M < 15 \text{ GeV}$) in single-polarised pp collisions at $\sqrt{s} = 115 \text{ GeV}$ and an acceptance of $2 < \eta^{\text{lab}} < 5$ with selected current and upcoming data sets on Siverts asymmetries. (right) Expected precision on Siverts Drell–Yan asymmetries for LHCb-FT (LHCSpin). Data points are for different ranges in laboratory rapidity (different symbols, as labelled) and increasing with x for increasing invariant mass of the lepton pairs ($4 \text{ GeV} < M < 9 \text{ GeV}$). Phenomenological curves are based on Refs. [38, 39]. (Left figure adapted from [2, 40], right one taken from [5].)

osity. In an ambitious program of collecting several fb^{-1} (as assumed for many of the performance studies shown in this section), a breakthrough advance in the understanding of parton distribution functions for gluons, antiquarks and heavy quarks at $x > 0.5$, where they are now almost unconstrained, can be expected. Such integrated luminosities could be collected in principle by running continuously with the maximum instantaneous luminosities of a few $10^{32} \text{ cm}^{-2} \text{ s}^{-1}$ allowed by the SMOG2 target. By contrast, the running scenario currently envisaged by the LHCb Collaboration is aiming at fixed-target data of the order of 0.1 fb^{-1} per year. This can be realised with minimal interference with the core LHCb program, given the common trigger and DAQ bandwidth and, particularly for heavy targets, the contamination of the LHC vacuum. Samples of this size would already allow copious production of Drell-Yan and heavy-flavor states, including $b\bar{b}$ mesons (see, for instance, Table 4 or Ref. [42]). LHCb-FT with nuclei could in principle be used for heavy-ion physics (cf. section 3) and corresponding studies are to be performed.

Implementation: The main challenges are related to the optimisation of the target design and to the integration of the data acquisition and offline computing strategies with the core LHCb program. The latter requires a substantial effort that will be implemented in progressive stages.

Estimated cost and time scale: The cost of the proposed new target setup is a minor fraction of the approved LHCb upgrade project. The collaboration is also evaluating more ambitious proposals that could be realised at LHCb on the time scale of LHC Run 4, including the polarised target (cf. section 2.1.3) and the crystal target (cf. section 2.2) proposals.

2.1.3 LHCSpin

The project has several ambitious goals rewarding new-era quantitative searches in QCD, through the study of nucleons internal dynamics. By using a transversely polarised gaseous target, one of the main measurements will allow to study quark transverse-momentum distributions (TMDs) in proton-proton collisions at the unique kinematic conditions described above through single transverse spin asymmetries.

The LHCb detector has been designed and optimised for heavy-flavor physics, so final states with c or b quarks, carrying information on the gluon dynamics inside nucleons, will be efficiently reconstructed and will allow to extend the measurements of spin asymmetries to the hardly known gluon sector.

Due to the possibility of parallel data taking with the LHCb main stream physics, it is possible to project statistical uncertainties for different data taking periods. As an example, for Drell-Yan transverse single-spin asymmetries in 4, 12, and 24 months of data taking, considering 8h/day and 20 days/month data of duty time, absolute statistical uncertainties of 0.015, 0.01, and 0.008 can be reached, respectively.

Implementation: The proposed target is based on the technology that has been applied successfully at the 27.6 GeV HERA electron ring in 1995 to 2005 for the HERMES experiment [43]. The target consists of a chamber with an open T-shaped tubular structure, the

Storage Cell (SC), into which a thermal beam of H atoms from an Atomic Beam Source (ABS) is injected and radially trapped. The LHC beam passes the cell through the straight beam tube. The SC can be opened during injection and kept at different temperatures in order to optimise density and polarisation. A transverse magnetic field (~ 300 mT) defines the direction of polarisation. A sample of gas is continuously extracted from the SC and analysed on-line by a polarimeter with respect to nuclear polarisation and atomic fraction, a key parameter related to the degree of polarisation. This allows to determine the polarisation of target atoms as seen by the beam along the SC to a precision of a few %. The SCs straight beam tube is assumed to be 10 mm in diameter and 300 mm in length, coated with Amorphous Carbon. By running the SC at about 100 K, an ice layer is formed providing an optimum surface which, according to the experience at HERMES, suppresses atomic recombination quantitatively, a major cause of depolarisation. At 100 K and with an injected flow rate of 6.5×10^{16} H/s, an areal density of more than 10^{14} H/cm² can be obtained. Assuming 1A for the HL-LHC proton-beam current an instantaneous luminosity of close to 10^{33} cm⁻² s⁻¹ could be achieved [44], which corresponds to about 10 fb⁻¹ per year. Whether LHCb will be able to cope with the corresponding event rate in addition to the collider data is an issue to be investigated. An advantage of a gaseous target is, however, the absence of diluting material. This is important for event-rate limited situations, as the event rate from the polarised target does not explode artificially due to presence of unpolarized scattering centres.

A different limitation might be the presently foreseen location upstream of the nominal LHCb IP. It will—in the present detector configuration—reduce substantially the coverage in rapidity and thus at high- x of the partons in the polarised (target) nucleon and needs to be investigated further.

Various effects are already being studied that may disturb a proper functioning of the polarised gas target, including wake fields and wall impedance, instabilities due to electron clouds, and depolarisation of the target gas by the bunch fields. No showstoppers have been found to date. Work on a conceptual design is in progress and discussions with machine experts are ongoing. The aim of these studies is to have a prototype target chamber ready for installation during LS3, enabling in-situ tests with gas injection. This set-up could be extended in steps by adding the ABS and the polarimeter during shorter stops of the machine.

A detailed R&D program, which benefits from the experience achieved with the installation and running of the unpolarised fixed target SMOG2, is going on and will take at least three years for addressing all the important issues connected to the implementation of the target system into the LHC. After this process, and if no showstopper has been identified, LHC Spin will be proposed for installation during the LHC LS3.

Collaboration strength: The main proponents form a group of experts with long experience on the polarised physics, HEP detectors and data analysis. A growing list of institutes includes, at the moment: INFN and University of Cagliari (Italy), INFN and University of Ferrara (Italy), INFN-Frascati (Italy), Jülich Laboratory (Germany), High Energy Physics Laboratory Gatchina (Russia), University of Erlangen (Germany), Univer-

sity of Virginia (US). Other groups from INFN Italy and in EU expressed their interest. For this purpose, a parallel discussion session has been organised during the SPIN2018 international conference organised by the group in Ferrari. LHCSpin had also been invited, in October 2018, to present the project at the Institute of Nuclear Theory, Seattle for involving the relevant American community, already present with few groups, and a dedicated meeting will be organised in Russia due to the expressed significant interest of the Russian colleagues.

Estimated cost and time scale: A rough estimation of the cost for the hardware R&D and the final construction is of the order of 2 M€.

2.1.4 ALICE-FT

One of the main strengths of ALICE in fixed-target mode would be its large rapidity coverage. Assuming a target location at $Z = 0$, the ALICE muon spectrometer (and future Muon Forward Tracker) would access the mid- to backward rapidity in the centre-of-mass frame ($-2.3 < y_{\text{cms}} < -0.8$).² In addition, the long absorber in front of the muon tracking station is an asset for background rejection and Drell–Yan studies at low energy. The ALICE central barrel offers a complementary coverage to the muon arm by accessing the very backward rapidity region ($-5.7 < y_{\text{cms}} < -3.9$), reaching the end of phase space for several processes. Thanks to its excellent particle identification capabilities, particle detection and identification down to low p_T , unique measurement of soft probes and open heavy flavors can be pursued. Another asset of the ALICE apparatus is the capability to operate with good performance in a high particle density environment. Access to most central AA collisions at $\sqrt{s_{NN}} = 72$ GeV should be possible if the interaction rate remains low. In addition, the ALICE Collaboration could potentially devote a significant data taking time to a fixed-target program (especially with the proton beam), allowing the collection of large integrated luminosities and the investigation of several target species. Two main solutions are being investigated to deliver fixed-target collisions to ALICE: an internal gaseous target or an internal solid target (coupled to a bent crystal to deflect the beam halo). On the one hand, a gas-jet or a storage cell (with levelled gas pressure) would allow to deliver about 45 pb^{-1} of proton-polarised hydrogen collisions to ALICE per year (260 pb^{-1} in case of proton-unpolarised H_2 collisions), and 8 nb^{-1} of Pb-Xe collisions. With such a system the target can be polarised, but requires large space to be installed (most likely outside the ALICE barrel magnet), requiring thus the need of additional detectors for vertexing and additional studies of the tracking performance of the TPC in such conditions. A simple unpolarized storage cell might potentially be used closer to the ALICE IP. On the other hand, the usage of an internal solid target coupled to a bent crystal has the advantage of more portability, allowing one to install the target closer to the nominal ALICE IP and thus benefiting of the optimal performance of the current ALICE apparatus. With such a device 37 pb^{-1} (6 pb^{-1}) of p -C (p -W) collisions, and 5 nb^{-1} (3 nb^{-1}) of Pb-C (Pb-W)

²This is considering an incident proton beam on the target. For an incident lead beam, the muon spectrometer rapidity coverage is $-1.8 < y_{\text{cms}} < -0.3$ and central barrel coverage $-5.2 < y_{\text{cms}} < -3.4$. Here, rapidities are computed for massless particles.

collisions could be registered in ALICE per year. Studies are ongoing on the integration and compatibility of a fixed target with the ALICE apparatus and its operation in collider mode.

2.2 LHC-FT: crystals

The LHC-FT crystal proposal discussed in the QCD working group aims at measuring the magnetic dipole moment (MDM) of short-lived baryons that contain a charm or a bottom quark. The key experimental element is to use a setup with bent crystals inside the LHC. Such a setup might also be used for measuring the electric dipole moments of the same hadrons, which would be a probe of CP violation. Both possibilities are described in [8]. Recently, the possibility to use the same technology for measuring the MDM of the τ lepton has been discussed in [10].

Physics motivation. Hadrons consisting of both light and heavy quarks play a special role in QCD: their binding is dominated by large-distance, non-perturbative dynamics, whilst the presence of a heavy quark mass brings in a simplifications due to heavy-quark symmetry. Next to their masses, the magnetic moments of baryons are among the most prominent quantities characterising their static properties. The significant range of model predictions for the magnetic moments of selected heavy baryons is shown in figure 13. Further model comparison and discussion can for instance be found in [45–47]. Of particular interest are modern effective theory approaches based on the heavy quark limit, e.g., the prediction in row 15 of the figure, which was obtained in heavy-baryon chiral perturbation theory. The prospect of having experimental data for magnetic moments might trigger further theory activity in this direction.

Experimental setup. The possibility to measure the MDM of heavy and strange baryons at the LHC has been explored in recent years [7, 8, 48, 49] and relies on the precession of their spin in external electromagnetic fields. The experimental setup is based on three main elements: i) a source of polarised particles with known direction and polarisation, ii) an intense electromagnetic field able to induce a sizeable spin precession during the lifetime of the particle, iii) a detector to measure the final polarisation vector by analysing the angular distribution of the decay particles. For short-lived, positively-charged charm and beauty baryons, e.g., Λ_c^+ , Ξ_c^+ , Ξ_b^+ and Ω_b^+ , an intense electromagnetic field, such as the one between the atomic planes of bent crystals, is necessary to induce spin precession. For this purpose, a fixed-target experiment is proposed to extract protons from the LHC beam halo with a bent crystal. These protons will then hit a dense target and produce charged heavy baryons that will then be channelled in bent crystals positioned in front of the detector.

The LHC interaction point IP8, where the LHCb detector sits, has been identified as a most suitable location of the experiment. This is motivated by the fixed-target like geometry of the apparatus, the only one operating at LHC that is fully instrumented in the forward region ($2 < \eta < 5$). A main challenge of the experiment is represented by the limited coverage of the LHCb detector acceptance in the very forward region, approximately greater than 15 mrad, and the limited particle identification information

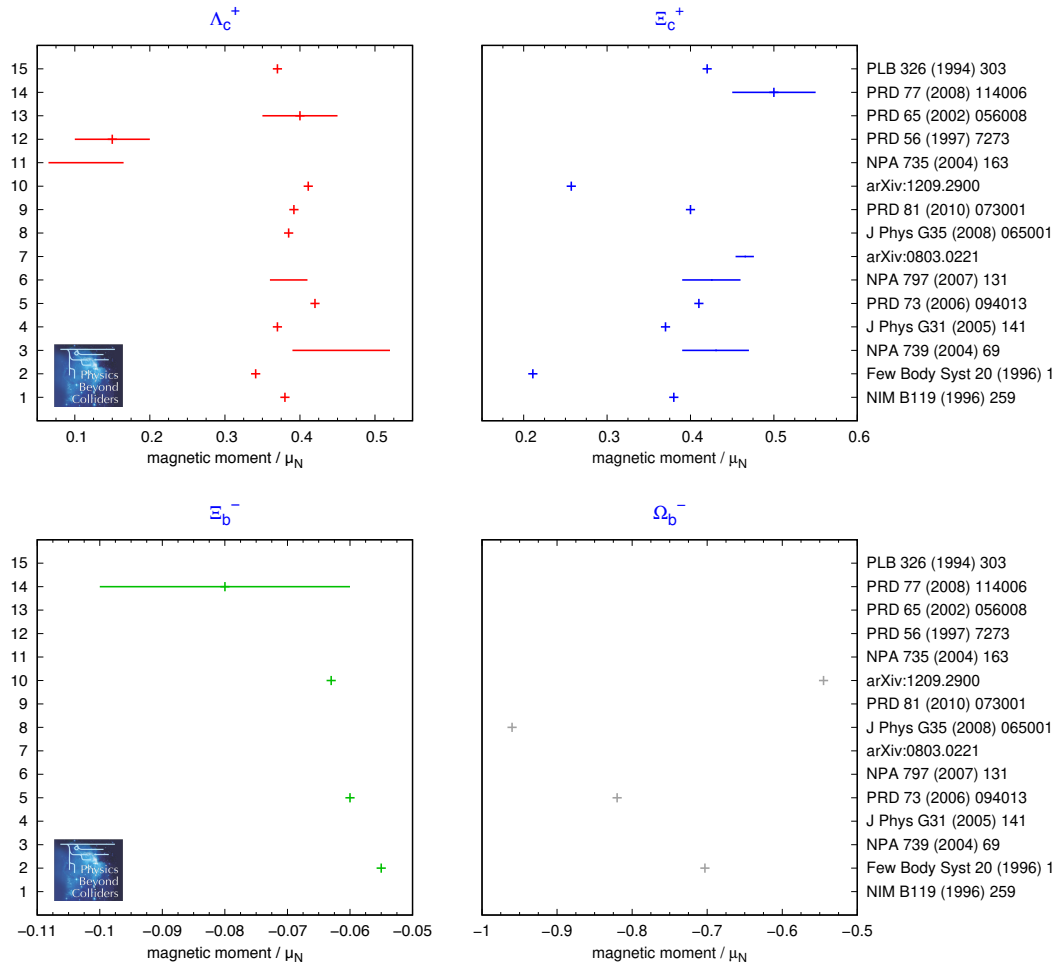


Figure 13. Spread of theoretical predictions for the magnetic moments of heavy baryons. Values in rows 1 to 10 are from different quark models, 11 from a soliton approach, 12 to 14 from sum rules, and 15 from chiral perturbation theory.

for high-momentum tracks above 100 GeV. Detector simulations have been conducted to demonstrate the feasibility of the experiment under realistic operational conditions and to estimate sensitivities [8, 49]. The clear signal signature combined with precise kinematical information compensates the lower vertex reconstruction performance from the upstream configuration.

Implementation: The location of the target and bent crystals is upstream of the vertex locator detector (VELO) vacuum tank and of a new sector valve that will be installed during LS2 to isolate from the LHC vacuum the region upstream of the VELO. This means about 1.16 m upstream of the position of the nominal proton-proton collision point at the LHCb interaction point. The proposal is to run the fixed-target configuration in parallel with standard proton-proton collisions in order to maximise the time of running, collecting both types of collisions at the same time. It has been shown that with the performance of the

Phase-I upgrade LHCb detector, a W target of 2 cm thickness hit by a proton flux of 10^7 protons/s is the upper limit for a parallel parasitic operation not affecting LHCb data taking of proton-proton collisions (i.e., an increase of less than 10% in occupancies due to the fixed-target collisions).

The proposed fixed-target setup can also be used for other flavor-physics studies complementary to those of the LHCb core physics or as a standard fixed target experiment, reaching luminosities similar to those discussed by the AFTER@LHC collaboration [5, 50].

Estimated performance and time scale: About 2.4×10^{14} protons on target (PoT) with a target thickness of 2 cm could be reached with three years of data taking, either with two weeks per year of dedicated detector running at 10^8 p/s or with parallel detector operation at 10^7 p/s. This would lead to MDM sensitivities of about $10^{-3} \mu_N$, $10^{-1} \mu_N$, and $10^{-3} \mu_N$ level [8] for charm, beauty and strange baryons, respectively (where μ_N is the nuclear magneton). Figure 14 shows the sensitivities for a scenario (labelled S1) with 10^{15} PoT and a target thickness of 0.5 cm (which is equivalent to 2.4×10^{14} PoT and a 2 cm target). Extending the detector coverage down to 10 mrad would significantly reduce the crystal bending angle required. The enhanced channelling efficiency and particle identification for tracks of 300 GeV would improve the reconstruction of signal events. Combined with longer running time and an increase of the proton flux in Run 5, this would improve sensitivities by about one order of magnitude. This is shown as scenario S2 in figure 14 for an integrated 10^{17} PoT and a 0.5 cm target (equivalent to 2.4×10^{16} PoT and a 2 cm target).

Challenges: Studies and R&D are ongoing to assess other challenges of the proposal. These include, on one hand, the compatibility with the machine, its operation mode, maximum reachable proton flux and the design of the collimation system (absorber) downstream the detector, along with the operation mode of the LHCb detector (parasitic as described above or dedicated short runs with only fixed-target collisions). On the other hand, the feasibility of the ≈ 15 mrad bent crystal, mandatory to optimise the acceptance coverage of the LHCb detector, will be a key milestone for the realisation of the experiment. In 2017, the double crystal scheme has been demonstrated at SPS energies and with a second crystal of lower bending without target.³ In 2016, the channelling of 6.5 TeV protons extracted from the LHC halo was demonstrated [51]. The viability of this technique, although in another energy and lifetime regime, was proved by the E761 Collaboration [52] through the measurement of the MDM of Σ^+ baryons produced using a 800 GeV proton beam impinging on a Cu target.

The sensitivity reach for measuring MDMs strongly relies on the self-polarisation of baryons in high-energy hadron collisions. It is clear that only in case of large polarisation a meaningful measurement (as depicted in figure 14) of the MDMs can be performed. While it has been known for a long time that Λ and other hyperons are produced transversely polarised, the magnitude and kinematic dependence of polarisation is poorly known for

³S. Montesano, Testing the double-crystal setup for physics beyond colliders experiments in the UA9-SPS experiment, <http://ipac2018.vrws.de/papers/tupaf043.pdf>, 2018.

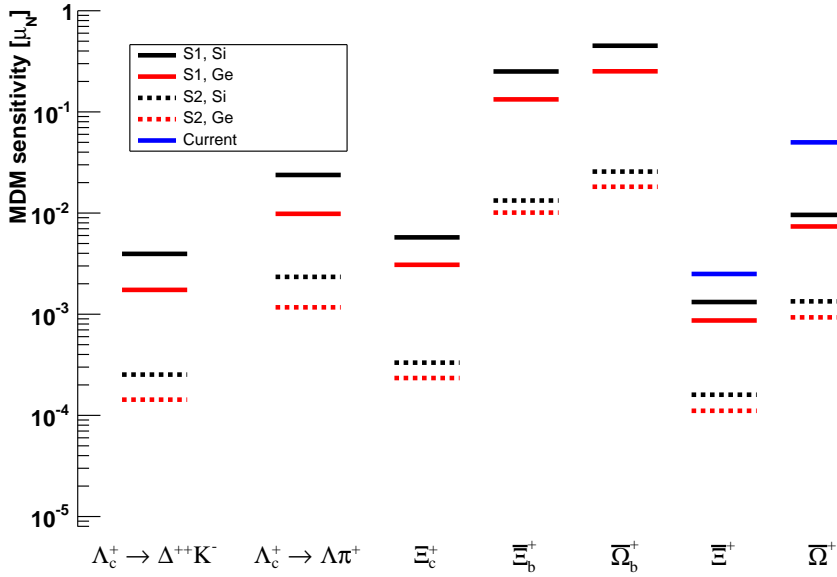


Figure 14. Estimated MDM sensitivities, for Si and Ge with crystal parameters optimised for S1 and S2 scenarios (see text). A total of 10^{15} and 10^{17} protons on a 0.5 cm thick target have been considered for S1 and S2, respectively. For comparison purposes, the Λ_c^+ case has been studied in the $\Delta^{++}K^-$ and $\Lambda\pi^+$ final states. Blue lines show the sensitivity of the current Ξ^- and Ω^- MDM measurements. (Figure from Ref [8].)

many of the baryons considered here. Corresponding systematic uncertainties have not been worked out. Valuable input to that can come from the SMOG data already recorded during LHC Run 2 and more so from future SMOG2 data at the same centre-of-mass energy of ≈ 115 GeV.⁴ Production cross sections, estimated initially from $c\bar{c}$ production at PHENIX at 200 GeV and scaled to 115 GeV, are consistent with the first measurement of J/Ψ and D^0 production in fixed-target configuration at the LHC [54].

2.3 COMPASS++

For more than four decades the M2 beam line of the SPS has provided secondary beams of muons and hadrons to the EHN2 experimental area.⁵ Several experiments dedicated to QCD utilised those beams, starting with EMC [55] in the 1970s. Currently, COMPASS [56] is in the process of completing its COMPASS-II program [57] with a remaining one-year muon run on a transversely polarised ^6LiD target in 2021. The versatility of the beam line with respect to particle species and energies has allowed a broad physics program on hadron structure spectroscopy, including polarisation dependence and modifications in the nuclear environment.

The COMPASS++ project of a “New QCD facility at the M2 beam line of the CERN SPS” [11] continues in this tradition. Among others, it addresses such open questions as

⁴See for instance Ref. [53] for a first sample of reconstructed Λ_c^+ .

⁵Low-intensity electron beams have been used as well, mainly for calibration purposes.

- the proton charge radius,
- quark structure of light mesons, in particular of the pion,
- kaon polarisabilities from the Primakov reaction,
- strange-meson spectroscopy,

and further complementary measurements, e.g., as input to the interpretation of cosmic-ray measurements (cf. Section 4). A summary of topics (including details on running time and on beam, target, as well as detector requirements) is presented in Table 2 and will be discussed in parts below. It should be noted that some of the programs (e.g., the last two in above list) require extensive modifications of the M2 beam line in order to provide RF-separated hadron beams. The feasibility is discussed in the parallel PBC “Conventional Beams” activity [12].

2.3.1 μp elastic scattering and the proton charge radius

The hydrogen atom is the most simple and abundant atom around. As such it has received enormous attention and served as testing ground for various benchmark calculations in QED. Nevertheless, it still confronts the field with open questions, in particular about its nucleus, the proton. As discussed before (cf. Sec. 2.1), the investigation of the proton structure, e.g., its description in terms of quark and gluon degrees of freedom in the framework of QCD, is a wide field of intense experimental and theoretical research. But even such a seemingly simple property as the charge radius has still not been measured precisely despite decades of activities. Two complementary approaches have traditionally been used to provide insights into the size of the proton, employing on one side hydrogen spectroscopy by measuring Lamb shifts (or more generally atomic energy-level splittings) and on the particle physics side using elastic lepton-proton scattering. The results of these approaches had seemed to agree and converged to a value of around 0.88 fm [58], until—close to ten years ago—new spectroscopy results became available using muonic hydrogen [59]. They disagreed by more than 5σ with the earlier measurements of the proton radius, both using elastic scattering but also ordinary-hydrogen spectroscopy, and suggested a smaller radius of about 0.84 fm. Further excitement was spurred by the results using muonic deuterium that also suggested a smaller charge radius. This triggered an ongoing debate about possible signs of lepton universality.

On the other hand side, electron-scattering results do not provide a coherent picture either. In particular, different fitting strategies to available scattering data (even using the same data) result in different proton radii. One should remember that the radius is not measured directly in elastic scattering, but rather deduced from extrapolating the slope of the electromagnetic form factors to zero four-momentum transfer squared, i.e.,

$$\frac{1}{6}r_p^2 = - \left. \frac{d}{dQ^2} \right|_{Q^2=0} G_E(Q^2) \quad (2.1)$$

Program	Physics Goals	Beam Energy [GeV]	Beam Intensity [s ⁻¹]	Trigger Rate [kHz]	Beam Type	Target	Earliest start time, duration	Hardware additions
muon-proton elastic scattering	Precision proton-radius measurement	100	4 · 10 ⁶	100	μ [±]	high-pressure H2	2022 1 year	active TPC, SciFi trigger, silicon veto,
Hard exclusive reactions	GPD <i>E</i>	160	2 · 10 ⁷	10	μ [±]	NH ₃ [↑]	2022 2 years	recoil silicon, modified polarised target magnet
Input for Dark Matter Search	\bar{p} production cross section	20-280	5 · 10 ⁵	25	<i>p</i>	LH2, LHe	2022 1 month	liquid helium target
\bar{p} -induced spectroscopy	Heavy quark exotics	12, 20	5 · 10 ⁷	25	\bar{p}	LH2	2022 2 years	target spectrometer: tracking, calorimetry
Drell-Yan	Pion PDFs	190	7 · 10 ⁷	25	π [±]	C/W	2022 1-2 years	
Drell-Yan (RF)	Kaon PDFs & Nucleon TMDs	~100	10 ⁸	25-50	<i>K</i> [±] , \bar{p}	NH ₃ [↑] , C/W	2026 2-3 years	"active absorber", vertex detector
Primakov (RF)	Kaon polarisability & pion life time	~100	5 · 10 ⁶	> 10	<i>K</i> ⁻	Ni	non-exclusive 2026 1 year	
Prompt Photons (RF)	Meson gluon PDFs	≥ 100	5 · 10 ⁶	10-100	<i>K</i> [±] π [±]	LH2, Ni	non-exclusive 2026 1-2 years	hodoscope
<i>K</i> -induced Spectroscopy (RF)	High-precision strange-meson spectrum	50-100	5 · 10 ⁶	25	<i>K</i> ⁻	LH2	2026 1 year	recoil TOF, forward PID
Vector mesons (RF)	Spin Density Matrix Elements	50-100	5 · 10 ⁶	10-100	<i>K</i> [±] , π [±]	from H to Pb	2026 1 year	

Table 2. Summary of physics programs within the COMPASS++ project (from [11], including the physics goals, beam and target requirements, running time, and detector upgrades (where applicable). The table is segmented into projects requiring **muon beams** (in blue), **conventional hadron beams** (in green), and **RF-separated hadron beams** (in red), the latter also separated by double horizontal lines from the presently available beams.

for which the electric form factor $G_E(Q^2)$ can be obtained from the elastic-scattering cross-section

$$\frac{d\sigma^{\mu p \rightarrow \mu p}}{dQ^2} = \frac{\pi\alpha^2}{Q^4 m_p^2 \vec{p}_\mu^2} \left[(G_E^2 + \tau G_M^2) \frac{4E_\mu^2 m_p^2 - Q^2(s - m_\mu^2)}{1 + \tau} - G_M^2 \frac{2m_\mu^2 Q^2 - Q^4}{2} \right], \quad (2.2)$$

where $Q^2 = -t = -(p_\mu - p_{\mu'})^2$, $\tau = Q^2/(4m_p^2)$ and $s = (p_\mu + p_p)^2$. The squared centre-of-momentum energy s is given in the laboratory system by $s = 2E_\mu m_p + m_p^2 + m_\mu^2$ with E_μ being the energy and \vec{p}_μ the three-momentum of the incoming muon when colliding with a proton at rest.

The situation has not improved over the past years. In contrary, new results feed even more the confusion with hydrogen spectroscopy now also suggesting a lower radius [60],⁶

⁶In that work a strong correlation between the values of Rydberg constant and the proton radius in

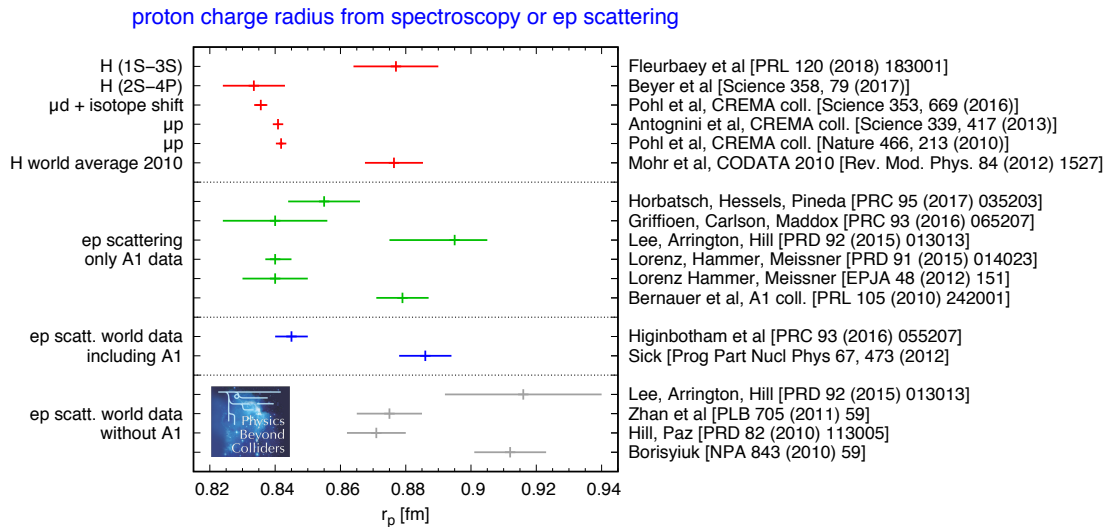


Figure 15. Overview of recent determinations of the proton charge radius r_p from spectroscopy of ordinary or muonic hydrogen (upper part) and from analyses of ep scattering data (lower three parts). The latter are grouped in analysis using only the MAMI A1 data (green), using all the world data (blue), and using the world data excluding the A1 data (grey). Some analyses use dispersion relations and thus additional data from the time-like region (Lorenz, Hammer, Meissner and Hill, Paz). The analysis of Horbatsch, Hessels, Pineda uses additional input from χ PT.

though also the larger value for the radius has been reproduced in spectroscopy [61]. The situation is illustrated in figure 15. Recently, preliminary results from hydrogen spectroscopy and from the Jefferson Lab PRad Collaboration support again a small radius (not included in the figure).⁷

One thus faces a complicated experimental situation both within spectroscopy and from elastic ep scattering experiments. In that respect, μp scattering at high energy at COMPASS++ is placed in a unique position and could be of particular interest. Using a muon beam it intrinsically has smaller QED corrections compared with ep and the contribution from the magnetic form factor $G_M(Q^2)$ to the cross section is suppressed due to the muon mass. As such extracting $G_E(Q^2)$ from the cross section is facilitated, and COMPASS++ has the potential to clarify theoretical and systematic uncertainties of the G_E extraction at low Q^2 . Still, the ultimate precision on r_p extracted from the slope of G_E at $Q^2 = 0$ remains to be quantified. The range in Q^2 , $0.001 \text{ GeV}^2 < Q^2 < 0.02 \text{ GeV}^2$, is indeed not larger than those for existing ep measurements, which actually yield very different radii depending on the choice of the fitting range and fitting functions, as was shown in figure 15. Technically, the low Q^2 to be accessed requires novel measurement methods. The plan is to use an active target by reconstructing the momentum transfer from the spectroscopy measurements was pointed out.

⁷A radius of $0.830 \pm 0.008_{\text{stat}} \pm 0.018_{\text{sys}}$ fm was reported by PRAD as their *Preliminary Result* at the recent 5th Joint Meeting of the APS Division of Nuclear Physics and the Physical Society of Japan.

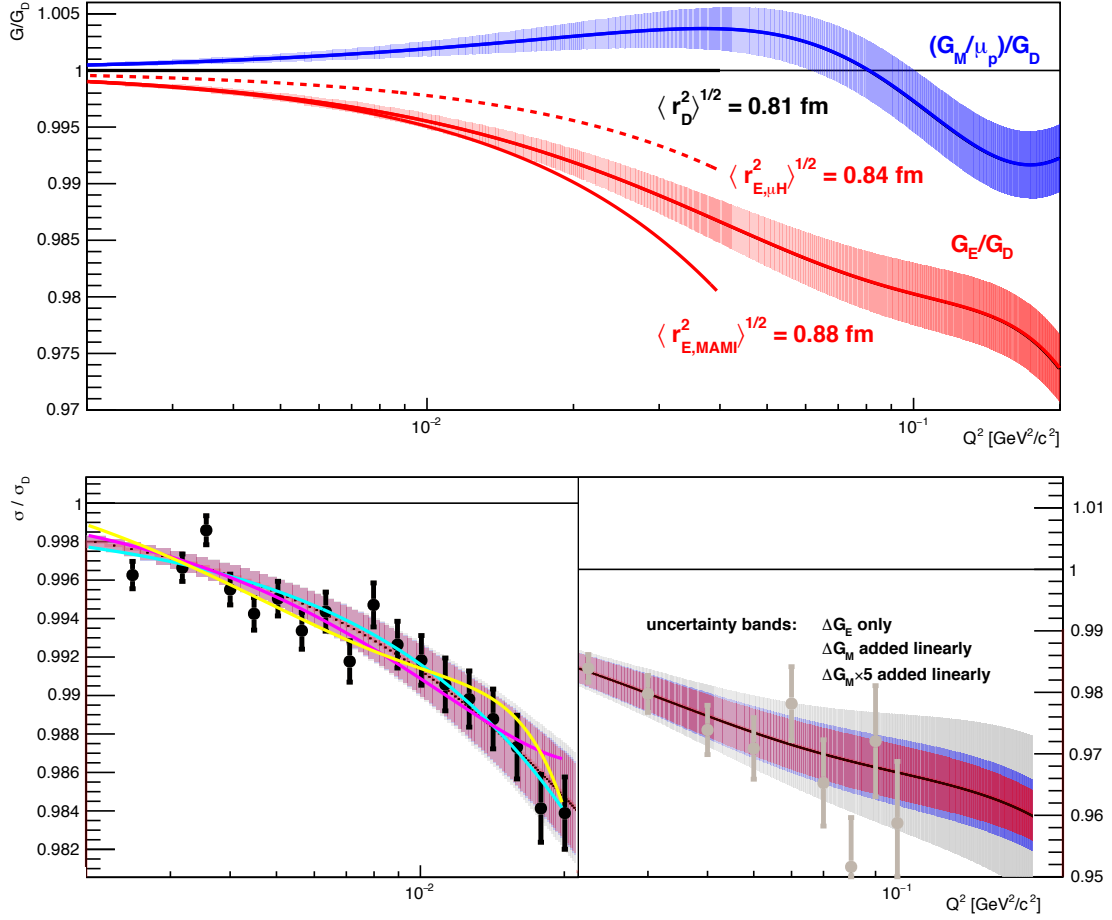


Figure 16. (Top) Proton form factors G_E and G_M (as labelled) from fits to MAMI data [64], shown as ratios to the dipole form factor G_D . Indicated as well are the curves for proton charge radii of 0.81, 0.84, and 0.88 fm. (Bottom) Ratio of the cross section (using the MAMI form-factor parameterisations) over the one using the dipole form factor. The innermost (red) uncertainty band corresponds to the effect of the uncertainty of G_E only, while for the (blue) middle band the uncertainty from G_M was added linearly, and for the outer (grey) band the contribution from ΔG_M was increased by a factor of five. Pseudo-data (points) were sampled according to the form factors from Ref. [64] and reflect the envisaged statistical precision of the COMPASS++ measurement. Only the low- Q^2 points in black were used in the various fits (polynomial in Q^2) to the pseudo-data shown as magenta (linear), purple (quadratic) and yellow (3rd order) curves. Pseudo-data points in grey require a different detector setup and are shown here for completeness. Only statistical uncertainties are shown as expected to dominate the systematic point-to-point uncertainty.

recoiling proton in a time-projection chamber (TPC) with pressurised pure hydrogen that also acts as the target. Such a target has been developed by PNPI [62, 63], and is in the testing phase for a similar experiment using electron scattering at Mainz.

Performance expectations: The design goal is to measure the electric form factor to such precision as to be sensitive to the proton charge radius at a level of 0.01 fm. Figure 16

(top) shows the electric and magnetic form factors from Ref. [64] scaled to the specific dipole form factor $G_D = [1 + r_D^2 Q^2/12]^{-2}$, one frequently used parameterisation of the form factor corresponding to an exponential charge distribution of the proton. The figure also shows in the bottom the elastic cross section (again normalised to the one for the dipole form), including the present uncertainty band resulting from the precision of the MAMI data, in comparison to the expected statistical precision of the COMPASS++ data (here from a Monte Carlo simulation that used the same form factor parameterisation as used for the curves).

The linear, purple, and yellow curves in figure 16 show polynomial fits to the pseudo-data, in particular fits that are linear, quadratic, and cubic in Q^2 , respectively. From these fits, the proton radius could indeed be extracted with high statistical precision: the quadratic fit in Q^2 is preferred by the data and gives $r_p = 0.877(13)$ fm, consistent with the value $r_p = 0.879$ fm used to generate the pseudo-data. However, it is clear from the spread of results in figure 15 from the same data set but using different fitting Ansätze that the ultimate goal for the precision on the radius extraction requires careful systematic studies using a similar selection on fitting approaches. Furthermore, the insensitivity of the proton radius fits to experimental systematics, e.g., from the luminosity normalisation (including all efficiency corrections) needs to be demonstrated.

Implementation considerations: As low values of momentum transfer have to be reconstructed, the proposal foresees usage of a variable high-pressure TPC with pure hydrogen that acts as a target and at the same allows reconstruction of Q^2 from the recoiling proton. Variation of gas pressure allows coverage of various regions in Q^2 . Such a setup is currently developed for a future measurement at MAMI. Usage of a TPC, however, puts stringent requirements on the maximum beam intensity. The currently tested upper limit of $2 \times 10^6 \text{ s}^{-1}$ is an order of magnitude below the full available muon-beam intensity. Further studies are needed on whether the wider beam profile of the M2 beam compared to the MAMI beam can be exploited in favour of larger beam intensities.

A further challenge concerns triggering, which currently also limits the manageable beam intensity. Triggering on the recoiling proton is not sufficient, but the present muon trigger is not suitable for muon trajectories with very small scattering angles imposed by the Q^2 range probed. The substantial background rate from very-small-angle muon scattering poses a challenge that requires additional tracking instrumentation (e.g., additional SciFi or silicon pixel detectors) and/or a trigger-less readout, the timeline of which is, however, not yet well defined.

Last but not least, the efficient use of the M2 muon beam might require coexistence of several PBC projects, e.g., MUonE (cf. Sect. 2.4) and NA64 μ (cf. Ref. [9]). Parallel installation of the proton-radius project and MUonE is discussed in more detail in Sect. 5.

Timelines: The earliest possible scenario for test runs is in 2021, with physics data taking in 2022, feasible if decision is taken sufficiently early.

Worldwide landscape: The discrepancies in the proton radius measurements spurred a whole range of activities, both on the spectroscopy as well as on the elastic-scattering

side. Here, only the latter is considered as relevant to the COMPASS++ proposal.

- The MUSE collaboration at PSI [65] will use low-energy μ^\pm and e^\pm scattering to reduce systematics but also to compare them directly for hints of lepton-flavor violation. Full commissioning is foreseen for this Fall (2018) and first data taking of 20 weeks between May and December 2019. Further data taking planned in 2020, and analysis as well as publication foreseen for 2021/22. The goal is to achieve sub-% relative precision over a Q^2 range of 0.002–0.07 GeV² to extract the proton radius to a precision of 0.007 fm.
- The PRad collaboration at Jefferson Lab [66] already took the presently lowest Q^2 data in ep elastic scattering and presented preliminary results this year. The analysis of the slope favours a generally lower (preliminary) value of the proton radius of $0.830 \pm 0.008_{\text{stat}} \pm 0.018_{\text{syst}}$ fm. The experiment exploits a simultaneous measurement of the well-known Møller scattering as reference to reduce systematics. Final results are expected to come out in 2019.
- At MAMI a similar approach as proposed here using a TPC as an active target will be employed in a future measurement,⁸ likely in 2020. Ongoing are runs with low beam-energy and via initial-state radiation [67]. Furthermore, MAGIX/MESA⁹ plans to run from 2021/22 on.
- Data at very-low Q^2 are expected to come from the ULQ² (“Ultra-Low Q²”) and ProRad (“Proton Radius”) experiments at Tohoku Low-Energy Electron Linac (Japan) and the PRAE facility in Orsay (France), respectively. ULQ², to start in 2019, aims at an absolute cross section measurement with 10^{-3} precision to obtain Rosenbluth separated $G_E(Q^2)$ and $G_M(Q^2)$ within $0.0003 \leq Q^2[\text{GeV}^2] \leq 0.008$, using a 10–60 MeV e^- beam.¹⁰ ProRad [68] will utilise a 30–70 MeV e^- beam and aims at a 0.1% precision on the elastic cross section.

2.3.2 Pion PDFs from Drell-Yan production

The pion is the lightest hadron and plays a fundamental role in QCD. Despite its importance little is known about its internal structure and the reason for its small mass. The simplest possible process for measuring pion PDFs, deep-inelastic lepton-pion scattering, is experimentally not feasible. As such other direct or indirect means are needed to constrain the pion PDFs, also to match the ongoing improvements in lattice calculations. Two approaches are highlighted here. In the so-called Sullivan process [69], one uses deep-inelastic lepton scattering off the pions radiated from a proton by tagging the recoil neutron. Its interpretation in terms of pion PDFs is however complicated by the fact that the pion is off shell and that one needs to know the pion flux in the proton. A direct approach avoiding these problems is pion-induced Drell–Yan, where typically a secondary pion beam is steered onto a solid fixed target to compensate for the limited beam intensity.

⁸https://www.blogs.uni-mainz.de/fb08-mami-experiments/files/2017/11/ep_-proposal.pdf

⁹<http://magix.kph.uni-mainz.de/physics.html>

¹⁰<https://www.jlab.org/indico/event/280/session/0/contribution/31/material/slides/0.pdf>

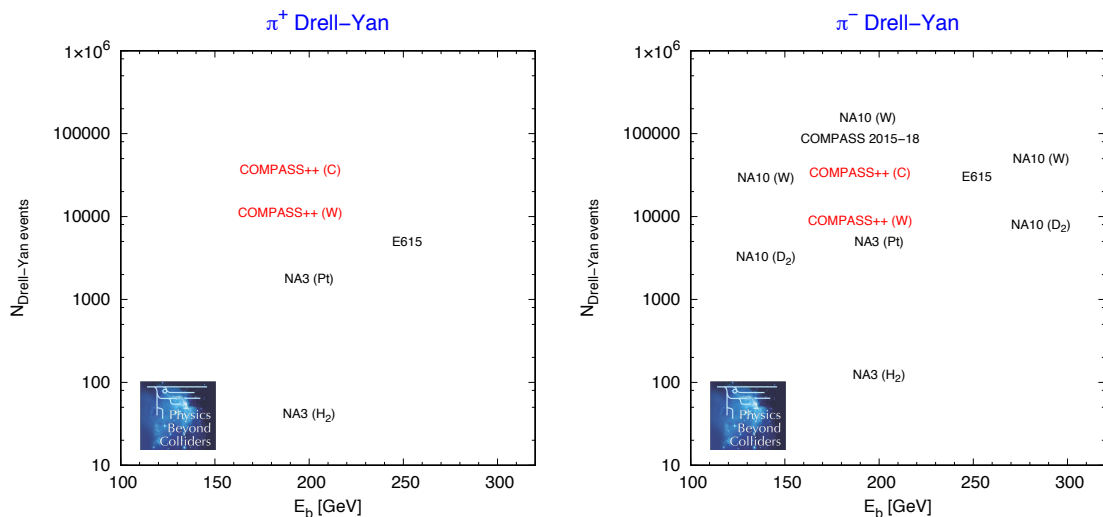


Figure 17. Overview of pion-induced Drell-Yan event yields for π^+ (left) and π^- (right) from past experiments and the proposed COMPASS++ running of 280 days at a beam energy of 190 GeV. In addition to the pion beam energies, the various target nuclei at the different experiments are indicated. (Numbers compiled from Table 3 in the LoI [11])

The theoretical framework of using Drell-Yan for PDF determinations is well established and used extensively for nucleon and nuclear PDFs. Nevertheless, data on pion-induced Drell-Yan are sparse, especially for π^+ beams, as can be seen in figure 17. That in turn affects the flavor separation of pion PDFs. Accordingly, phenomenological work is rather limited with important work dating back to the 1990s: SMRS [70], GRV [71], and GRS [72]. However, only the valence and gluon distributions (the latter mainly through prompt-photon production) were constrained in those works. A recent analysis [73], including also data from leading-neutron production in deep-inelastic scattering at HERA, results in much improved sea-quark and gluon distributions, the latter contributing about 1/3 of the pions momentum. Although claimed to be small, the model dependence inherent to employing the Sullivan process will make it desirable to have complementary data that can directly constrain the sea-quark contribution.

The differences in cross sections for π^+ and π^- induced Drell-Yan are highly sensitive to the pion's sea. More specifically, for an iso-scalar target, assuming charge conjugation, $SU(2)_f$ symmetry for valence quarks and $SU(3)_f$ symmetry for sea quarks, the leading-order sea-quark distribution can be uniquely constrained through the two linear combinations [74]

$$\Sigma_{\text{val}}^{\pi D} = -\sigma^{\pi^+ D} + \sigma^{\pi^- D}, \quad \Sigma_{\text{sea}}^{\pi D} = 4\sigma^{\pi^+ D} - \sigma^{\pi^- D}. \quad (2.3)$$

$\Sigma_{\text{sea}}^{\pi D}$ contains only contributions of sea-valence and sea-sea terms, i.e., no valence-valence contribution, of pion and proton quark distributions. In contrast, $\Sigma_{\text{val}}^{\pi D}$ receives only contributions from valence-valence combinations. The proton PDFs and the pion valence-quark PDFs are known well enough in order to extract the pion sea-quark PDF.

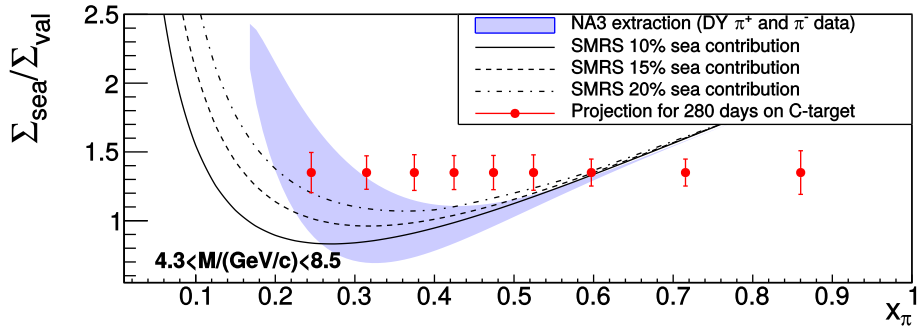


Figure 18. COMPASS++ projections for ratio of the cross-section combinations in (2.3), for 280 days of running on a carbon target at a beam energy of 190 GeV. The SMRS curves correspondent to three different sea-quark distributions from Ref. [70], while the shaded area represents a prediction based on the extraction of the pion valence and sea distributions by NA3 [75]. (Figure from [11])

Performance expectations and worldwide landscape: COMPASS++ proposes to use the M2 pion beams at 190 GeV on an iso-scalar carbon target. Two years (2×140 days) of data taking at high beam intensity would allow an improved extraction of the pion PDFs for $x_\pi > 0.1$. Figure 18 illustrates the impact of the COMPASS++ data on the $\Sigma_{\text{sea}}/\Sigma_{\text{val}}$ ratio.¹¹ Such measurement would be a unique possibility for separating valence and sea quarks in the pion for $x_\pi \gtrsim 0.1$, with strong complementarity to the pion-structure studies in ep scattering (off virtual pions via the Sullivan process) foreseen at JLab12 and at a future EIC.¹² There is presently no competition in this sector as no other facility provides high-intensity high-energy pion beams. It should be noted that parallel to the data on the Drell–Yan process a rather large data set on J/ψ production will be collected, which would allow detailed studies of charmonium production.

2.3.3 Kaon polarisability from the Primakov reaction

The electric and magnetic polarisabilities of a meson, α and β , characterise its response to a quasistatic electromagnetic field. For pions and kaons, they can be computed in chiral perturbation theory (χ PT), which makes them prominent observables for the quantitative investigation of QCD in the low-energy limit. The currently most precise measurement of the electric pion polarisability is $\alpha_\pi = (2.0 \pm 0.6_{\text{stat}} \pm 0.7_{\text{syst}}) \times 10^{-4} \text{ fm}^3$, which is in good agreement with the predictions of χ PT and dispersion relations. This result was obtained by COMPASS [76] in the so-called Primakov reaction $\pi^- Z \rightarrow \pi^- \gamma Z$ using a 190 GeV negative pion beam and a Ni target, making the assumption $\alpha_\pi + \beta_\pi = 0$. The latter is motivated by χ PT [77], where $\alpha_\pi + \beta_\pi = 0$ is nonzero only at two-loop level.

The prediction of one-loop χ PT for the charged kaon polarisability is $\alpha_K = -\beta_K = (0.64 \pm 0.10) \times 10^{-4} \text{ fm}^3$ [78]. Experimentally, only an upper limit $\alpha_K < 200 \times 10^{-4} \text{ fm}^3$ (CL=90%) was established from the analysis of X-ray spectra of kaonic atoms [79].

¹¹The SMRS curves are ad hoc assumptions for the sea distributions as data could not constrain them in that analysis.

¹²See, e.g., the presentation by T. Horn at <https://www.jlab.org/conferences/ugm/program.html>.

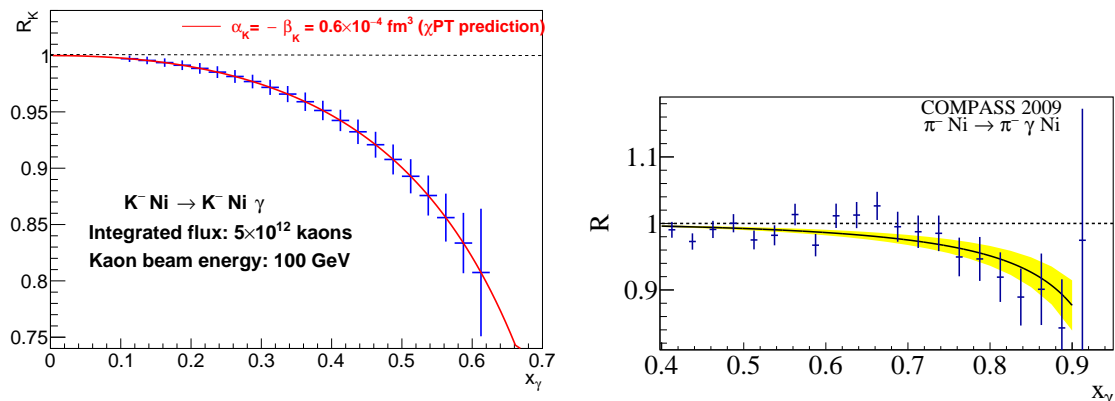


Figure 19. Left: projected data for the scaled Primakov cross section R_K with a 100 GeV kaon beam (figure 37 of [11]). x_γ is the energy of the produced photon normalised to the beam energy. The red curve shows the prediction from χ PT. Right: the corresponding measurement of R_π for the pion, published in [76].

A measurement of the kaon polarisability via the reaction $K^-Z \rightarrow K^- \gamma Z$ along the lines of the measurement of the pion polarisability performed by COMPASS, is challenging. The kaon component in a conventionally produced hadron beam is too small at high beam energies to collect the required amount of data on a reasonable timescale. Also, it is difficult to identify beam particles with high enough purity. To this end, a RF-separated hadron beam, in which kaons are enriched, would provide a unique opportunity to perform the first measurement of the kaon polarisability. Additional difficulties for the kaon polarisability measurement are the small kinematic gap between the threshold in the invariant mass $M_{K-\gamma}$ and the first resonance $K^*(892)$, when compared to the pion case with the $\rho(770)$ resonance, and the one order of magnitude smaller Primakov cross section compared to the case of the pion.

Performance expectations: For a kaon polarisability measurement with a 100 GeV RF-separated kaon beam with intensity $5 \times 10^6 \text{ s}^{-1}$, an estimate of the achievable precision has been given in the COMPASS++ LoI [11]. Projected data for the ratio R_K of the differential cross section for the physical kaon over the expected cross section for a hypothetical point-like kaon are shown in figure 19, along with the published results for a pion beam [76]. Assuming an integrated flux of 5×10^{12} kaons after one year of data taking, this estimate finds the achievable statistics to be about 6×10^5 $K^- \gamma$ events in the kinematic range $0.1 < x_\gamma < 0.6$ and $M_{K-\gamma} < 0.8 \text{ GeV}$, where, x_γ is the energy of the produced photon normalised to the beam energy. The relation between R_K and α_K under the hypothesis $\alpha_K + \beta_K = 0$ approximately reads

$$R_K - 1 = -\frac{3m_K^3}{2\alpha_{\text{em}}} \frac{x_\gamma^2}{1-x_\gamma} \alpha_K^3, \quad (2.4)$$

where α_{em} is the fine structure constant. Note that polarisation effects in case of the kaon are amplified by the factor $(m_K/m_\pi)^3 \approx 44$ when compared to the pion. The statistical

accuracy of the α_K extraction under the assumption $\alpha_K + \beta_K = 0$ is estimated to be $0.03 \times 10^{-4} \text{ fm}^3$ if the relation (2.4) is used. This corresponds to a 5% error w.r.t. the predicted value from one-loop χ PT. The experimental systematic uncertainty is expected to be smaller than the statistical one [11]. An additional theory uncertainty will come from corrections to (2.4) from higher-order contributions in the chiral expansion, which remain to be calculated.

Challenges and timelines: No specific additions to the experiments are foreseen. Potential difficulties might be the above-mentioned small kinematic gap between the threshold in the invariant mass $M_{K-\gamma}$ and the first resonance $K^*(892)$ and the smaller Primakov cross section compared to the case of the pion. The main experimental challenge for this measurement lies in the availability of RF-separated beams, which puts the time window for the required 1-year data-taking period at earliest after LS3.

Worldwide landscape: This would be a unique benchmark measurement for low-energy QCD in the three-flavour sector, and we are not aware of any other existing or planned facility that would be able to perform it.

2.3.4 Strange meson spectroscopy with kaon beams

Baryon and meson spectroscopy has been a vital tool for the understanding of the QCD bound states. However, while the spectrum of non-strange mesons has seen tremendous progress, also thanks to the activities of the COMPASS collaboration, the spectrum of mesons carrying strangeness with masses beyond 1 GeV is known with much less precision, not to say *terra incognita* when going beyond the ground states. This is illustrated in figure 20, which shows the known strange mesons in comparison to the prediction of states from a relativistic quark-model [80]. A more precise knowledge of the kaon spectrum would have a broad impact, as excited kaons appear in many processes in modern hadron and particle physics, e.g., in the study of CP violation in heavy-meson decays, which are studied at LHCb and Belle II.

COMPASS has already developed a powerful partial-wave analysis framework during its previous spectroscopy program with non-strange mesons [15]. The M2 hadron beam, in fact, has a kaon component. However, it is too weak to efficiently exploit it for a detailed spectroscopy program for strange mesons. An alternative could be the use of high-intensity RF-separated hadron beams of at least 50 GeV beam energy, whose feasibility is studied in a parallel PBC activity [12].

Performance expectations: The goal of a kaon spectroscopy program with RF-separated beams would be to map out the complete spectrum of excited kaons with unprecedented precision [11].

Challenges and timelines: The main experimental challenges—beyond the already mentioned ambitious requirement of RF-separated beams—are high-precision vertex reconstruction, photon detection with electromagnetic calorimeters to reconstruct neutral hadrons, and final-state particle identification (for instance, kaons have to be distinguished

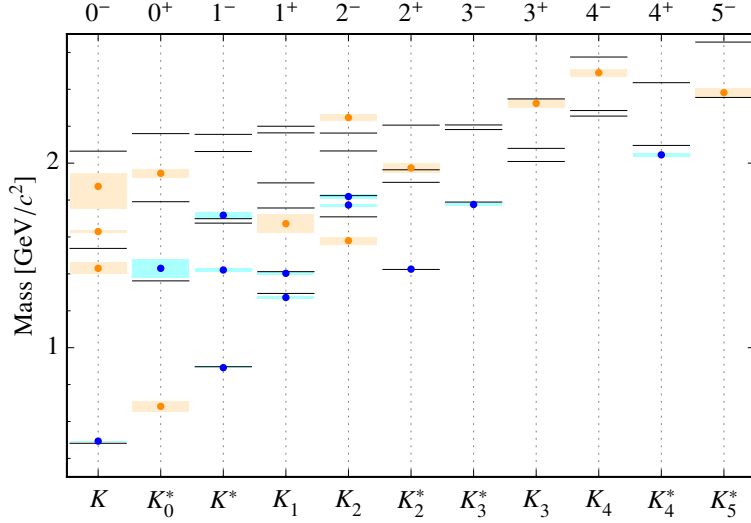


Figure 20. Excitation spectrum of strange mesons grouped by their J^P quantum numbers. Known states from the PDG (points and shaded boxes representing the central value and uncertainty of the measurements, respectively) are compared to the relativistic quark-model prediction of Ref. [80] (black lines). States included also in the PDG summary table are shown in blue. (Figure from [11])

from pions with high efficiency in the kinematic range of 1 GeV up to the beam momentum). As for the Primakov measurement (section 2.3.3), these requirements situate this 1-year measurement earliest after LS3.

Worldwide landscape: There are proposals and plans for future measurements of strange mesons at other facilities.

- The investigation of τ decays, in which strange mesons can appear in subsystems, will be pursued at Belle2, BES III and LHCb to study strange mesons. The largest possible mass of the strange subsystem is limited by the rather low τ mass of 1.8 GeV, so that many of the observed or predicted kaon states are out of reach.
- GlueX will study strange mesons in photo-production at JLab12. Achievable photon energies are limited by the maximum energy of 12 GeV of the electron beam delivered to Hall D. Measurements using a secondary K_L beam are considered as well [81].
- At J-PARC, a new beam line with a separated kaon beam is under discussion, which aims for a K^- intensity of 10^7 per spill at much lower beam momentum of 2–10 GeV. At such low momenta, the separation between beam and target excitations would become difficult and might lead to larger systematic uncertainties.

In comparison, the COMPASS++ measurement would profit from a high-intensity high-energy kaon beam that allows for excellent precision and clear separation of the strange-meson from the recoiling system. It is as such unique and complementary to other world-wide activities.

2.3.5 Selected other COMPASS++ measurements and summary

The realisation of RF-separated beams opens up the possibility of a wide program of Drell–Yan measurements. Similarly to the pion PDFs (sect. 2.3.2), kaon PDFs can be studied in unpolarized Drell–Yan. Prompt-photon production will further help constraining the gluon distribution of the kaon. As discussed already for LHC-F'T (sect. 2.1) a transversely polarised target permits a series of measurements related to transverse-momentum distributions like the Sivers function. Especially attractive in that respect would be a high-intensity \bar{p} beam. The kinematics (see, e.g., figure 30 in LoI [11]) would be such that the region $x \gtrsim 0.1$ in both beam and target would be probed, e.g., valence quarks in the polarised proton would annihilate with (valence) anti-quarks in the anti-proton.

Nevertheless, the overall rate is rather low. Table 5 in LoI [11] quotes about 5 to 8×10^4 DY events with $M > 4\text{ GeV}$ for 140 days of beam time, thus remaining unclear whether it would be competitive with pp proposals at larger \sqrt{s} , which profit from the abundance of anti-quarks at low x in the unpolarized proton. In the area of low-energy observables, a parasitic running of one year along the kaon Primakov measurement would allow a direct measurement of the neutral pion lifetime. COMPASS++ measurements of \bar{p} cross sections for air showers, possible with the existing M2 proton beam, are discussed in Sec. 4.

Altogether, the COMPASS++ proposal comprises a diverse physics program centred around its main pillar of hadron structure. The skeleton of the *Future QCD Facility* is an upgraded COMPASS spectrometer with a number of new elements for different physics programs (see Table 2). The whole program would require up to 11 or 12 years of running time, but in view of competing experiments the overall beam time request might be reduced after further prioritisation of measurements. The earliest starting year of the program is 2022 as a one year long approved extension of the COMPASS-II program is scheduled to run in 2021.

For the moment it is quite difficult to give a solid cost estimates for new detectors and for upgrade and renewal of the COMPASS spectrometer, a total budget in the range of 10 to 20 M CHF seems to be reasonable. According to the previous experience of the COMPASS Collaboration, in order to carry out the COMPASS++ program, a new collaboration of approximately 250 physicists has to be established.

The main challenge for the long-term program is a newly designed and constructed RF-separated hadron beam, which would become a very versatile and world-wide unique beam line for the foreseeable future. For that, studies of feasibility and estimated beam parameters have started in the PBC Conventional Beam WG [12].

2.4 MUonE

Physics motivation. The long-standing 3 to 4σ discrepancy between the experimental value and theoretical prediction for $(g - 2)_\mu$ is among the most prominent problems of the Standard Model. Future measurements at FNAL and J-PARC aim at improving the accuracy of the E821 experiment at BNL by a factor of 4. At the same time, it is essential to consolidate the theoretical prediction and, if possible, further decrease its uncertainty. Reviews of the current state of these efforts can for instance be found in [82, 83]. By far

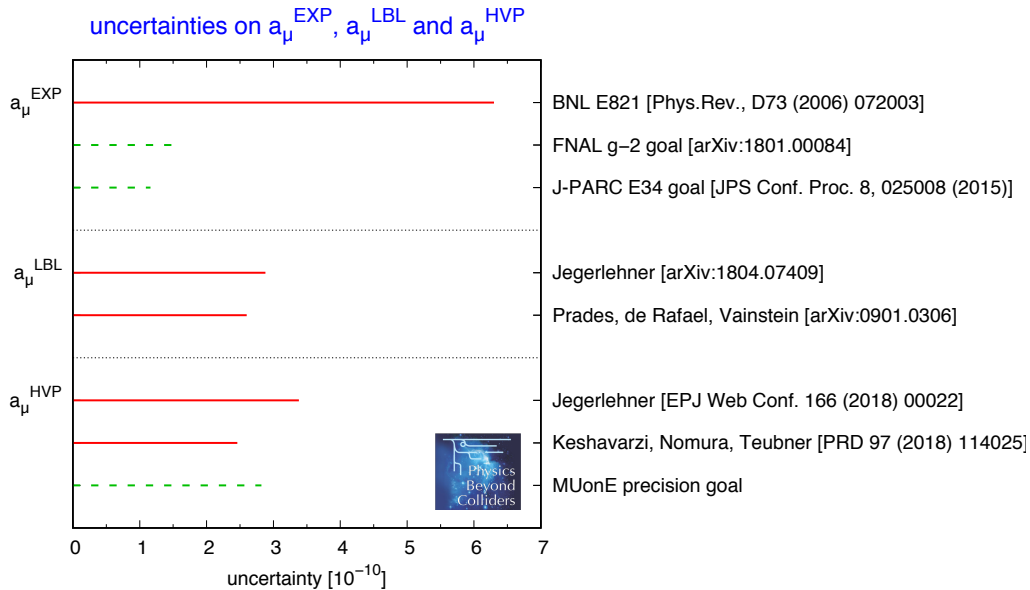


Figure 21. Top part: current experimental precision on a_μ and the accuracy goals of the planned experiments at FNAL and J-PARC. Central part: accuracy of two current determinations of the contribution to a_μ from light-by-light scattering (LBL). Bottom part: accuracy of two current determinations of the contribution of hadronic vacuum polarisation (HVP) to a_μ , as well as the ultimate precision aimed at by MUonE. The latter is given as a 0.3% statistical error and a systematic error of the same size, added in quadrature. Numbers have in part been taken from the review [82].

the most important uncertainties on $a_\mu = (g-2)_\mu/2$ are due to the leading order hadronic vacuum polarisation (termed HVP in the sequel) and to the hadronic contribution to light-by-light scattering. Figure 21 gives an overview of the situation.

The currently most precise way of calculating the leading hadronic contribution is to use a time-like dispersion relation, which relies on the knowledge of the e^+e^- annihilation cross section into hadrons from the π^0 mass threshold upwards. The low energy range is affected by large non perturbative effects, and experimental data from e^+e^- machines are needed. At present, large amounts of data have been collected at different machines for many exclusive and inclusive channels, through direct energy scan or radiative return methods. The overall data set allows a determination of leading hadronic contribution with an uncertainty of the order of 0.4–0.5%. In the near future new precise data will be available, notably from BES III and Belle 2, as well as CMD2 and SND at Novosibirsk. However, the estimate of the systematic uncertainties, of both experimental and theoretical origin, related to each channel and to the global combination (e.g. the correlation among different channels) is very delicate. In this situation, corroboration from independent methods, like the space-like approach [84] with muon-electron scattering data of the MUonE project [85] would be extremely valuable. Concerning the evaluation of a_μ^{HVP} in lattice QCD, in the last few years there has been a lot of progress on the leading hadronic contribution to $(g-2)_\mu$ (as well as the hadronic light-by-light one). In February 2018, a dedicated workshop was held

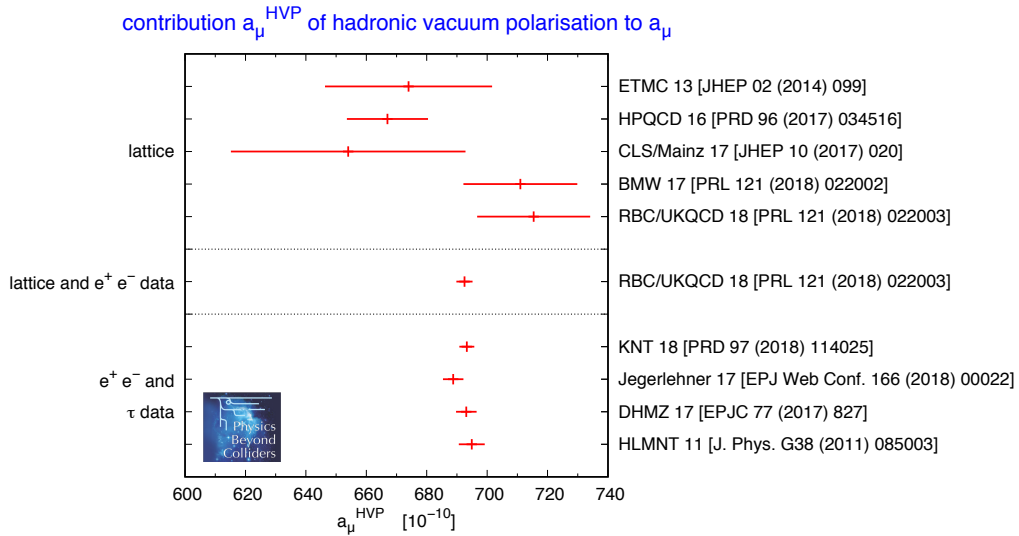


Figure 22. Selected current determinations of the contribution a_μ^{HVP} to the anomalous magnetic moment of the muon. Detailed information can e.g. be found in the reviews [82, 83].

at KEK, Japan, where the recent developments of these determinations were presented.¹³ Although their progress is very interesting and promising, the lattice calculations of the leading hadronic contribution to a_μ are not yet competitive with the dispersive ones. This is clearly visible in figure 22, where the only lattice determination with competitive errors [RBC/UKQCD18] is using a hybrid method with e^+e^- data as input.

The review in Ref. [82] concluded that “Therefore, the very different Euclidean approaches, lattice QCD and the proposed alternative direct measurements of the hadronic shift $\Delta\alpha(-Q^2)$ [85], in the long term will be indispensable as complementary cross-checks.”

Hadronic vacuum polarisation from elastic μe scattering. The MUonE experiment aims to measure the leading order hadronic contribution to $(g-2)_\mu$ with a statistical precision of 0.3%. The goal in accuracy and the novel technique will make this measurement an important ingredient to reinforce the SM prediction on $(g-2)_\mu$ and eventually to clarify any possible hint of new physics when compared with the expected measurements at FNAL and J-PARC.

The method is based on a sum rule, which relates the leading order hadronic contribution to a_μ to the running fine structure constant $\alpha(t)$ as [85]

$$a_\mu^{\text{HVP}} = \frac{\alpha(0)}{\pi} \int_0^1 dx (1-x) \Delta\alpha_{\text{had}}(t(x)), \quad (2.5)$$

where $\Delta\alpha(t) = 1 - \alpha(0)/\alpha(t)$ and $\Delta\alpha_{\text{had}}(t)$ is its hadronic component, which is obtained by subtracting the purely leptonic part. The scaling variable x is related to the timelike

¹³All presentations can be found at <https://kds.kek.jp/indico/event/26780>.

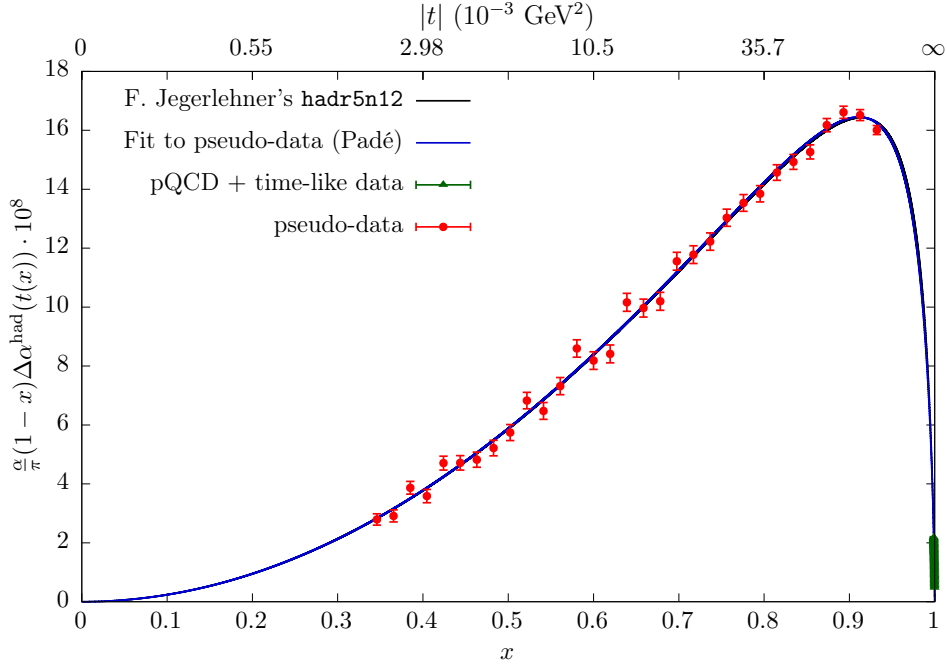


Figure 23. Integrand of the sum rule (2.5), together with pseudodata and a fit described in the text below.

momentum transfer by

$$t(x) = -\frac{x^2 m_\mu^2}{1-x}. \quad (2.6)$$

The integrand of the sum rule (2.5) is shown in figure 23. The peak of the spectrum is at $x \approx 0.914$, which corresponds to $t \approx -0.108 \text{ GeV}^2$.

In order to have a systematic error compatible with the statistical one, a systematic uncertainty at 10^{-5} level is required on the knowledge of the μe cross section. Although this is not a request on the knowledge of the absolute cross section (i.e. the running of α will be obtained by the ratio between a signal and a normalisation region both of them obtained by μe data itself) it poses severe requests on the knowledge of the following quantities:

Multiple scattering: Multiple scattering (MS) effects in the target affect the reconstructed angle and if not properly taken into account result in a systematic error. Preliminary studies indicate that an accuracy of the order of 1% is required on the knowledge of the MS effects. Such accuracy will require dedicated test beams where the results of data will be compared with the prediction from (GEANT) simulation. Preliminary results from a test beam in 2017 are encouraging.¹⁴ A corresponding publication is being prepared. It is important to stress that the MS effects (especially the tails) will be monitored during the run by looking at specific observables like acoplanarity.

¹⁴See the presentation <https://indico.cern.ch/event/686555/contributions/2971020>.

Tracking uniformity, alignment and reconstruction of angles: It is important to keep the systematic error arising from non-uniformity of the tracking efficiency and angle reconstruction at the 10^{-5} level. The use of state-of-the-art silicon detectors is sufficient to ensure the required uniformity. The relative alignment of the silicon detectors will be monitored with the high statistics provided by the muon beam; absolute calibration on the transverse plane can be achieved taking advantage of the constrained kinematic of two-body elastic scattering. The longitudinal position of the silicon detector must be monitored in real time at the 10 microns level; this precision can be achieved with commercial laser systems based on interferometry.

PID: A μ - e separation at 10^{-5} is required in the 2-3 mrad region where there is an ambiguity between the outgoing electron and muon. Given the high momentum of the emitted particle in this range (70 GeV) a high granularity electromagnetic calorimeter followed by a muon detector should be sufficient to reach this accuracy.

Knowledge of the Beam: A high intensity muon beam of the energy of 150 GeV as used by COMPASS at M2 with a few percent momentum spread would be suited for the measurement. There are discussions with the beams experts about the possibility to have the shape of the M2 beam adapted to the MUonE apparatus, i.e. a width of several centimetres and parallel. A 0.8% percent accuracy of the beam momentum, as obtained by the spectrometer used by COMPASS, would be useful to over-constrain the $\mu - e$ kinematics and control the systematic effects arising from beam spread, reconstruction and MS.

Background: Background events will be rejected by cutting on the numbers of the hit recorded in the tracker, and on the elasticity band. A rejection of more than 10^5 has been obtained by Monte Carlo simulation.

Theory: A complete fixed order calculation of QED NNLO radiative corrections, consistently matched with resummation of higher-orders and implemented into a Monte Carlo event generator, will be required to control the theoretical systematics at the 10^{-5} level and, in turn, to extract the leading order hadronic contribution to $(g-2)_\mu$ with the aimed accuracy. A core of theoretical Italian groups in Padova, Parma and Pavia, together with international collaborators, have started to work on the MUonE project.¹⁵ Results of this activity are presented in [86–89].

The systematic error on the normalisation as well as uncertainty on the model dependence of the multiple scattering, on the beam spectrum and on the alignment of the detector will be correlated in x . Other systematic errors like PID and background subtraction are expected to affect only some specific x values.

The integral in the region $0.93 < x < 1$, accounting for 13% of the total a_{mu}^{HVP} integral, cannot be reached by the proposed MUonE experiment. However, it can be determined us-

¹⁵See the workshops <https://agenda.infn.it/internalPage.py?pageId=0&confId=13774> at Padova and <https://indico.mitp.uni-mainz.de/event/128> at Mainz.

ing timelike data and perturbative QCD, and/or lattice QCD results, with a tiny estimated uncertainty of about one per mil.

In an exercise to validate the method at the level of statistical errors and fitting, pseudodata was generated and subsequently fitted, as shown in figure 23. The fit result is $a_\mu^{\text{HVP}} = (686.9 \pm 2.3) \times 10^{-10}$, compared with an input value $a_\mu^{\text{HVP}} = 688.54 \times 10^{-10}$ used to generate the pseudo-data. The error reflects only the statistical uncertainty on the pseudodata and corresponds to 0.33%, consistent with the ultimate accuracy goal of the experiment. The additionally used information from timelike data and perturbative QCD is represented by the points close to $x = 1$ in the figure.

Collaboration, estimated timeline and cost Several groups from Italy (Bologna, Ferrara, Milano Bicocca, Padova, Pavia, Pisa, Trieste), Poland (Kracow), Russia (Novosibirsk), UK (Liverpool and London) and USA (Virginia University) have started to work on MUonE. Many of them are experts in the field of precision physics. Years 2018-2019 will be devoted to detector optimisation studies, simulation, Test Run and theory improvement with a final goal to present a Letter of Intent to the SPSC. The detector construction is expected during LS2 and the plan is to install the detector (or a staged version of it) and start data taking in the period 2021-2024. A very preliminary estimate of the cost gives less than 10 M CHF.

According to current estimates (which will be refined in the course of further studies), a running time of around 3 years will be required to achieve the 0.3% statistical accuracy goal quoted above. A staged approach is being envisaged.

2.5 NA60++

Physics motivation. Experiments at high-energy heavy-ion colliders (RHIC, LHC) investigate the properties of a Quark-Gluon Plasma state at high energy density and initial temperature, but at low baryochemical potential μ_B (typically a few MeV). In this region of the QCD phase diagram the transition between quark-gluon plasma (QGP) and hadronic matter is a rapid cross-over with no latent heat. It occurs at a pseudo-critical temperature $T_c \sim 155$ MeV. High-energy collider experiments cannot access the large- μ_B region of the phase diagram, whose study requires lower collision energies. In this area, QCD-inspired model computations suggest that a first-order phase transition may occur. This implies a second order critical end point (CP) of the cross-over line. Experimentally, information on this region is relatively poor, and its study is of chief interest for our understanding of ultra-relativistic heavy-ion physics. The global landscape of heavy-ion experiments is mapped out in section 3, see i.e. the figures 32, 33 there. In section 3 the uniqueness of NA60++ as compared to the other experiments is also discussed.

The NA60++ project aims at measuring the properties of the QGP and the nature of the phase transition by performing an energy scan in the range accessible to the CERN SPS (beam energies in the range 20-160 GeV/nucleon, corresponding to $\sqrt{s_{\text{NN}}} \sim 6 - 17$ GeV). Such an experiment could address several fundamental and still open physics questions, and in particular

- (i) can a signal of the first-order phase transition to QGP be detected?

- (ii) can we observe a signal corresponding to the restoration of chiral symmetry?
- (iii) can we study the transport properties of the high- μ_B QGP?

An experiment based on a muon tracking system and a sophisticated vertex spectrometer gives access to these questions. With such a set-up, the dimuon invariant mass spectrum can be studied from threshold up to the J/ψ mass region and beyond, discriminating between prompt and non-prompt sources. The vertex spectrometer can also be used to detect hadronic decays of particles containing strange and heavy quarks. Its layout is conceptually similar to that of the past NA60 experiment, which took data in 2003-2004 with indium and proton beams on various nuclear targets at top SPS energy and performed accurate measurements of muon pair production.

This brings us to the observables whose measurement can answer the physics questions posed above. The nature of the phase transition can be investigated by studying the evolution of the temperature of the system, for various collision energies, as a function of its energy density. The temperature can be precisely extracted by a measurement of the mass spectrum of the thermal muon pairs in the mass region 1.5-2.5 GeV, while the energy density is estimated via charged multiplicity measurements in the vertex spectrometer. In this way a “caloric curve” for the phase transition can be determined and the flattening related to a first order phase transition experimentally detected, see left plot in figure 24. The feasibility of the temperature measurement via thermal dimuons was clearly demonstrated by NA60, which obtained at top SPS energy average temperatures of the order of 200 MeV for the created strongly interacting system.

The approach to the restoration of chiral symmetry, expected in the proximity of the phase transition to the QGP, should modify in a detectable way the spectral function of the vector/isovector mesons (ρ - a_1). A strong broadening of the ρ was already observed by NA60, and it is considered a manifestation of chiral restoration. Additionally, while the a_1 cannot be directly observed in the dilepton spectrum, chiral mixing of the vector and axial vector spectral functions is expected to increase the dilepton yield by $\sim 30\%$ in the mass region 1-1.5 GeV, see right plot in figure 24. This is a direct manifestation of chiral restoration and NA60++ aims at measuring the related yield excess for the first time. Such a study is particularly intriguing at low beam energies where the contribution of the QGP phase, which would constitute a background to this measurement, becomes less important.

When decreasing the incident beam energy, the initial energy density of the created strongly interacting system also decreases, while the net baryon content increases, leading to a high- μ_B QGP if the critical temperature is attained. At high energy, it has been shown that such a system can selectively melt the quarkonium states according to their binding energy, via a colour screening mechanism in the QGP. At low energies, one should therefore observe the suppression effect to become weaker and then disappear when the initial temperature of the system does not exceed the critical temperature. By measuring the J/ψ or $\psi(2S)$ decay to $\mu^+\mu^-$, and possibly the $\chi_c \rightarrow J/\psi \gamma$ process, one could therefore track the onset of the deconfinement transition. See figure 25 for the evaluation of the J/ψ nuclear modification factor.

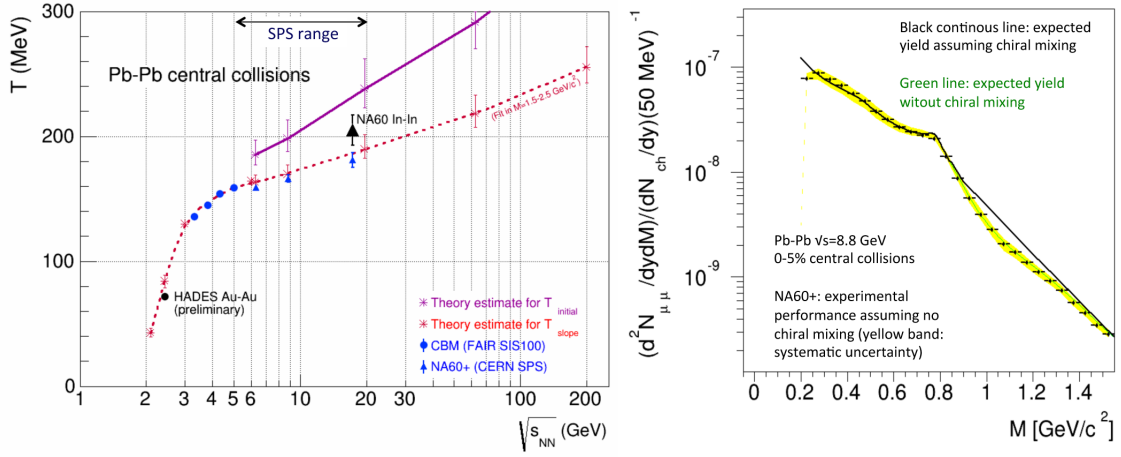


Figure 24. Left: medium temperature evolution vs. $\sqrt{s_{NN}}$ in central Pb-Pb collisions. T_{initial} (magenta points) and T_{slope} (red points) are theoretical estimates for the initial medium temperature and the temperature from dilepton spectra respectively [90], and a coarse graining approach in URQMD [91, 92]. Blue triangles and squares are the expected performance from NA60++ and CBM. The only existing measurements at present are from NA60 In-In data [93, 94] and from HADES preliminary Au-Au data [95]. Right: NA60++ projection for the acceptance corrected thermal dimuon mass spectrum at $\sqrt{s_{NN}} = 8.8$ GeV in case of no chiral mixing (the yellow band is the systematic uncertainty from combinatorial background subtraction) compared to the theoretical expectation (green dashed line). The black line above 1 GeV is the expectation from full chiral mixing [90]. The experimental precision makes the experiment fully sensitive to the yield increase of $\sim 30\%$ expected in $1 \text{ GeV} < M < 1.4 \text{ GeV}$ in case of chiral mixing.

In addition to charmonium measurements, also the detection of open charm mesons and baryons represents an important observable in the low SPS energy range. Their hadronic decay products can be measured in the vertex spectrometer, see figure 26 for the expected performance of the D^0 measurement. An indirect measurement via muon pairs from simultaneous semileptonic decays of meson or baryon pairs is also feasible, see figure 26. Indeed the charm diffusion coefficient is predicted to be larger in the hadronic phase at temperatures approaching the critical temperature T_c from below than in the QGP phase at temperatures larger than T_c , and the system is expected to spend a relatively longer time in the hadronic phase when the collision energy becomes lower. For what concerns hadronisation mechanisms, recombination effects could lead to a large enhancement of the Λ_c/D ratio. The enhancement could be larger at low SPS energy than at RHIC and LHC energies, because of the larger baryon content of the system.

Detector. This rich physics program can be addressed by an experiment which includes a high-resolution vertex spectrometer, consisting of 5 silicon pixel tracking planes immersed in a 1.2 Tm dipole field. The tracker will be based on a new generation of CMOS Monolithic Active Pixel Sensors (MAPS), developed in close synergy with the ALICE experiment, immersed in a dipole magnetic field. The goal is to obtain very large area sensors up to $\sim 14 \times 14 \text{ cm}^2$, retaining a thickness of $50 \mu\text{m}$ or less. The vertex spectrometer will be followed

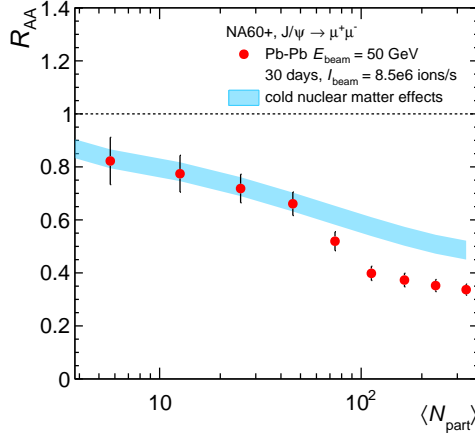


Figure 25. NA60++ projected performance for the nuclear modification factor of J/ψ production in Pb–Pb collisions at $E_{lab} = 50$ GeV as a function of the number of participants N_{part} , compared with expectations from an estimate for cold nuclear matter effects similar as at full SPS energy, shown as a blue band. An extra anomalous suppression of J/ψ in the quark gluon plasma on the level of 20% is assumed to settle in for $N_{part} > 50$.

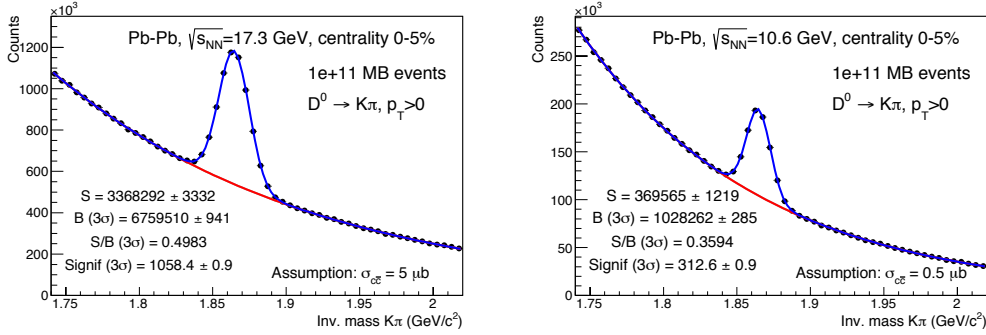


Figure 26. NA60++ projection for the D^0 invariant-mass distribution from $5 \cdot 10^9$ central Pb–Pb events at beam energies of $\sqrt{s_{NN}} = 17.3$ GeV (left) and 10.6 GeV (right) with a vertex detector based on MAPS. The yield per event is estimated assuming $\sigma_{c\bar{c}} = 5 \mu b$ at $\sqrt{s_{NN}} = 17.3$ GeV (based on [96, 97] and POWHEG) and $\sigma_{c\bar{c}} = 0.5 \mu b$ at $\sqrt{s_{NN}} = 10.6$ GeV.

by a thick absorber (mainly graphite) that will filter out hadrons and finally by a muon spectrometer, with a toroidal magnet and several large planes of tracking and triggering detectors. In particular, for the 4 tracking planes, the use of GEM detectors providing spatial resolution $< 100 \mu m$, time resolution < 10 ns and sustaining high particle rates (the current requirement is ~ 10 kHz/cm²) is currently foreseen, with a total surface of the order of 100 m². Finally, for the muon triggering detectors, which will be placed behind a further hadron absorber, the default choice is the use of RPCs, which have been shown to provide good resistance to ageing and can easily sustain the expected maximum rate of ~ 100 Hz/cm².

Uniqueness. This rich physics programme can only be pursued at the CERN SPS. Although other facilities for the study of ultra-relativistic heavy-ion collisions in the high- μ_B domain are being built (FAIR, NICA) they are either lacking the necessary interaction rate (NICA) or reach too low energy (SIS100 @FAIR) to address all the physics topics detailed above. Similarly, the beam energy scan program at RHIC (BES-II) covers the same energy range as the CERN SPS, but with interaction rates lower by orders of magnitude.

Location. In order to access all the observables detailed above, a Pb ion beam intensity $\sim 10^7\text{s}^{-1}$ impinging on a ~ 4 mm Pb target is required, leading to interaction rates of the order of 1 MHz. This choice is dictated in particular by the need of a high precision for the temperature measurement and by the relatively low charmonium production cross section at SPS energy. Such an intensity can be provided by using the existing ECN3 underground hall in the CERN North Area.

Collaboration, estimated timeline and cost. At present a proto-collaboration is established with about 60 physicists from the following institutions:

University of Lyon, CNRS/IN2P3, France, University of Frankfurt, Germany, University of Heidelberg, Germany, Technical University Munich, Germany, Saha Institute of Nuclear Physics, India, INFN Cagliari, Italy, University of Cagliari, Italy, INFN Padova, Italy, University of Padova, Italy, INFN Torino, Italy, Politecnico di Torino, Italy, University of Torino, Italy, University of Piemonte Orientale, Italy, Tohoku University, Japan, CERN, Switzerland, Rice University, USA, Stony Brook University, USA.

The estimated cost is in the 15-25 MCHF range. As indicated in figure 1 for the timeline, the experiment might take data during LHC run 4 and run 5.”

2.6 NA61++

Physics motivation. The continuation of the NA61/SHINE programme concerns measurements of hadron and nuclear fragment production properties in reactions induced by hadron and ion beams after the Long Shutdown 2. The measurements are requested by heavy ion, cosmic ray and neutrino communities and they will include:

- (i) measurements of charm hadron production in Pb+Pb collisions for heavy ion physics,
- (ii) measurements of nuclear fragmentation cross section for cosmic ray physics,
- (iii) measurements of hadron production induced by proton and kaon beams for neutrino physics. NA61/SHINE is the only experiment which will conduct such measurements in the near future.

The objective of **charm hadron production measurements** in Pb+Pb collisions is to obtain the first data on mean number of $c\bar{c}$ pairs produced in the full phase space in heavy ion collisions. Moreover, first results on the collision energy and system size dependence will be provided. This, in particular, should significantly help to answer the questions:

- (i) What is the mechanism of open charm production?

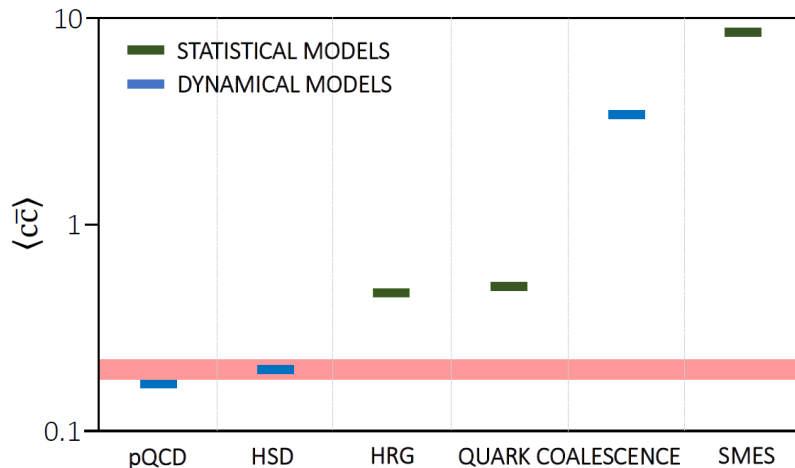


Figure 27. Mean multiplicity of charm quark pairs produced in central Pb+Pb collisions at $158A$ GeV/ c calculated within dynamical models (blue bars): pQCD-inspired [98, 99], HSD [100], and Dynamical Quark Coalescence [101], as well as statistical models (green bars): HRG [48], Statistical Quark Coalescence [102], and SMES [103]. The width of the red band, at the location assuming HSD predictions, shows the foreseen accuracy of the NA61++ result. (Figure taken from [13].)

The mechanism for open charm production is either of dynamical or of predominantly statistical nature. NA61++ offers the unique possibility to single out the production mechanism, see figure 27.

- (ii) How does the onset of deconfinement impact open charm production?

The charm production in deconfined matter (dominantly $\bar{c}c$ pairs) is expected to be more abundant than in the confined phase (dominantly $D\bar{D}$ -pairs) due to the higher production energy (about 1 GeV) of the latter. A model computation for the energy dependence is shown in figure 28.

- (iii) How does the formation of quark-gluon plasma impact J/ψ production?

J/ψ -suppression has been used as an important indication for the formation of the quark-gluon plasma. So far it has been accessed by an assumed proportionality of the mean multiplicity of $\bar{c}c$ -pairs to that of Drell-Yan pairs, $\langle c\bar{c} \rangle \sim \langle DY \rangle$. This assumption is challenged by the fact that the ratio $\sigma_{J/\psi}/\sigma_{\pi}$ is independent of centrality and close to the prediction of the hadron-resonance gas, see figure 29.

The objective of **nuclear fragmentation cross section measurements** is to provide high-precision data needed for the interpretation of results from current-generation cosmic ray experiments. The proposed measurements are of paramount importance to extract the characteristics of the diffuse propagation of cosmic rays in the Galaxy. A better understanding of the cosmic-ray propagation is needed to

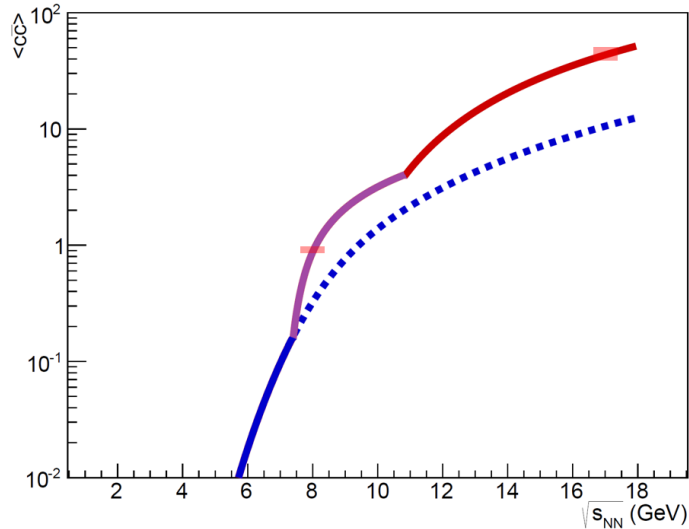


Figure 28. Energy dependence of $\langle c\bar{c} \rangle$ in central Pb+Pb collisions calculated within the SMES model. The red bars show the foreseen accuracy of the NA61/SHINE results for two energies: 40A GeV ($\sqrt{s_{NN}} = 8.6$ GeV) and 150A GeV ($\sqrt{s_{NN}} = 16.7$ GeV), assuming the SMES model yields [103]. (Figure taken from [13].)

- (i) study the origin of Galactic cosmic rays and
- (ii) evaluate the cosmic-ray background for signatures of astrophysical dark matter.

The objectives of **new hadron production measurements for neutrino physics** are

- (i) to improve further the precision of hadron production measurements for the currently used T2K replica target, paying special attention to the extrapolation of produced particles to the target surface,
- (ii) to perform measurements for a new target material (super-sialon), both in thin target and replica target configurations, for T2K-II and Hyper-Kamiokande,
- (iii) to study the possibility of measurements at low incoming beam momenta (below 12 GeV) relevant for improved predictions of both atmospheric and accelerator neutrino fluxes,
- (iv) to ultimately perform hadron production measurements with prototypes of Hyper-Kamiokande and DUNE targets.

Detector. The new measurements require upgrades of the NA61/SHINE detector that shall increase the data taking rate to about 1 kHz. These are:

- (i) construction of a new Vertex Detector,
- (ii) replacement of the TPC read-out electronics,

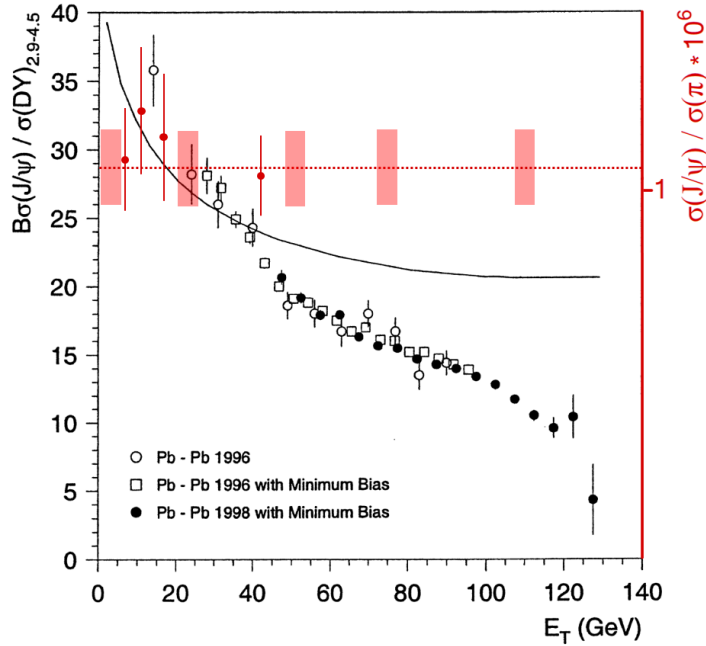


Figure 29. The ratio of $\sigma_{J/\psi}/\sigma_{DY}$ (left) and $\sigma_{J/\psi}/\sigma_{\pi}$ (right) as a function of transverse energy in Pb+Pb collisions at 158A GeV. The $\sigma_{J/\psi}/\sigma_{DY}$ ratio was measured by NA50 [104], and was used to calculate the $\sigma_{J/\psi}/\sigma_{\pi}$ ratio in [105]. Red bars mark the expected accuracy of the $\sigma_{J/\psi}/\sigma_{c\bar{c}}$ result of NA61/SHINE 2020+ assuming $\sigma_{c\bar{c}} \propto \sigma_{\pi}$ and scaled to the $\sigma_{J/\psi}/\sigma_{DY}$ ratio in peripheral collisions. (Figure taken from [13].)

- (iii) construction of a new trigger and data acquisition system,
- (iv) upgrade of the Projectile Spectator Detector.

Furthermore, the construction of new Time-of-Flight detectors would be highly desirable for potential future measurements of hadron production in C+C and Mg+Mg collisions which are expected to be needed to understand the onset of fireball phenomenon. The detector upgrade is planned to be executed during the LS2 and the measurements are scheduled in the period 2021-2024. The total upgrade cost is estimated to be about 2M CHF.

Collaboration, estimated timeline and cost. The collaboration consists of about 150 physicists from 30 institutions and 14 countries. Detailed description can be found in Ref. [13].

2.7 DIRAC++

The DIRAC++ proposal aims at performing the first high-precision measurement of the scattering lengths in the πK system, and at further improving the accuracy of the corresponding results in the $\pi\pi$ sector. As mentioned in section 1, these are key quantities for the study of QCD in the low-energy limit, where much of the dynamics follows from chiral symmetry breaking and can be described within chiral perturbation theory (χ PT).

Precise measurements in the πK sector. The S wave πK scattering lengths $a_{1/2}$ and $a_{3/2}$ (where the subscripts denote the isospin channel) are zero in the limit of chiral symmetry and hence particularly sensitive to chiral symmetry breaking. An overview of theoretical predictions is shown in figure 30. Experimentally, the combination $|a_{1/2} - a_{3/2}|$ can be extracted from the lifetime of the short-lived πK atoms $A_{\pi^+ K^-}$ and $A_{\pi^- K^+}$ in the ground state; the relation between the two quantities has a theoretical precision of 1%. Such an extraction has been achieved by the DIRAC experiment at the CERN PS with a proton beam momentum of 24 GeV/c: the DIRAC collaboration observed 349 ± 62 πK atomic pairs after breakup of the produced πK atoms, measured the πK atom lifetime, and extracted $|a_{1/2} - a_{3/2}|$ with a precision of 34% [106].

As estimated in [107], the number of $A_{\pi^+ K^-}$ and $A_{\pi^- K^+}$ produced per time unit at SPS CERN at $E_p = 450$ GeV would be 53 ± 11 and 24 ± 5 times higher than in the DIRAC experiment. For an experimental setup with the same parameters as in the DIRAC experiment and 5 months running time, this results in an expected number $n_A = 13000$ of πK atomic pairs. The statistical (systematic) precision of the πK scattering length $|a_{1/2} - a_{3/2}|$ is estimated to be around 5% (2%) [108]. As seen in figure 30, such a precision is highly competitive at the scale of theoretical predictions, concerning both their spread and quoted errors.

Figure 31 illustrates the gain in statistics between the PS and the SPS. Shown is the distribution of atomic πK pairs in their relative momentum Q , from which the number of produced atoms extracted. The points with errors and the left scale refer to the DIRAC measurement, where $\pi^- K^+$ and $\pi^+ K^-$ 349 ± 62 atomic pairs were observed. The blue

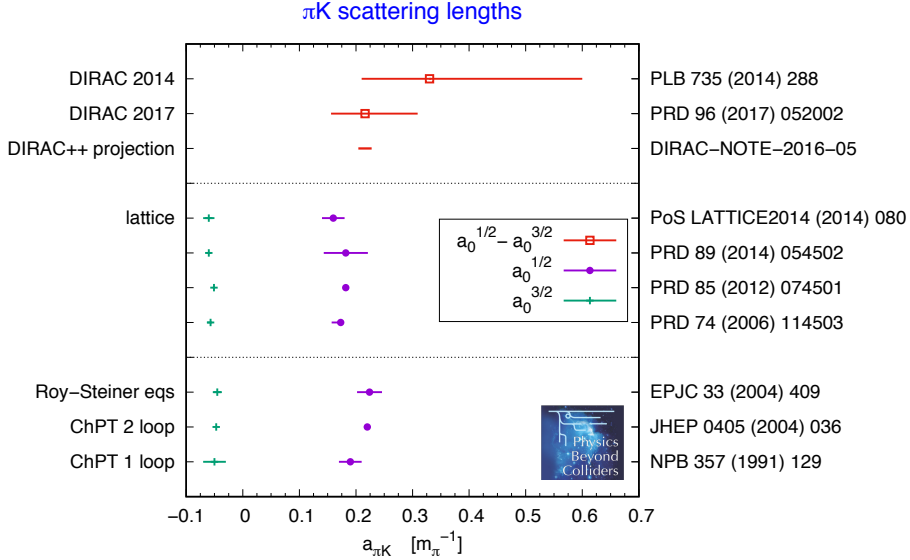


Figure 30. Theoretical predictions for the πK scattering lengths in the isospin 1/2 and 3/2 channels, together with the DIRAC measurements of the difference $a_0^{1/2} - a_0^{3/2}$ and the projected uncertainty of a measurement with DIRAC++.

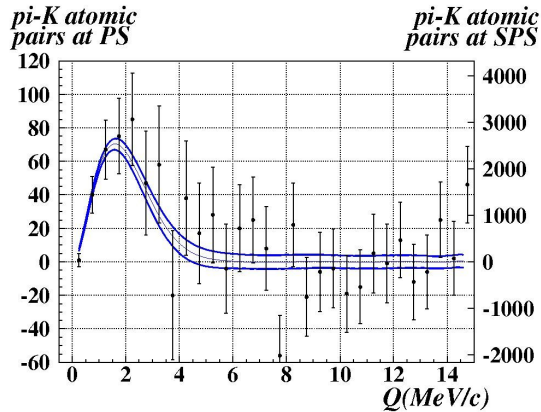


Figure 31. Change of statistical uncertainties on atomic πK pairs between the PS (DIRAC) and the SPS (DIRAC++), as explained in the text.

error band and the scale on the right correspond to the projection of 13000 atomic pairs produced at DIRAC++ during 5 months of data taking. The PS and SPS distributions are normalised to the same area in the interval of Q from 0 to 1.5 MeV/c.

Improvements in the $\pi\pi$ sector. In the same experiment, a large number of $\pi^+\pi^-$ atoms would be observed. Theoretical calculations of the S -wave $\pi\pi$ scattering lengths a_0 and a_2 have reached a high degree of accuracy: lattice calculations quote a relative precision of 4-10% and 1% for a_0 and a_2 , respectively [109–112]. Chiral Perturbation Theory predicts a_0 and a_2 with a precision of 2.3% and $|a_0 - a_2|$ with an accuracy of 1.5% [113]. For the short-lived $\pi^+\pi^-$ atom ($A_{2\pi}$) in the ground state, the lifetime is related to the scattering length combination $|a_0 - a_2|$. The most accurate experimental measurements of a_0 and a_2 have a precision of 6% and 22% respectively and were done by NA48 using kaon decays [114, 115]). The combination $|a_0 - a_2|$ can also be extracted from the lifetime of the short-lived $\pi^+\pi^-$ atom ($A_{2\pi}$) in the ground state. This was done by DIRAC [116] with an accuracy around 4% and a value consistent with the NA48 results.

With a proton beam momentum 450 GeV/c, the number of $A_{2\pi}$ generated per time unit would be 12 ± 2 times higher than in the DIRAC experiment. The expected number of $\pi\pi$ atomic pairs detected simultaneously with πK atomic pairs would be $n_A = 4 \times 10^5$. The statistical (systematic) precision of $\pi\pi$ scattering lengths $|a_0 - a_2|$ is estimated to be around 0.7% (2%), thus improving the current precision by a factor of two.

One may wonder whether the πK scattering lengths could be extracted from charmed meson decays, in analogy to the method used by NA48 for $\pi\pi$. However, an analysis in the strange sector is expected to be more delicate because of prominent resonances on top of the πK continuum, starting with $K^*(892)$ not far away from the threshold at 633 MeV.

Long-lived atoms. A sample of 436_{-61}^{+157} atomic pairs from the breakup of long-lived $A_{2\pi}$ atoms was observed by DIRAC [117]. From this sample, the collaboration extracted the lifetime of the $2p$ state, which is three orders of magnitude larger than the one of $A_{2\pi}$

in the ground state ($\tau_{2p} = 0.45_{-0.30}^{+1.08} \times 10^{-11}$ s vs $\tau_{1s} = 3.15_{-0.26}^{+0.28} \times 10^{-15}$ s) [118]. At the SPS, the 450 GeV/c proton beam and experimental adaptations envisaged for DIRAC++ (see below) open up new possibilities for study of long-lived $\pi\pi$ and πK atoms [107]. The number of $A_{2\pi}$, $A_{\pi^+K^-}$ and $A_{\pi^-K^+}$ detected per unit of time would be increased by factors of 609, 26553 and 12024, respectively and the background would be decreased by about two orders of magnitude compared to the DIRAC experiment. This would allow one to apply a resonance method for measuring only one parameter, the Lamb shift, and evaluating from this parameter the linear combination $2a_0 + a_2$ [119]. Combined with the measurement of $|a_0 - a_2|$, this would allow for the experimental separation of both scattering lengths from measurements with $\pi\pi$ atoms.

Required upgrades and additions to experimental equipment. For an experimental setup at the SPS, parts of the original DIRAC detector can be re-used. A scheme currently under investigation is the use of two magnets, a new small one, and the DIRAC magnet as second one. The use of modern coordinate detectors is foreseen. This modification will enlarge the setup acceptance and will allow the experiment to work with a higher proton beam intensity than DIRAC, thus improving the statistical precision significantly. A rough estimate of the cost of such a new set up is 3 million CHF.

Collaboration. Based on the experience with the original DIRAC experiment, it is hoped that a collaboration of adequate strength to build and operate DIRAC++ would form if a Letter of Intent were positively reviewed by the SPS Committee.

3 Summary of heavy-ion measurements

The currently running and planned heavy ion experiments sweep over a large temperature and density regime in the phase structure, scanning $\sqrt{s_{NN}}$ from about 2 GeV to LHC energies. Combined, the experiments will unravel the phase structure of QCD, see figures 32 and 33.

In combination, the heavy ion experiments at CERN already offer a unique opportunity with their positioning from the very high energy regime covered by LHC, and the connected regime covered by the fixed target experiments at SPS and LHC.

Moreover, the SPS experiments cover a specifically interesting energy regime. In this regime several anomalies in the energy dependence of hadron production properties have been observed in central lead-lead collisions. They are interpreted as the beginning of the creation of QGP (the onset of deconfinement, OD), see figure 32. This regime possibly also include the critical end point in the QCD phase diagram (CP), see figure 32. They are complementary to the other experiments in this regime, RHIC BES-II (running (2019), NICA (starting 2020). They are unique in their access to open charm (NA61++, NA60++) and the precise determination of the caloric curve (NA60++), for more details see the chapters 2.5, 2.6, as well as connecting to CBM, FAIR and J-PARC-HI with high interaction rates at lower collision energies. In summary this offers the opportunity at SPS CERN for significantly contributing to the resolution of the density region potentially hosting the critical end point of QCD.

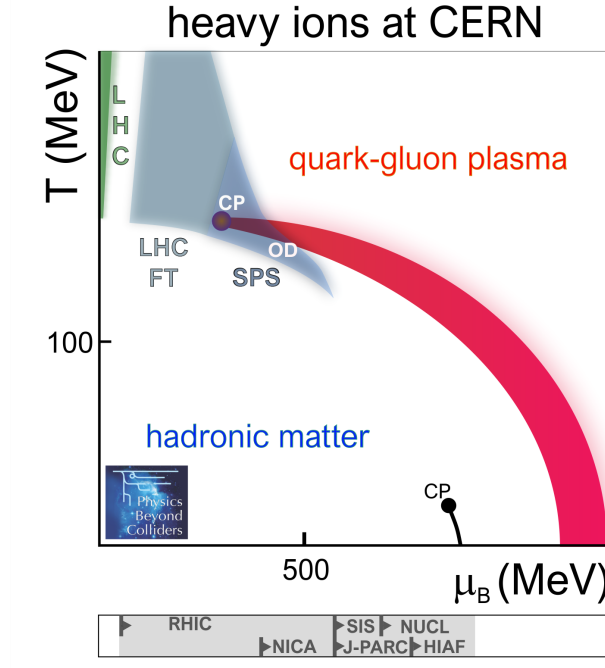


Figure 32. Phase diagram of QCD and density range of running or planned experiments. The density range of LHC, LHC-FT and SPS experiments is indicated with the shaded areas in the figure. The lower boundary of the grey and blue shaded area follows the chemical freeze-out. The upper boundary relates to the parameters at the early stage of the collisions. The potential critical end point is labelled with CP, the onset of deconfinement with OD. The back line at small temperatures and high densities signifies the nuclear liquid-gas transition, also ending in a critical end point CP. The density range of other experiments is indicated in the bar below the figure. This includes RHIC at BNL, NICA at JINR, SIS100 at FAIR, J-PARC-HI at J-PARC, the Nuclotron at JINR (NUCL), and HIAF at HIRFL.

The FT experiments at LHC cover an energy regime overlapping with that of RHIC, but allow for different and partially more accurate measurements. For example, the large pA rates are orders of magnitudes larger than those reached at RHIC in collider mode. The high statistics data for heavy flavour azimuthal correlations ($D - D, J/\psi - D$) together with measurements of the D-meson elliptic flow and the nuclear modification factor allow for a study of the QGP transport properties (\hat{q} and charm quark diffusion coefficients), for more details see [5].

4 Measurements for cosmic-ray physics and for neutrino experiments

Precise measurements of cosmic-ray fluxes up to very high energies, ranging from about tens of MeV up to hundreds of TeV, have become available for many particle species. High-precision data on the interaction (production) cross sections of typical cosmic-ray particles with (from) nuclei most abundant in the universe are needed for the interpretation of results from current- and future-generation cosmic-ray experiments. In this respect a

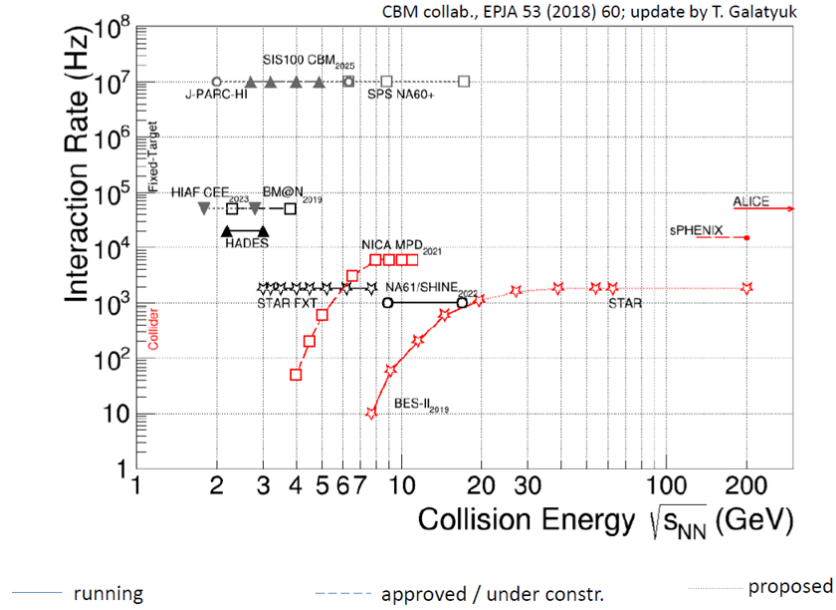


Figure 33. Interaction rate of running or planned experiments (figure taken from [120], update by T. Galatyuk). The fixed target experiments at CERN have large interaction rates relevant for the accuracy required for the physics questions at hand. They cover a very interesting regime in the collision energy $\sqrt{s_{NN}}$, see figure 32, complementary to other running or planned experiments.

better understanding of the cosmic-ray propagation is needed to study the origins of galactic cosmic rays and to evaluate the cosmic-ray background for signatures of astrophysical dark matter cosmic-ray acceleration.

Anti-protons are of special interest as expected to be a result of the diffuse propagation of primary cosmic rays in the galaxy. Recently, the AMS experiment reported anti-proton to proton flux ratios for 1–400 GeV [121] with much higher precision than earlier PAMELA data [122] (see figure 34). Precision knowledge of anti-proton production cross sections over a wide range of energy and initial-state nuclei opens the portal to indirect detection of dark matter or unknown astrophysical mechanisms of cosmic-ray acceleration. Nuclei that are abundant in the galaxy play a particular role, as prime candidates for anti-proton sources. Data from NA61/SHINE [17] and from LHCb [16] with the current SMOG fixed-target system have already been used in analyses and demonstrated the usefulness of such measurements [123]. This is illustrated in figure 35 in which different parameterisations of the \bar{p} production cross section in proton-He collision is compared to the LHCb SMOG data, clearly favouring one over the other parameterisation [123].

In the case of cosmic neutrinos, atmospheric neutrinos are sources of background in terrestrial studies of galactic neutrino generation and propagation. Heavy-quark decay constitutes a major uncertainty that can be addressed, e.g., by charm production cross sections in pA and AA collisions. In particular, charm production at large- x_F , e.g., very forward and at high-energies, strongly depends on the charm content of the nucleon, il-

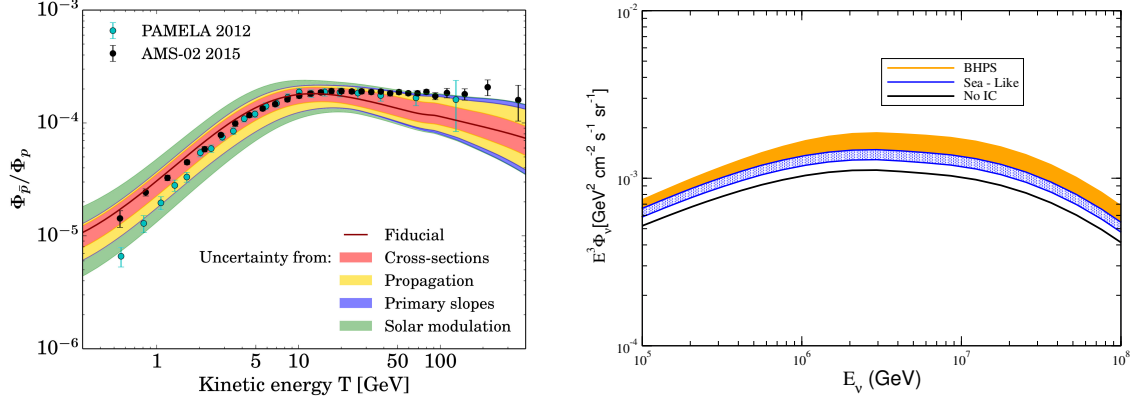


Figure 34. Examples of QCD-related limitations in flux calculations for cosmic-ray physics. (left) The combined total uncertainty on the predicted secondary \bar{p}/p ratio, superimposed to PAMELA [122] and AMS [121] data. (right) Predictions for high-energy atmospheric neutrinos from collisions of cosmic rays with atmospheric nuclei. The different curves correspond to different assumptions on the high- x charm content of the proton [5, 124]. (Figures taken from [5, 125].)

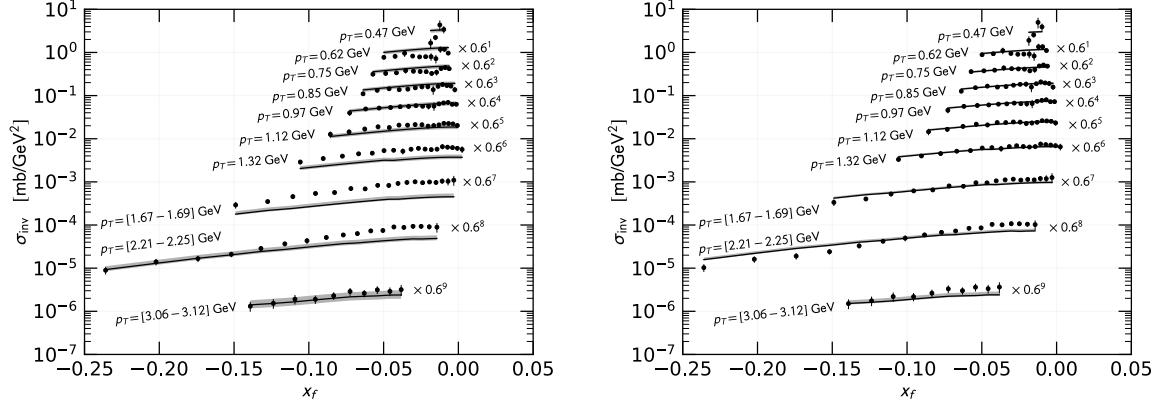


Figure 35. Comparison of two parameterisations [123] for the p He cross section with the LHCb data [16]. (Figure taken from [123].)

illustrated in figure 34 for three models for charm in the projectile proton [5, 124]. The capability to measure charm production in fixed-target mode at the LHC has been already demonstrated by LHCb using few nb^{-1} of data collected with the SMOG target with helium and argon [54]. The use of a hydrogen target and the large increase in luminosity allowed by the SMOG2 target upgrade are expected to provide precise measurements on the amount of intrinsic charm in nucleons.

Last but not least accelerator-based neutrino experiments (cf. Refs. [126–129]) rely on a precise description of particle production in primary and follow-up interactions of beam and secondary hadrons in the often extended nuclear targets. It is, however, far from trivial to predict those precisely from standard Monte Carlo simulations due to the complexity and ranges of different interactions involved. Measurements of particle fluxes using replica targets or thin targets of the same material under similar conditions can provide

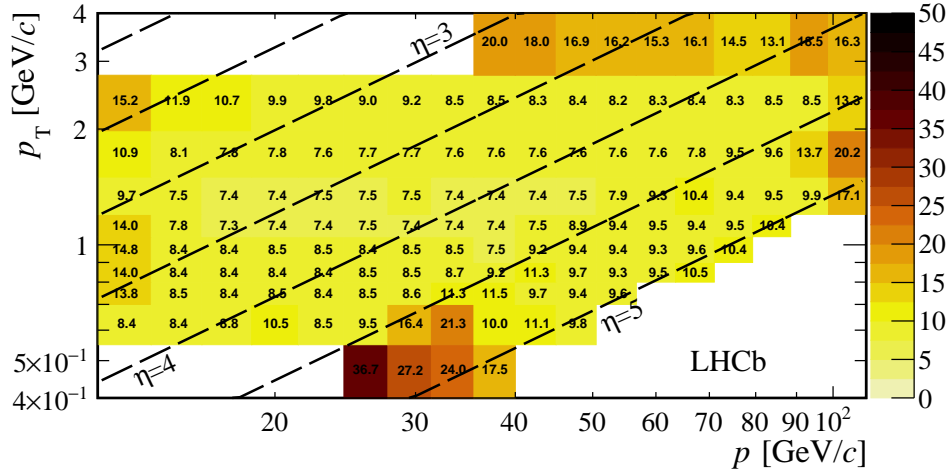


Figure 36. Relative precision (in %) of recent LHCb results [16] on \bar{p} production in p He collision at $\sqrt{s}=110$ GeV. The integrated luminosity used in this measurement amounts to 0.5 nb^{-1} . With SMOG2 it should be possible to collect about 100 nb^{-1} in an hour beam time. Moreover, SMOG2 will significantly reduce the systematic uncertainty on the luminosity, the dominating uncertainty of the present measurement.

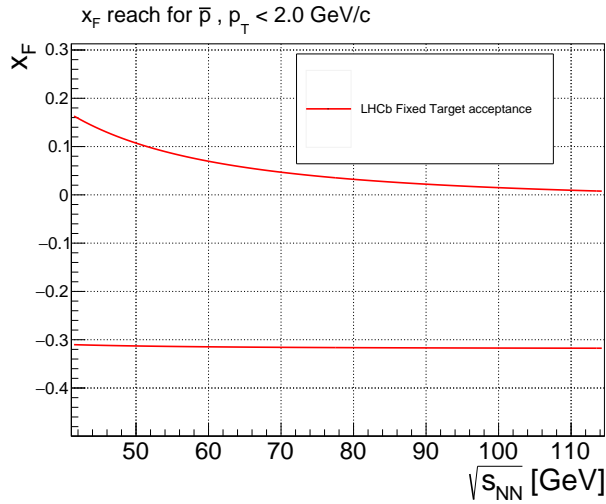


Figure 37. Acceptance in Feynman- x of LHCb-FT (SMOG2) for p_T up to 2 GeV in \bar{p} production. Note that the majority of the production is in the range $|x_F| < 0.1$.

important input to these simulations. For example, the NA61/SHINE collaboration has performed several of such measurements that have been exploited in flux calculations for the T2K long-baseline neutrino experiment [130–133]. NA61/SHINE plans to continue this program including measurements for present and future J-PARC long-baseline experiments (T2K, T2K-II, Hyper-K), and the future Long-Baseline Neutrino Facility (LBNF) beam for DUNE [129], strongly endorsed by those collaborations [13].

Among the various PBC-QCD proposals, COMPASS++, LHC-FT (AFTER@LHC, LHCb-FT, and ALICE-FT), as well as NA61++ have cosmic-ray and neutrino-flux related measurements as part of their program. They are discussed below.

Anti-proton production and nuclear fragmentation:

- **LHCb-FT** (SMOG2 [41, 42]) plans to perform similar measurements as those mentioned above using a He target [16], but with hydrogen and deuterium under the same kinematic condition to provide the production in pp collision and to constrain isospin violations, which affect the prediction for the anti-neutron contribution to the antiproton flux. The better control over the gas density provided by SMOG2 will reduce the systematic uncertainty on the luminosity, which is one of the largest limitations to the precision of the current measurement with He, which is depicted in figure 36, with the reach in x_F for $p_T < 2$ GeV of the \bar{p} shown in figure 37. Measurements at lower \sqrt{s} are also foreseen.
- **ALICE-FT** could employ the central barrel to measure very slow \bar{p} with almost zero momentum. The production of such slow \bar{p} with the LHC proton beam correspond to the highest possible energies in the inverse kinematics, where the nuclear target (C, N, O, He) travels at TeV energies, hit an interstellar p at rest and produces a \bar{p} in the limit of $x_F \rightarrow 1$ [5]. Using, e.g., a ${}^4\text{He}$ target would then correspond to the high-energy tail of the ${}^4\text{He} + p \rightarrow \bar{p} + X$ process (${}^4\text{He}$ as projectile), which is one of the leading process in the cosmic \bar{p} spectrum. Similarly, using C, N or O targets, one can study the high-energy \bar{p} tail for $(\text{C,N,O})+p \rightarrow \bar{p} + X$. As an example, the yield of low-momentum \bar{p} in the range $0.3 \text{ GeV} < p_T^{\bar{p}} < 4 \text{ GeV}$ is shown in figure 38 for 45 pb^{-1} .
- **NA61++** proposes to measure a range of nuclear fragmentation cross sections relevant for the production of Li, Be, B, C and N nuclei. In addition, (anti)proton and (anti)deuteron cross sections will be studied under the same kinematic conditions allowing for determinations of d/p and \bar{d}/\bar{p} ratios. Details are to be worked out and will be subject to a future addendum to the NA61/SHINE proposal. For guidance, from 60M pp collisions recorded between 2009 and 2011, 13k \bar{p} and 10 \bar{d} are expected based on simulations [13]. 600M events each are foreseen to be taken with a liquid-hydrogen target at beam energies of 40 GeV, 180 GeV, and 350 GeV, respectively, running each 100 days at a rate of 6M pp -events/day. Yields of \bar{p} and \bar{d} after selection and identification requirements are estimated based on the preliminary p and d analyses of already existing NA61/SHINE 158GeV pp data [134] as well as an analysis of other statistically limited \bar{d} production data [135], and are summarised in Table 3, taking into account the about 1 kHz rate limit of NA61++ read-out (a rate that also saturates the available radiation budget in the case of PbPb collision). The acceptance, estimated based on the published analysis of pp data from 2009 [17], is depicted for protons and anti-protons in figure 39.

Table 3. Estimated \bar{p} and \bar{d} event yields for 100 days running each at 40 GeV, 180 GeV, and 350 GeV beam momentum and a liquid-hydrogen target at NA61++ and a 1 kHz read-out rate.

beam momentum	40 GeV	180 GeV	350 GeV
\sqrt{s}	8.8 GeV	18.4 GeV	25.7 GeV
beam time	100 d	100 d	100 d
pp collisions	6×10^8	6×10^8	6×10^8
estimated \bar{p} events	1.3×10^4	1.4×10^5	2.3×10^5
estimated \bar{d} events	10	110	180

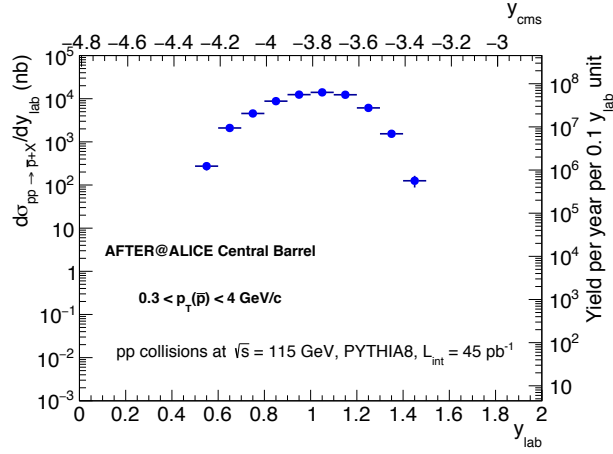


Figure 38. Expected kinematic coverage of \bar{p} production for ALICE-FT (for details, see [5]; figure taken from [5]).

- **COMPASS++** proposes, similarly as NA61++, to measure \bar{p} production with a liquid-hydrogen target, but also with a ^4He target. \bar{p} will be accepted in a momentum range of 10–45 GeV (where an absence of a RICH signal is used for particle-ID in the range of 10–18 GeV) and 2.4–8 in pseudo-rapidity. A 1% relative statistical precision in each of 20×20 bins in momentum and pseudo-rapidity is envisaged using a beam intensity of 10^5 p/s on target, corresponding to a trigger rate of 25kHz. With a total of 10s beam per minute, 2.5×10^5 collision events will be collected. An estimated \bar{p} identification efficiency of 70%, 4 hours (6 hours incl. contingency) will be required for each combination of target and beam setting.

Charm: **LHC-FT** offers a unique opportunity to study high- x parton distributions, as discussed already in Sec. 2.1. **LHCb-FT**, in particular, has excellent acceptance and identification capabilities for various charm-sensitive channels. In addition to the discussion in Sec. 2.1, example prospects for measuring charm at LHCb with SMOG2 are given in Table 4. Please note that

- the list is far from being exhaustive, e.g., different target gases are possible;
- extrapolations are currently crude estimates;

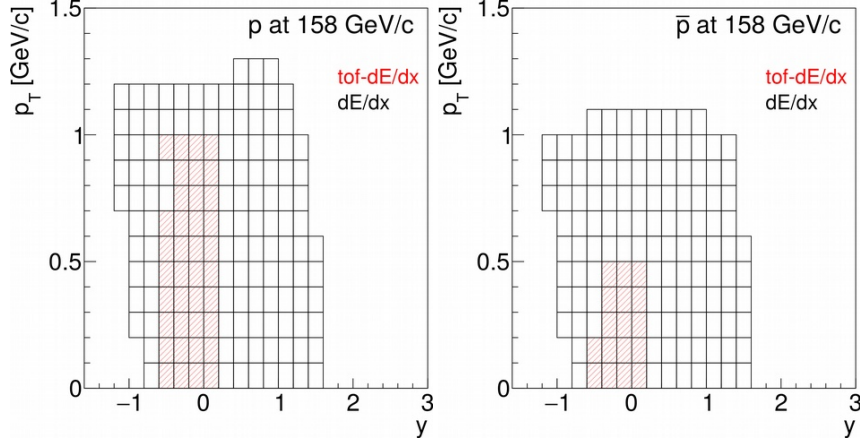


Figure 39. Accepted range in p_T and rapidity y (calculated in the collision centre-of-mass system) for proton and anti-proton production in pp collision at $\sqrt{s} = 158$ GeV. (Figures taken from [17].)

Table 4. Current and estimated yields in charm events as well as for $\Upsilon(1S)$ production and Drell–Yan for SMOG and SMOG2 at LHCb-FT.

	SMOG published pHe@87 GeV	SMOG largest sample pNe@68 GeV	SMOG2 example pAr@115 GeV
Integrated luminosity	7.6 nb^{-1}	$\sim 100 \text{ nb}^{-1}$	$\sim 45 \text{ pb}^{-1}$
Systematic unc. on J/ψ cross section	7%	6–7%	2–3 %
J/ψ yield	400	15k	15M
D^0 yield	2000	100k	150M
Λ_c^+ yield	20	1k	1.5M
$\psi(2S)$ yield	negl.	150	150k
$\Upsilon(1S)$ yield	negl.	4	7k
DY $\mu^+\mu^-$ yield ($5 \text{ GeV} < M < 9 \text{ GeV}$)	negl.	5	9k

- assuming quarkonium absorption by the nuclear target leads to a decrease of its cross section by a factor 0.75 (0.6) in $p\text{Ne}$ and 0.5 (0.4) in $p\text{Ar}$ for J/ψ (ψ') with respect to $p\text{He}$;
- the smaller systematic uncertainty with SMOG2 is expected from the reduction of the dominant uncertainty on the luminosity (6%) for SMOG data.

Hadron production measurements for accelerator-based neutrino experiments: NA61++ proposes a series of measurements for J-PARC and LBNF in order to

- improve further the precision of hadron production measurements for the currently used T2K replica target, paying special attention to the extrapolation of produced particles to the target surface,

- perform measurements for a new target material (super-sialon), both in thin target and replica target configurations, for T2K-II and Hyper-Kamiokande,
- study the possibility of measurements at low incoming-beam momenta (below 12 GeV) relevant for improved predictions of both atmospheric and accelerator neutrino fluxes,
- ultimately perform hadron production measurements with prototypes of Hyper-Kamiokande and DUNE targets.

5 Compatibility of COMPASS++ and MUonE at the M2 beam line

The proposed measurements of elastic μp scattering by COMPASS++ and of elastic μe scattering by MUonE are both envisaged to take place (or at least start) during Run 3 of the LHC, given the scientific urgency of the physics problems they address and the activity of related experiments elsewhere in the world. The question therefore arises whether and under which condition a concurrent running of both experiments might be possible. This initiated a study within the PBC QCD working group, whose status is presented in this section. Preliminary answers were already provided at the 2018 June PBC workshop.¹⁶

Compatible locations for μ - e and the μ -proton-radius foreseen setups. Concerning the setup, several options were studied. The μ - e is a long setup and among the two options studied (upstream or downstream of EHN2 Hall) the retained option is presently upstream (figure 40 top), within a possible available space in the M2 beam-line. The μ -proton-radius requires the usage of several components of the COMPASS spectrometer, therefore it should be installed, as shown in figure 40 (bottom). Dedicated studies were performed¹⁷ showing that an adequate μ -beam tuning can be achieved for the two experiments running in parallel.

Optimum μ -beam energies for μ - e and the μ -proton-radius. Presently, the optimum beam energies for the two measurements are different. Quoted is maximum 100 GeV for μ -proton-radius and (at least) 150 GeV for μ - e . Figures 41 (top and bottom) illustrate this issue. The μ -proton-radius will also need data taken < 100 GeV to get an accurate measurement at the lowest foreseen $Q^2 = 10^{-4}$, in order to check the quality of the extrapolation to $Q^2 = 0$. One should definitely *study the option of running μ -proton-radius at 150 GeV*.

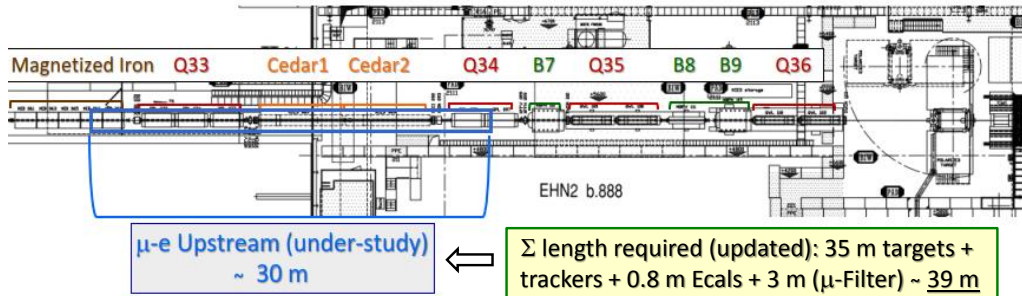
Optimum μ -beam intensities for μ - e and the μ -proton-radius. The values of intensities quoted in the μ -proton-radius proposal [136] and in the μ - e proposal [85] (and subsequent presentations) are quite different. Even though they cannot be taken yet as finalised parameters, they differ by at least one order of magnitude. Therefore raising a

¹⁶See the presentation by A. Magnon at <https://indico.cern.ch/event/706741/timetable/#20180614.detailed>.

¹⁷This was presented by L. Gatignon at the Conventional Beams PBC General Meeting on 13 June 2018. An ATS Note by D. Banerjee and J. Bernhard is in preparation.

μ -e setup upstream of present COMPASS experiment, i.e. within M2 beam-line

- More upstream of Entrance Area of EHN2 (Proposed by Johannes B. & Dipanwita B.)
 - Pro: Could allow running μ -e/ μ -p_{Radius} in parallel.
 - Questions: will require displacements (also removal) of some M2 components.
 - Beam(s) compatibility for μ -e & μ -p_{Radius} : Optic's wise is OK (June 11-2018 CBWG EHN2 Status)



μ -p_{Radius} requires usage of full COMPASS spectrometer

Setup for the COMPASS measurement

- TPC and silicon telescopes in the nominal COMPASS target region
- trigger: two scenarios under investigation
 - SciFi with high segmentation for a "kink trigger"
 - high-rate triggerless readout (requires new readout scheme for the silicon detectors)
- spectrometer in usual (open) configuration for scattered muon momentum measurement
- e.m. calorimetry for control of radiative effects and measurement of muon-electron scattering (similar / competing process)

Optimum location for Si trackers, TPC and trigger components is Upstream of SM1

Christian Dreisbach (christian.dreisbach@cern.ch) Proton Radius at COMPASS 18

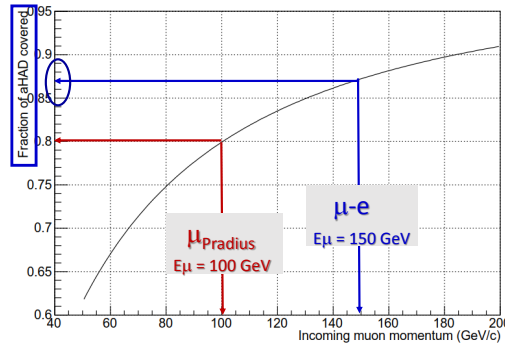
Figure 40. Foreseen setups: (Top) μ -e and (Bottom) μ -proton-radius setups.

critical issue, concerning compatibility, see illustration in figure 42. To optimise the overall use of the μ -beam it would be of *great interest for μ -proton-radius to improve their setup*, with the goal of running at a higher beam intensity.

Deterioration of the μ -beam purity from interactions with the μ -e setup. Several remarks were expressed by the μ -proton-radius proponents concerning the option of

What will be optimum μ -beam energy for μ -e measurement ?

Fraction of a_{μ}^{HLO} which can be accessed, from the μ -e measurement vs the incoming beam p_{μ}



From U. Marconi & G. Venanzoni

In view of the accessed fraction of a_{μ}^{HLO} vs μ -beam momentum, the assumed 150 GeV energy is a clear lower limit to run this experiment

What will be optimum μ -beam energies for μ -p_{Radius} measurement ?

(Proposal p.2&3) The low Q^2 region is vital to constrain the parametrisation of the form factors and thus give more comfort for their extrapolation to $Q^2 = 0$. A lower limit of $Q^2 = 10^{-4}$ is desirable. On the other hand the region of large $Q^2 (> 10^{-3})$ gives sensitivity to the charge radius.

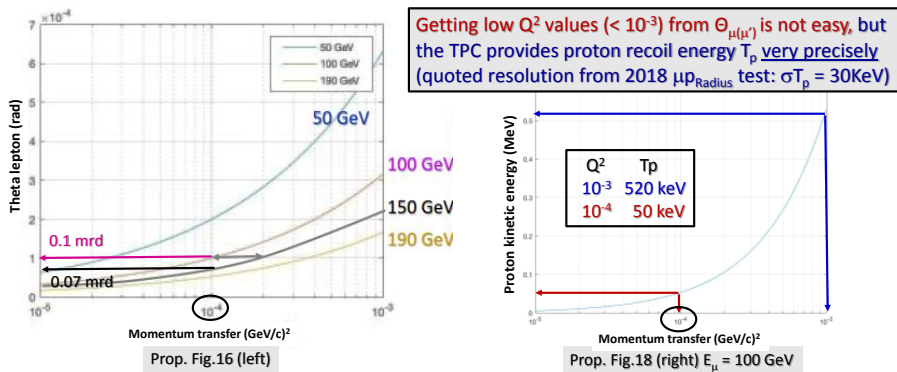


Figure 41. Quoted optimum energies: (Top) at least 150 GeV for μ -e and (Bottom) 100 GeV and below for μ -proton-radius.

the μ -e setup located upstream: "Such hybrid solution *will not be compatible with the very strict requirements* of the proton radius measurement using high energy μ p elastic scattering within the COMPASS setup". One remark concerned the generated background, resulting from interaction of the muons with the μ -e setup. A quantification was performed,¹⁸ using both Geant4 and Fluka softwares. A sketch of the assumed material-input for μ -e is shown in figure 43 (top) and results from simulations are shown in figure 43 (bottom).

These 1st estimates of the pollution from the μ -e setup (upstream) are *quite promising*. Note also that the two different simulations (Geant4 and Fluka) provide *very consistent* results.

¹⁸The simulation was done by D. Banerjee and M. V. Dick.

What will be optimum μ -beam intensities for μ -p_{Radius}

- For low Q² use of a TPC is mandatory
 - ==> Proposal (Sections 3.4 - 3.5): Instant beam rate of $\sim 2 \times 10^5 \mu/s$ is quoted (running at two different target pressures)
 - ==> From 2018 μ p_{Radius} tests TPC could stand up to $\sim 10^6 \mu/s$ (on-going analysis will confirm)
- ==> New TPC set-up, also trigger-less readout could increase present beam rate limitation by a factor of 10 - under study

Presently, μ -intensities for μ -p_{Radius} $\leq 10^6 \mu/s$

... and μ -e measurements

- To achieved the statistical accuracy of 0.3% on the a_μ^{HLO} , the required Luminosity is $L = 1.5 \times 10^7 \text{ nb}^{-1}$ (see arXiv:1609.08987v2)
- Assuming the full target consisting of 60 “modules” having each a 1cm Beryllium target, and an average intensity of the μ -beam of $\langle I_\mu = 1.3 \times 10^7 \text{ s}^{-1} \rangle$ corresponding to $\sim 5 \times 10^7 \text{ s}^{-1}$ (*) during the SPS spill and $2 \times 10^7 \text{ s/yr}$ (**) such required Luminosity can be collected in 2 (rather 3 or more ?) years of data taking.
 - (*) Intensity for 160 GeV μ -beam up to $5 \times 10^7 \text{ s}^{-1}$
 - (**) Optimistic (rather $1 \times 10^7 \text{ s/yr}$)

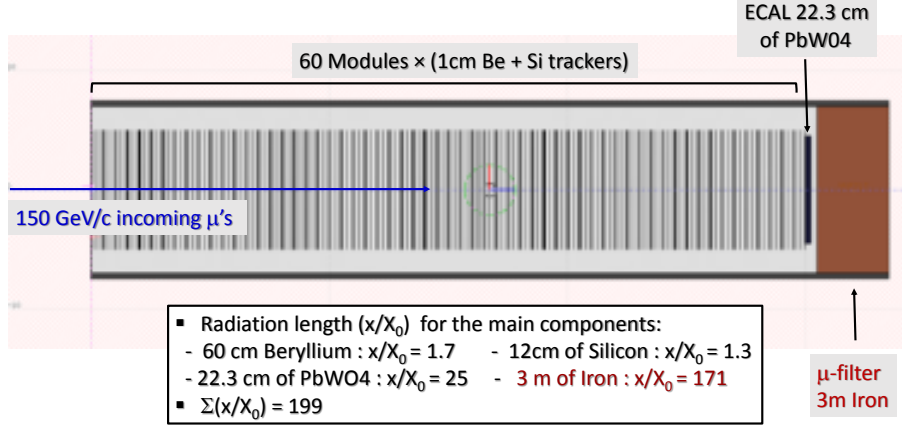
Quoted μ -Intensities for μ -e is $5 \times 10^7 \text{ s}^{-1}$ (during SPS spill)
 ==> NOT compatible with μ -p_{Radius} using the present TPC technology

1

Figure 42. Quoted expected optimum intensities: (Top) μ -proton-radius and (Bottom) μ -e.

Deterioration of the μ -beam angular divergence from MSC in the μ -e material, also momentum distribution spreading from energy losses. The large amount of radiation lengths of the μ -e setup quoted in figure 43 (top), in particular downstream, generates a significant beam divergence from Multiple SCattering (MSC). In addition, the μ 's loose energy which results in a shift and a spreading of the energy distribution. Concerning the MSC a dedicated optical beam tuning (suggested by J.Bernhard) has been proposed and studied. Also suggested is the use of a ¹²C μ -filter instead of Iron, which results in an additional reduction of the beam spreading from MSC. The (preliminary) *quite promising* results are shown in figure 44 (top). However, the effects from the μ -beam energy losses in the μ -e material which impact is shown on figure 44 (bottom) cannot be reduced. We need a *precise evaluation* of the sensitivity of μ -proton-radius measurement to such degradation of the incoming μ -beam energy (see below) and not ignore the potential of the COMPASS spectrometer to measure $E_{\mu'}$ (E_μ) precisely, and "tag" events issued from

MUonE setup used for background simulations (using Fluka and Geant4)
and located upstream of EHN2 experimental Hall



Simulation of background components for 150 GeV incident muon at the
"TPC2" position, 40m $>$ μ -filter

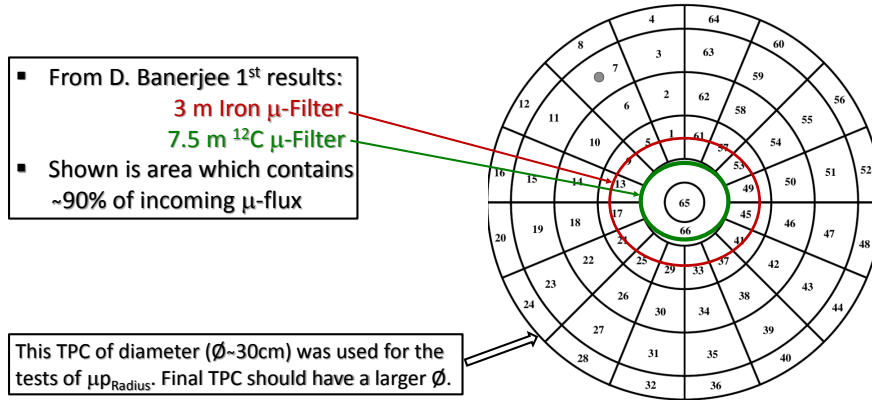
Particle	$R = \Sigma/\mu$	σR
Proton	3×10^{-7}	1.7×10^{-7}
A_Proton	1×10^{-7}	1.0×10^{-7}
e-	0.00094	9.7×10^{-6}
e+	0.00092	9.6×10^{-6}
γ	0.008	2.8×10^{-5}
Neutron	2×10^{-7}	1.4×10^{-7}
A_Neutron	2×10^{-7}	1.0×10^{-7}
$\mu+$	0.893016	3.0×10^{-4}
$\mu-$	1×10^{-7}	1.0×10^{-7}
$\pi+$	2.7×10^{-6}	5.2×10^{-7}
$\pi-$	1.9×10^{-6}	4.4×10^{-7}
K+	1×10^{-7}	1.0×10^{-7}
K-	3×10^{-7}	1.7×10^{-7}

Annotations in the table:
 $e^{\pm} \leq 10^{-3}$
 $\gamma \leq 10^{-2}$
 Hadrons: $\leq 5 \times 10^{-7}$

Figure 43. (Top) Assumed μ -e setup composition and estimated radiations length. (Bottom) Fraction (per- μ) of background components entering the acceptance of the TPC used to detect the recoil low-energy proton and located 40m downstream, as shown in figure 40 (Bottom)

the low energy tail.

Option of having a hole of appropriate size in the downstream μ -e heavy components. In order to reduce significantly the μ -beam deterioration, question was asked about the possibility to make a hole in the central part of the ECAL and μ -filter (heavy material) of the μ -e setup. Such hole should have an appropriate size to not interfere with (at least 90%) of the μ -beam. Figure 45 (top) shows a few μ -e selected kinematics for which a sample of outgoing scattered μ and e tracks for events produced both upstream



- Calculation by M. v. Dijk of the μ -momentum at the position of the μ -p-radius TPC assumes mono-energetic incoming μ 's of 150 GeV, upstream of the μ -e setup including ECAL and 3 m long Iron μ -filter
- P_{μ} distribution is degraded, in particular low energy tail (plot below)

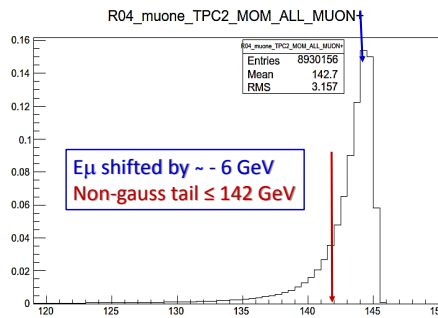


Figure 44. (Top) Reduction of the μ -beam size spreading from the MSC angular divergence from a dedicated M2 μ -beam tuning, optimised for the μ -proton-radius TPC position (red). Also additional reduction by replacing the Iron μ -filter by a longer ^{12}C filter (green). (Bottom) Impact on the μ energy distribution of the energy losses produced by the full μ -e setup.

and downstream of the setup are illustrated in figure 45 (bottom). The conclusion is that such an option will seriously degrade the PID performances, in particular for the Signal (S.2) region where the μ and e angles are ambiguous and PID mandatory.

Preliminary conclusions about μ -e and μ -proton-radius compatibility.

1. The option of having the μ -e installed upstream of EHN2 looks quite promising. It guarantees, at least that the two projects can be setup together, with a priori, *no interference* concerning their installation. More technical input is expected from the EN/EA/LE group, in particular about the real available space and the required modifications/adjustments for some M2 components.

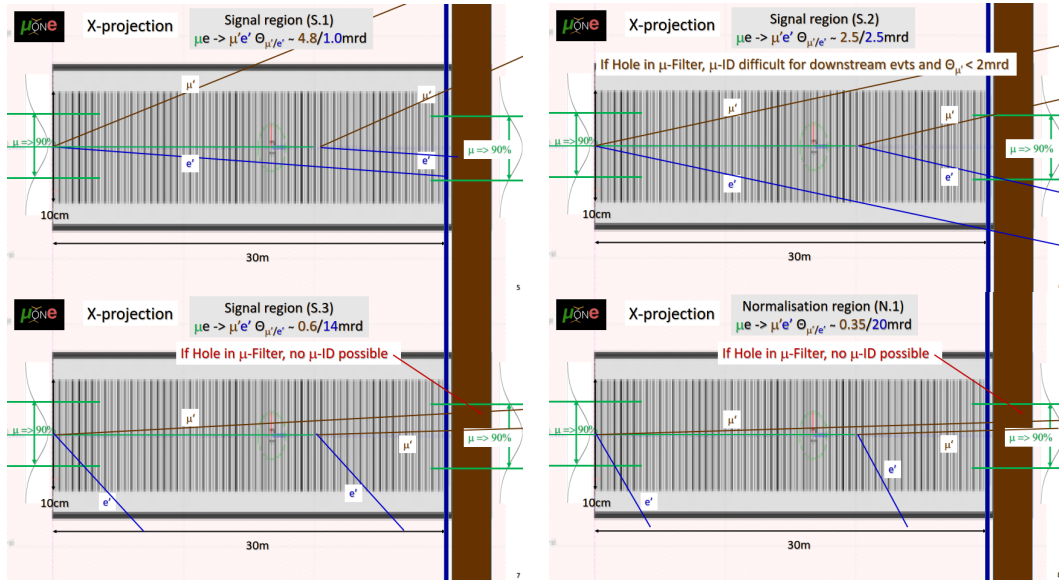
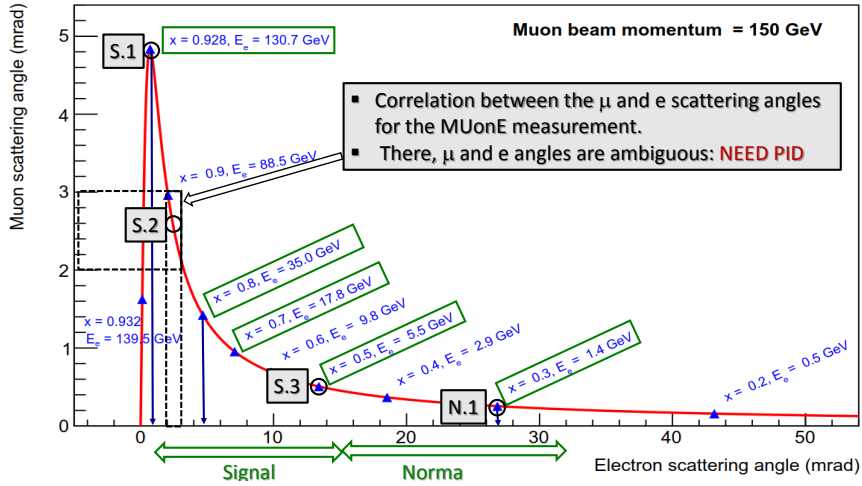
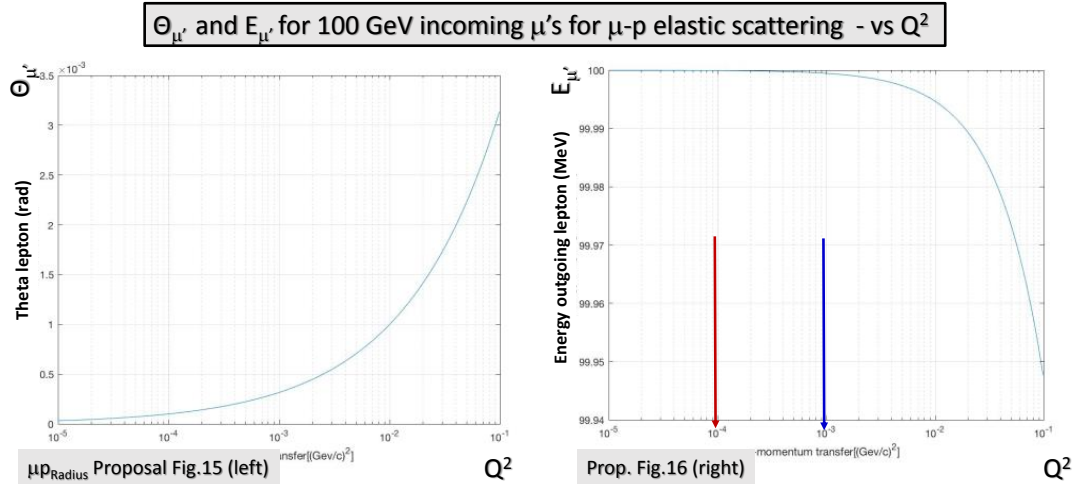


Figure 45. (Top) Selected μ - e kinematics used to test the impact on the PID of a hole in both ECAL and μ -filter. (Bottom) corresponding sample of tracks for μ - e scattered events.

2. Concerning a possible beam sharing: 1/- compatible beam energies is not granted. However, at this stage, we cannot exclude possible compromises which could allow a "partial" sharing, 2/- about beam intensities, compatibility appears to be a real problem, and given the present information(s) a *true show-stopper*. More studies are requested from μ -proton-radius to progress on this issue.
3. To proceed with further investigations, one will need more input about the overall issue of "feasibility", in particular for the very challenging μ - e project.



Recall (proposal): Getting Q^2 values ($< 10^{-3}$) from the $E_{\mu(\mu')}$, also scattering angle $\Theta_{\mu(\mu')}$ is not easy.

But the TPC provides proton recoil energy T_p very precisely (quoted resolution from 2018 μ p_{Radius} test: $\sigma T_p = 30\text{KeV}$) $\implies Q^2 10^{-4} / T_p = 50 \text{ keV}$ $\implies Q^2 10^{-3} / T_p = 520 \text{ keV}$

Figure 46. Scattering angle $\theta_{\mu'}$ and energy $E_{\mu'}$ for the outgoing muon, assuming an incoming energy E_{μ} of 100 GeV.

4. Given the "revised mandate" of the Physics Beyond Colliders Study group this should leave enough time for the future projects to provide the required additional input(s).

Additional remarks concerning the μ -proton-radius measurement. Concerning the impact on the μ -proton-radius measurement of the expected degradation of the incoming μ -beam energy (see above) it is interesting to quote inputs from the proposal. In section 2.2.2 of version 1 of the proposal [136] we read "All kinematic quantities only depend on Q^2 and are almost independent of the beam energy, except for the muon scattering angle shown in Fig. 16a for three different possible values of the incoming muon energy". Also interesting are the proposal plots (see figure 46) which confirm that getting the low Q^2 values from the scattered muon angle $\theta_{\mu\mu'}$ also outgoing $E_{\mu'}$ versus incoming E_{μ} is very difficult. For low Q^2 , its precise value is provided by the measurement of T_p given by the TPC, see figure 41 (bottom).

6 Conclusions

We conclude this report with a brief summary of the proposals and their physics highlights.

Experiments with gas targets at the LHC (**LHC-FT gas**) open up a unique region of acceptance in hadron-hadron reactions. Drell-Yan as well as heavy flavour production in such a setup would significantly improve the determination of PDFs, both in the proton and in nuclei. Especially in the region of large parton momentum fraction x , such measurements would be highly competitive and timely for the analysis of data taken at the LHC in collider mode.

A programme with polarised gas targets at the LHC would allow measurement of asymmetries in Drell-Yan production that address core issues in QCD spin physics, most notable the Sivers effect. This would be unique and highly complementary to existing and future measurements in lepton-proton collisions, because the asymmetries in question have a process dependence between pp and ℓp that is predicted by theory.

A critical question for the realisation of such a programme is the impact of a fixed target on the LHC beams. Furthermore, the target location with respect to the detector has a significant impact on the acceptance. This directly influences the kinematic and hence physics reach of a setup.

A measurement of the magnetic moments of short lived heavy baryons with bent crystals at the LHC (**LHC-FT crystal**) would yield interesting information for heavy-quark physics. This proposal is also of interest from a technological side, and it offers the possibility to be adapted to other goals such as measuring the magnetic moment of the τ lepton. The proposed measurements are challenging, and further R&D is necessary to establish their feasibility.

The measurement of μp elastic scattering at high energy, proposed by **COMPASS++**, would be unique and could significantly improve our understanding of elastic lepton-proton scattering at low momentum transfer. Progress in this area would be highly welcome, given the unsettled discrepancies in the determination of the electromagnetic proton radius by different methods. The per mil point-to-point cross-section precision required for the proposed measurement is challenging and will require further R&D in instrumentation and data acquisition.

The partonic structure of the pion is of special interest in QCD, given the special role of the pion in chiral symmetry breaking. A measurement campaign of Drell-Yan production with conventional π^+ and π^- beams would significantly improve our knowledge of pion PDFs, providing for the first time a handle on separating sea quarks from valence quarks at momentum fractions x above 0.1. Planned investigations of pion PDFs at JLab 12 and the EIC make use of pions radiated from a target proton. The interpretation of such measurements is delicate because these pions are off shell, and detailed pion Drell-Yan data would provide a most valuable baseline for the field.

A broad range of unique possibilities would be opened up by RF-separated beams at the SPS, whose production was studied in the PBC Conventional Beams working group [12]. Highlights among the experiments proposed by COMPASS++ are the detailed investigation of the kaon excitation spectrum, which remains poorly known, and the use of the Primakov process to gain information on the electromagnetic kaon polarisabilities. Drell–Yan or prompt-photon production with RF-separated kaon beams would allow the investigation of kaon structure at the quark-gluon level.

The quantitative understanding of chiral dynamics in channels that involve strange quarks remains a challenge. In addition to the kaon polarisabilities just mentioned, the elastic πK scattering lengths are benchmark quantities for the comparison of nonperturbative calculations in QCD with experiment. The study of mesonic atoms at the SPS proposed by **DIRAC++** could determine the difference $|a_{1/2} - a_{3/2}|$ with precision at par with current theory predictions, in addition to further improving our knowledge of the $\pi\pi$ scattering lengths.

The aim of the **MUonE** proposal is to extract the contribution of hadronic vacuum polarisation to $(g - 2)_\mu$ with a precision competitive with the one currently obtained from e^+e^- annihilation into hadrons and from hadronic τ decays. This would be an extremely valuable independent determination for the value $(g - 2)_\mu$ in the Standard Model. The uncertainties from pure lattice determinations are currently too large to be competitive. A measurement by MUonE would be timely in view of imminent measurements at FNAL and J-PARC. The envisaged accuracy puts highest demands on experimental and theoretical precision, and further work in both areas is required to establish the feasibility of this experiment.

With collision energies of $\sqrt{s_{\text{NN}}} \sim 5 - 17$ GeV at the SPS, the proposed experiments **NA60++** and **NA61++** cover a very important part of the density regime in the QCD phase diagram, that possibly contains the critical end point. In particular, with its open charm measurements, **NA61++** offers a unique possibility to access this regime, and to study effects related to the onset of deconfinement. This also allows to discriminate between competing phenomenological explanations for the production of charm pairs. **NA60++** offers a precise determination of the initial fireball temperature, that would allow to pin down the first order regime for baryon densities above the critical end point.

Several of the fixed-target projects discussed here also aim at providing input to the interpretation of data from cosmic-ray measurements and accelerator-based neutrino experiments. Particle fluxes from nuclear collisions at various collision energies could be measured at **NA61++**, **COMPASS++**, and **LHC-FT gas**, covering a range in \sqrt{s} from 8.8–115 GeV, with a special focus on \bar{p} production in view of high-precision results on the \bar{p} flux from AMS-02. Charm production in the atmosphere constitutes an important background for neutrino fluxes and can be better understood with data on the charm content at large- x in the nucleus, which is part of the LHC-FT gas program. Long-baseline

neutrino experiments require an excellent knowledge of the neutrino flux resulting from hadron-nucleus collision in the production target. Dedicated measurements using target replica are foreseen at **NA61++**.

In summary, the proposals discussed in the PBC QCD working group reveal a number of physics opportunities at the CERN accelerator complex, with the potential to significantly bring forward our understanding of strong interaction physics in a broad range of areas, from the quark-gluon structure of hadrons to low-energy dynamics and to the collective phenomena responsible for the QCD phase transition. Some of the measurements would greatly benefit other fields, from the interpretation of precision measurements probing the limits of the Standard Model to the propagation of cosmic rays.

For several proposals, further investigation is required to establish whether they are able to reach their physics goals. Further studies are also required to determine the technical boundary conditions for the optimal use of the M2 beam line of the SPS, which would be the location of the experiments proposed by COMPASS++ and MUonE, and also of a beam-dump experiment with muons proposed by NA64++ and discussed in the PBC BSM working group [9]. It is hoped that the extension of the PBC mandate until mid-2020 will help in making progress on several of these open issues.

Acknowledgments

Individual authors of this report have received financial support from ERC Ideas Consolidator Grant No. 771642 SELDOM (European Union); CNRS (France) via: COPIN-IN2P3 agreement, IN2P3 project "TMD@NLO", Franco-Spanish PICS "Excitonium", Quarkonium4AFTER project of the Franco-Chinese LIA FCPPL; the P2I Department of Paris-Saclay University (France); DFG Collaborative Research Centre SFB 1225 "ISO-QUANT" (Germany); BMBF grant 05P18VHFCA (Germany); INFN (Italy); GVA(Spain); Ikerbasque (Spain); MINECO (Spain); RFBR/CNRS grant 18-52-15007 (Russia and France).

List of Figures

- | | | |
|---|--|----|
| 1 | Schematic overview of the proposals discussed in the working group, together with their possible timelines. | 6 |
| 2 | Comparison of the kinematic coverage of the ALICE and LHCb detectors at the LHC and the STAR and PHENIX detectors at RHIC. | 11 |
| 3 | The ratios of the valence down to up distributions and of F_2^n/F_2^p for various PDF sets, compared to predictions from different nonperturbative models. | 11 |
| 4 | Parton-parton luminosities for 13 TeV proton-proton collisions for various PDF sets. | 12 |
| 5 | Schematic comparison of kinematical reach for heavy-quark production in pp collision at $\sqrt{s} = 115$ GeV for ALICE-FT and LHCb-FT. | 13 |

6	Kinematical reach in beam and target momentum fractions for Drell–Yan lepton-pair production in pp collisions at $\sqrt{s} = 115$ GeV with an acceptance of $2 < \eta_{\mu}^{\text{lab}} < 5$ and $p_{T,\mu} > 1.2$ GeV.	14
7	Proton PDF and $u\bar{u}$ luminosity profiling using 10 fb^{-1} of Drell–Yan data in pp collisions for the LHCb fixed-target conditions.	15
8	Impact of 10 fb^{-1} of pp and 100 pb^{-1} of $p\text{Xe}$ collisions on nuclear-modification factors R_q^{W} ($q = u, \bar{u}, d, \text{ and } \bar{d}$) from Drell–Yan data for LHCb fixed-target conditions.	15
9	Impact of 10 fb^{-1} of pp and 100 pb^{-1} of $p\text{Xe}$ collisions on nuclear-modification factors R_g^{Xe} through various gluon-sensitive probes for LHCb fixed-target conditions.	16
10	Schematic comparison of kinematical reach in x and Q^2 for Drell–Yan lepton-pair production in pp and $p\text{Xe}$ collisions at $\sqrt{s} = 115$ GeV with typical data sets used in proton and nuclear PDF fits.	17
11	Kinematic reach of future or planned polarised Drell–Yan experiments.	18
12	Schematic comparison of kinematical reach in x and Q^2 for Drell–Yan lepton-pair production in single-polarised pp collisions at $\sqrt{s} = 115$ GeV with selected current and upcoming data sets on Sivers asymmetries and expected precision on Sivers Drell–Yan asymmetries for LHCb fixed-target conditions.	18
13	Spread of theoretical predictions for the magnetic moments of heavy baryons.	23
14	Estimated magnetic dipole moment sensitivities for heavy baryons using bent crystals inside the LHC at LHCb.	25
15	Overview of recent determinations of the proton charge radius r_p from spectroscopy of ordinary or muonic hydrogen and from analyses of ep scattering data.	28
16	Proton form factors G_E and G_M from fits to MAMI data [64], compared to the curves for proton charge radii of 0.81, 0.84, and 0.88 fm, and ratio of the cross section (using the MAMI form-factor parameterisations) over the one using the dipole form factor, overlaid with pseudo-data that reflect the envisaged statistical precision of the COMPASS++ measurement and various polynomial fits to the pseudo-data.	29
17	Overview of pion-induced Drell–Yan event yields for π^+ and π^- from past experiments and the proposed COMPASS++ running.	32
18	COMPASS++ projections for ratio of certain cross-section combinations compared to three different scenarios for the sea-quark distributions and to a prediction based on the extraction of the pion valence and sea distributions by NA3.	33
19	Projected COMPASS++ data for the scaled Primakov cross section R_K for a kaon beam, compared to the prediction from χPT , and the corresponding (existing) measurement of R_{π} for the pion.	34
20	Excitation spectrum of strange mesons grouped by their J^P quantum numbers.	36

21	Current experimental precision on the anomalous magnetic moment a_μ of the muon (and the accuracy goals of the planned experiments at FNAL and J-PARC), of two current determinations of the contribution to a_μ from light-by-light scattering, of two current determinations of the contribution of hadronic vacuum polarisation to a_μ , and the ultimate precision aimed at by MUonE on the latter contribution.	38
22	Selected current determinations of the contribution of the hadronic vacuum polarisation to the anomalous magnetic moment of the muon.	39
23	Integrand of the sum rule that relates the leading-order hadronic contribution to a_μ to the running fine structure constant, together with MUonE pseudodata.	40
24	Medium temperature evolution vs. $\sqrt{s_{NN}}$ in central Pb-Pb collisions with expected performance from NA60++ and CBM and the only existing measurements (NA60 and HADES), as well as NA60++ projections for the acceptance-corrected thermal dimuon mass spectrum at $\sqrt{s_{NN}} = 8.8$ GeV in case of no chiral mixing compared to the theoretical expectation.	44
25	NA60++ projected performance for the nuclear modification factor of J/ψ production in Pb-Pb collisions at $E_{\text{lab}} = 50$ GeV as a function of the number of participants N_{part} , compared with expectations from an estimate for cold nuclear matter effects similar as at full SPS energy.	45
26	NA60++ projection for the D^0 invariant-mass distribution from $5 \cdot 10^9$ central Pb-Pb events at beam energies of $\sqrt{s_{NN}} = 17.3$ GeV and 10.6 GeV with a vertex detector based on MAPS.	45
27	Mean multiplicity of charm quark pairs produced in central Pb+Pb collisions at 158A GeV/c calculated within dynamical models and statistical models, compared to the foreseen accuracy of the NA61/SHINE 2020+ result.	47
28	Energy dependence of $\langle c\bar{c} \rangle$ in central Pb+Pb collisions calculated within the SMES model in comparison to the foreseen accuracy of the NA61/SHINE results for $\sqrt{s_{NN}} = 8.6$ GeV and $\sqrt{s_{NN}} = 16.7$ GeV.	48
29	The ratios $\sigma_{J/\psi}/\sigma_{\text{DY}}$ and $\sigma_{J/\psi}/\sigma_\pi$ as functions of transverse energy in Pb+Pb collisions at 158A GeV, in comparison to the expected accuracy of $\sigma_{J/\psi}/\sigma_{c\bar{c}}$ from NA61/SHINE 2020+.	49
30	Theoretical predictions for the πK scattering lengths in the isospin 1/2 and 3/2 channels, together with the DIRAC measurements of the difference $a_0^{1/2} - a_0^{3/2}$ and the projected uncertainty of a measurement with DIRAC++.	50
31	Change of statistical uncertainties on atomic πK pairs between the PS (DIRAC) and the SPS (DIRAC++).	51
32	Phase diagram of QCD and density range of running or planned experiments.	53
33	Interaction rate as a function of collision energy of running or planned experiments.	54
34	Examples of QCD-related limitations in flux calculations for cosmic-ray physics.	55

35	Comparison of parameterisations for the $p\text{He}$ cross section with the LHCb data.	55
36	Relative precision of LHCb results on \bar{p} production in $p\text{He}$ collision at $\sqrt{s}=110$ GeV.	56
37	Acceptance in Feynman- x of LHCb-FT (SMOG2) for \bar{p} production for p_T up to 2 GeV.	56
38	Expected kinematic coverage of \bar{p} production for ALICE-FT.	58
39	Accepted range in p_T and rapidity y (calculated in the collision centre-of-mass system) for p and \bar{p} production in pp collision at $\sqrt{s} = 158$ GeV.	59
40	Foreseen experimental setups for the μ - e and the μ -proton-radius measurements.	61
41	Quoted optimum energies for the μ - e and the μ -proton-radius measurements.	62
42	Quoted optimum intensities for the μ - e and the μ -proton-radius measurements.	63
43	Assumed μ - e setup composition and estimated radiations length; fraction of background components entering the acceptance of the COMPASS++ TPC used to detect the recoil low-energy proton and located 40m downstream.	64
44	Reduction of the μ -beam size spreading from the MSC angular divergence from a dedicated M2 μ -beam tuning, optimised for the μ -proton-radius TPC position, and additional reduction by replacing the Iron μ -filter by a longer ^{12}C filter. Impact on the μ energy distribution of the energy losses produced by the full μ - e setup.	65
45	Selected μ - e kinematics used to test the impact on the PID of a hole in both ECAL and μ -filter, and corresponding sample of tracks for μ - e scattered events.	66
46	Scattering angle $\theta_{\mu'}$ and energy $E_{\mu'}$ for the outgoing muon, assuming an incoming energy E_{μ} of 100 GeV.	67

List of Tables

1	Schematic overview of the physics topics addressed by the studies presented in the QCD working group.	9
2	Summary of physics programs within the COMPASS++ project, including the physics goals, beam and target requirements, running time, and detector upgrades (where applicable).	27
3	Estimated \bar{p} and \bar{d} event yields for 100 days running each at 40 GeV, 180 GeV, and 350 GeV beam momentum and a liquid-hydrogen target at NA61++ and a 1 kHz read-out rate.	58
4	Current and estimated yields in charm events as well as for $\Upsilon(1S)$ production and Drell–Yan for SMOG and SMOG2 at LHCb-FT.	59

References

- [1] J. Jäckel, M. Lamont and C. Vallée, *Summary Report of Physics Beyond Colliders at CERN*, Tech. Rep. [CERN-PBC-REPORT-2018-003](#), CERN, Geneva, Dec, 2018.
- [2] A. Accardi et al., *Electron Ion Collider: The Next QCD Frontier*, *Eur. Phys. J.* **A52** (2016) 268, [[1212.1701](#)].
- [3] R. Tribble, *Presentation at the EIC Users Meeting, Washington D.C., June 2018*, .
- [4] F. Bordry, M. Benedikt, O. Brüning, J. Jowett, L. Rossi, D. Schulte et al., *Machine Parameters and Projected Luminosity Performance of Proposed Future Colliders at CERN*, [1810.13022](#).
- [5] C. Hadjidakis et al., *A Fixed-Target Programme at the LHC: Physics Case and Projected Performances for Heavy-Ion, Hadron, Spin and Astroparticle Studies*, [1807.00603](#).
- [6] Hadjidakis, C., “Physics opportunities and feasibility studies with ALICE in a fixed-target mode, presented at the [PBC working group meeting in June 2018](#).”
- [7] UA9 collaboration, L. Burmistrov, G. Calderini, Y. Ivanov, L. Massacrier, P. Robbe, W. Scandale et al., *Measurement of Short Living Baryon Magnetic Moment using Bent Crystals at SPS and LHC*, Tech. Rep. [CERN-SPSC-2016-030](#). [SPSC-EOI-012](#), CERN, Geneva, Jun, 2016.
- [8] E. Bagli et al., *Electromagnetic dipole moments of charged baryons with bent crystals at the LHC*, *Eur. Phys. J.* **C77** (2017) 828, [[1708.08483](#)].
- [9] G. Lanfranchi, M. Pospelov, A. Rozanov, G. Ruoso and K. Jungmann, *Report of the BSM Working Group of the Physics Beyond Colliders at CERN*, Tech. Rep. [CERN-PBC-REPORT-2018-007](#), CERN, Geneva, Dec, 2018.
- [10] A. S. Fomin, A. Y. Korchin, A. Stocchi, S. Barsuk and P. Robbe, *Anomalous magnetic dipole moment of the τ lepton using bent crystal at the LHC*, [1810.06699](#).
- [11] LETTER OF INTENT WORKING GROUP collaboration, O. Yu. Denisov, *Letter of Intent (Draft 2.0): A New QCD facility at the M2 beam line of the CERN SPS*, [1808.00848](#).
- [12] L. Gagnon, D. Banerjee, J. Bernhard, M. Brugger, N. Charitonidis, G. L. D’Alessandro et al., *Report from the Conventional Beams Working Group to the Physics beyond Collider Study and to the European Strategy for Particle Physics*, Tech. Rep. [CERN-PBC-REPORT-2018-002](#), CERN, Geneva, Dec, 2018.
- [13] NA61/SHINE collaboration, A. Aduszkiewicz, *Study of Hadron-Nucleus and Nucleus-Nucleus Collisions at the CERN SPS: Early Post-LS2 Measurements and Future Plans*, Tech. Rep. [CERN-SPSC-2018-008](#) and [SPSC-P-330-ADD-10](#), CERN, Geneva, Mar, 2018.
- [14] NA61/SHINE collaboration, A. Aduszkiewicz, *Reply to the SPSC questions on Addendum CERN-SPSC-2018-008*, Tech. Rep. [CERN-SPSC-2018-019](#) and [SPSC-P-330-ADD-11](#), CERN, Geneva, Jun, 2018.
- [15] COMPASS collaboration, C. Adolph et al., *Resonance Production and $\pi\pi$ S-wave in $\pi^- + p \rightarrow \pi^- \pi^- \pi^+ + p_{recoil}$ at 190 GeV/c*, *Phys. Rev.* **D95** (2017) 032004, [[1509.00992](#)].
- [16] LHCb collaboration, R. Aaij et al., *Measurement of antiproton production in pHe collisions at $\sqrt{s_{NN}} = 110$ GeV*, *Phys. Rev. Lett.* (2018) , [[1808.06127](#)].

- [17] NA61/SHINE collaboration, A. Aduszkiewicz et al., *Measurements of π^\pm , K^\pm , p and \bar{p} spectra in proton-proton interactions at 20, 31, 40, 80 and 158 GeV/c with the NA61/SHINE spectrometer at the CERN SPS*, *Eur. Phys. J.* **C77** (2017) 671, [1705.02467].
- [18] R. D. Ball, E. R. Nocera and J. Rojo, *The asymptotic behaviour of parton distributions at small and large x* , *Eur. Phys. J.* **C76** (2016) 383, [1604.00024].
- [19] S. J. Brodsky and G. R. Farrar, *Scaling Laws at Large Transverse Momentum*, *Phys. Rev. Lett.* **31** (1973) 1153–1156.
- [20] W. Melnitchouk and A. W. Thomas, *Neutron / proton structure function ratio at large x* , *Phys. Lett.* **B377** (1996) 11–17, [nucl-th/9602038].
- [21] S. Dulat, T.-J. Hou, J. Gao, M. Guzzi, J. Huston, P. Nadolsky et al., *New parton distribution functions from a global analysis of quantum chromodynamics*, *Phys. Rev.* **D93** (2016) 033006, [1506.07443].
- [22] NNPDF collaboration, R. D. Ball et al., *Parton distributions from high-precision collider data*, *Eur. Phys. J.* **C77** (2017) 663, [1706.00428].
- [23] L. A. Harland-Lang, A. D. Martin, P. Motylinski and R. S. Thorne, *Parton distributions in the LHC era: MMHT 2014 PDFs*, *Eur. Phys. J.* **C75** (2015) 204, [1412.3989].
- [24] T.-J. Hou, S. Dulat, J. Gao, M. Guzzi, J. Huston, P. Nadolsky et al., *CT14 Intrinsic Charm Parton Distribution Functions from CTEQ-TEA Global Analysis*, *JHEP* **02** (2018) 059, [1707.00657].
- [25] S. J. Brodsky, P. Hoyer, C. Peterson and N. Sakai, *The Intrinsic Charm of the Proton*, *Phys. Lett.* **B93** (1980) 451–455.
- [26] S. J. Brodsky, A. Kusina, F. Lyonnet, I. Schienbein, H. Spiesberger and R. Vogt, *A review of the intrinsic heavy quark content of the nucleon*, *Adv. High Energy Phys.* **2015** (2015) 231547, [1504.06287].
- [27] NNPDF collaboration, R. D. Ball, V. Bertone, M. Bonvini, S. Carrazza, S. Forte, A. Guffanti et al., *A Determination of the Charm Content of the Proton*, *Eur. Phys. J.* **C76** (2016) 647, [1605.06515].
- [28] D. W. Sivers, *Single-spin production asymmetries from the hard scattering of pointlike constituents*, *Phys. Rev.* **D41** (1990) 83–90.
- [29] HERMES collaboration, A. Airapetian et al., *Single-spin Asymmetries in Semi-Inclusive Deep-Inelastic Scattering on a Transversely Polarized Hydrogen Target*, *Phys. Rev. Lett.* **94** (2005) 012002, [hep-ex/0408013].
- [30] J. C. Collins, *Leading-twist single-transverse-spin asymmetries: Drell–Yan and deep-inelastic scattering*, *Phys. Lett.* **B536** (2002) 43–48, [hep-ph/0204004].
- [31] H. Avakian, A. Bressan and M. Contalbrigo, *Experimental results on TMDs*, *Eur. Phys. J.* **A52** (2016) 150.
- [32] COMPASS collaboration, M. Aghasyan et al., *First measurement of transverse-spin-dependent azimuthal asymmetries in the Drell-Yan process*, *Phys. Rev. Lett.* **119** (2017) 112002, [1704.00488].
- [33] STAR collaboration, L. Adamczyk et al., *Measurement of the transverse single-spin asymmetry in $p^\uparrow + p \rightarrow W^\pm/Z^0$ at RHIC*, *Phys. Rev. Lett.* **116** (2016) 132301, [1511.06003].

- [34] A. Kusina, *private communication*, 2018.
- [35] LHCb collaboration, A. A. Alves, Jr. et al., *The LHCb Detector at the LHC*, *JINST* **3** (2008) S08005.
- [36] R. Abdul Khalek, S. Bailey, J. Gao, L. Harland-Lang and J. Rojo, *Towards Ultimate Parton Distributions at the High-Luminosity LHC*, *Eur. Phys. J.* **C78** (2018) 962, [[1810.03639](#)].
- [37] K. J. Eskola, P. Paakkinen, H. Paukkunen and C. A. Salgado, *EPPS16: Nuclear parton distributions with LHC data*, *Eur. Phys. J.* **C77** (2017) 163, [[1612.05741](#)].
- [38] M. G. Echevarria, A. Idilbi, Z.-B. Kang and I. Vitev, *QCD Evolution of the Sivers Asymmetry*, *Phys. Rev.* **D89** (2014) 074013, [[1401.5078](#)].
- [39] M. Anselmino, U. D'Alesio and S. Melis, *Transverse single-spin asymmetries in proton-proton collisions at the AFTER@LHC experiment in a TMD factorisation scheme*, *Adv. High Energy Phys.* **2015** (2015) 475040, [[1504.03791](#)].
- [40] Aschenauer, Elke C., *Transverse spin measurements at RHIC and TMDs at EIC, presented at the INT workshop on "Probing Nucleons and Nuclei in High-Energy Collisions"*, 2018.
- [41] P. Di Nezza, *The SMOG2 project*, Tech. Rep. [CERN-PBC-Notes-2018-007](#), Dec, 2018.
- [42] A. Bursche, H. P. Dembinski, P. Di Nezza, M. Ferro-Luzzi, F. Fleuret, G. Graziani et al., *Physics opportunities with the fixed-target program of the LHCb experiment using an unpolarized gas target*, Tech. Rep. [LHCb-PUB-2018-015](#). [CERN-LHCb-PUB-2018-015](#), CERN, Geneva, Dec, 2018.
- [43] HERMES collaboration, A. Airapetian et al., *The HERMES polarized hydrogen and deuterium gas target in the HERA electron storage ring*, *Nucl. Instrum. Meth.* **A540** (2005) 68–101, [[physics/0408137](#)].
- [44] E. Steffens, *Estimation of the performance of a HERMES-type gas target internal to the LHC*, *PoS PSTP2015* (2015) 019.
- [45] A. Faessler, T. Gutsche, M. A. Ivanov, J. G. Korner, V. E. Lyubovitskij, D. Nicmorus et al., *Magnetic moments of heavy baryons in the relativistic three-quark model*, *Phys. Rev.* **D73** (2006) 094013, [[hep-ph/0602193](#)].
- [46] N. Sharma, H. Dahiya, P. K. Chatley and M. Gupta, *Spin $1/2^+$, spin $3/2^+$ and transition magnetic moments of low lying and charmed baryons*, *Phys. Rev.* **D81** (2010) 073001, [[1003.4338](#)].
- [47] A. Bernotas and V. Simonis, *Magnetic moments of heavy baryons in the bag model reexamined*, [1209.2900](#).
- [48] V. G. Baryshevsky, *The possibility to measure the magnetic moments of short-lived particles (charm and beauty baryons) at LHC and FCC energies using the phenomenon of spin rotation in crystals*, *Phys. Lett.* **B757** (2016) 426–429.
- [49] A. S. Fomin et al., *Feasibility of measuring the magnetic dipole moments of the charm baryons at the LHC using bent crystals*, *JHEP* **08** (2017) 120, [[1705.03382](#)].
- [50] S. J. Brodsky, F. Fleuret, C. Hadjidakis and J. P. Lansberg, *Physics Opportunities of a Fixed-Target Experiment using the LHC Beams*, *Phys. Rept.* **522** (2013) 239–255, [[1202.6585](#)].
- [51] W. Scandale et al., *Observation of channeling for 6500 GeV/c protons in the crystal assisted collimation setup for LHC*, *Phys. Lett.* **B758** (2016) 129–133.

- [52] E761 collaboration, D. Chen et al., *First observation of magnetic moment precession of channeled particles in bent crystals*, *Phys. Rev. Lett.* **69** (1992) 3286–3289.
- [53] LHCb collaboration, *Measurement of J/ψ and D^0 production in pAr collisions at $\sqrt{s_{NN}} = 110$ GeV*, Tech. Rep. LHCb-CONF-2017-001. CERN-LHCb-CONF-2017-001, CERN, Geneva, Mar, 2017.
- [54] LHCb collaboration, R. Aaij et al., *First measurement of charm production in fixed-target configuration at the LHC*, Submitted to: *Phys. Rev. Lett.* (2018) , [[1810.07907](#)].
- [55] EUROPEAN MUON collaboration, J. J. Aubert et al., *A Large Magnetic Spectrometer System for High-Energy Muon Physics*, *Nucl. Instrum. Meth.* **179** (1981) 445–466.
- [56] NA58 COLLABORATION collaboration, G. Baum, J. Kynäräinen and A. Tripet, *COMPASS: a proposal for a common muon and proton apparatus for structure and spectroscopy*, Tech. Rep. CERN-SPSLC-96-14. SPSLC-P-297, CERN, Geneva, 1996.
- [57] COMPASS collaboration, Gautheron, F. and others, *COMPASS-II Proposal*, Tech. Rep. CERN-SPSC-2010-014. SPSC-P-340, CERN, Geneva, May, 2010.
- [58] P. J. Mohr, B. N. Taylor and D. B. Newell, *CODATA Recommended Values of the Fundamental Physical Constants: 2010*, *Rev. Mod. Phys.* **84** (2012) 1527–1605, [[1203.5425](#)].
- [59] R. Pohl et al., *The size of the proton*, *Nature* **466** (2010) 213–216.
- [60] A. Beyer, L. Maisenbacher, A. Matveev, R. Pohl, K. Khabarova, A. Grinin et al., *The rydberg constant and proton size from atomic hydrogen*, *Science* **358** (2017) 79–85, [<http://science.sciencemag.org/content/358/6359/79.full.pdf>].
- [61] H. Fleurbaey, S. Galtier, S. Thomas, M. Bonnaud, L. Julien, F. Biraben et al., *New Measurement of the $1S - 3S$ Transition Frequency of Hydrogen: Contribution to the Proton Charge Radius Puzzle*, *Phys. Rev. Lett.* **120** (2018) 183001, [[1801.08816](#)].
- [62] A. A. Vorobyov, G. A. Korolev, V. A. Schegelsky, G. Ye. Solyakin, G. L. Sokolov and Yu. K. Zalite, *A method for studies of small-angle hadron-proton elastic scattering in the coulomb interference region*, *Nucl. Instrum. Meth.* **119** (1974) 509–519.
- [63] S. Ilieva et al., *Nuclear-matter density distribution in the neutron-rich nuclei $^{12,14}\text{Be}$ from proton elastic scattering in inverse kinematics*, *Nucl. Phys.* **A875** (2012) 8–28.
- [64] A1 collaboration, J. C. Bernauer et al., *High-precision determination of the electric and magnetic form factors of the proton*, *Phys. Rev. Lett.* **105** (2010) 242001, [[1007.5076](#)].
- [65] MUSE collaboration, R. Gilman et al., *Technical Design Report for the Paul Scherrer Institute Experiment R-12-01.1: Studying the Proton "Radius" Puzzle with μp Elastic Scattering*, [1709.09753](#).
- [66] A. Gasparian et al., “High Precision Measurement of the Proton Charge Radius.” 2011.
- [67] M. Mihovilović et al., *First measurement of proton’s charge form factor at very low Q^2 with initial state radiation*, *Phys. Lett.* **B771** (2017) 194–198, [[1612.06707](#)].
- [68] M. Hoballah, S. Cholak, R. Kunne, C. Le Galliard, D. Marchand, G. Quémener et al., *Merits and constraints of low- K^2 experimental data for the proton radius determination*, [1811.03545](#).
- [69] J. D. Sullivan, *One-pion exchange and deep-inelastic electron-nucleon scattering*, *Phys. Rev.* **D5** (1972) 1732–1737.

- [70] P. J. Sutton, A. D. Martin, R. G. Roberts and W. J. Stirling, *Parton distributions for the pion extracted from Drell-Yan and prompt photon experiments*, *Phys. Rev.* **D45** (1992) 2349–2359.
- [71] M. Glück, E. Reya and A. Vogt, *Piononic parton distributions*, *Z. Phys.* **C53** (1992) 651–656.
- [72] M. Glück, E. Reya and I. Schienbein, *Piononic parton distributions revisited*, *Eur. Phys. J.* **C10** (1999) 313–317, [[hep-ph/9903288](#)].
- [73] P. C. Barry, N. Sato, W. Melnitchouk and C.-R. Ji, *First Monte Carlo Global QCD Analysis of Pion Parton Distributions*, *Phys. Rev. Lett.* **121** (2018) 152001, [[1804.01965](#)].
- [74] J. T. Londergan, G. Q. Liu, E. N. Rodionov and A. W. Thomas, *Probing the pion sea with π -D Drell-Yan processes*, *Phys. Lett.* **B361** (1995) 110–114.
- [75] NA3 collaboration, J. Badier et al., *Experimental Determination of the π Meson Structure Functions by the Drell-Yan Mechanism*, *Z. Phys.* **C18** (1983) 281.
- [76] COMPASS collaboration, C. Adolph et al., *Measurement of the charged-pion polarizability*, *Phys. Rev. Lett.* **114** (2015) 062002, [[1405.6377](#)].
- [77] Gasser, Jürg and Ivanov, Mikhail A. and Sainio, Mikko E., *Revisiting $\gamma\gamma \rightarrow \pi^+\pi^-$ at low energies*, *Nucl. Phys.* **B745** (2006) 84–108, [[hep-ph/0602234](#)].
- [78] F. Guerrero and J. Prades, *Kaon polarizabilities in chiral perturbation theory*, *Phys. Lett.* **B405** (1997) 341–346, [[hep-ph/9702303](#)].
- [79] G. Backenstoss et al., *K^- mass and K^- polarizability from kaonic atoms*, *Phys. Lett.* **43B** (1973) 431–436.
- [80] D. Ebert, R. N. Faustov and V. O. Galkin, *Mass spectra and Regge trajectories of light mesons in the relativistic quark model*, *Phys. Rev.* **D79** (2009) 114029, [[0903.5183](#)].
- [81] GLUEX collaboration, S. Adhikari et al., *Strange Hadron Spectroscopy with a Secondary KL Beam at GlueX*, [1707.05284](#).
- [82] F. Jegerlehner, *The Muon $g-2$ in Progress*, *Acta Phys. Polon.* **B49** (2018) 1157, [[1804.07409](#)].
- [83] H. B. Meyer and H. Wittig, *Lattice QCD and the anomalous magnetic moment of the muon*, *Prog. Part. Nucl. Phys.* **104** (2019) 46–96, [[1807.09370](#)].
- [84] C. M. Carloni Calame, M. Passera, L. Trentadue and G. Venanzoni, *A new approach to evaluate the leading hadronic corrections to the muon $g-2$* , *Phys. Lett.* **B746** (2015) 325–329, [[1504.02228](#)].
- [85] G. Abbiendi et al., *Measuring the leading hadronic contribution to the muon $g-2$ via μe scattering*, *Eur. Phys. J.* **C77** (2017) 139, [[1609.08987](#)].
- [86] P. Mastrolia, M. Passera, A. Primo and U. Schubert, *Master integrals for the NNLO virtual corrections to μe scattering in QED: the planar graphs*, *JHEP* **11** (2017) 198, [[1709.07435](#)].
- [87] S. Di Vita, S. Laporta, P. Mastrolia, A. Primo and U. Schubert, *Master integrals for the NNLO virtual corrections to μe scattering in QED: the non-planar graphs*, *JHEP* **09** (2018) 016, [[1806.08241](#)].
- [88] M. Fael, *Hadronic corrections to μ -e scattering at NNLO with space-like data*, [1808.08233](#).
- [89] M. Alacevich, C. M. Carloni Calame, M. Chiesa, G. Montagna, O. Nicrosini and F. Piccinini, *Muon-electron scattering at NLO*, [1811.06743](#).

- [90] R. Rapp and H. van Hees, *Thermal dileptons as fireball thermometer and chronometer*, *Physics Letters B* **753** (2016) 586 – 590.
- [91] S. Endres, H. van Hees, J. Weil and M. Bleicher, *Dilepton production and reaction dynamics in heavy-ion collisions at sis energies from coarse-grained transport simulations*, *Phys. Rev. C* **92** (Jul, 2015) 014911.
- [92] T. Galatyuk, *Future facilities for high μ_b physics, to be published in Quark Matter 2018 conference proceedings* .
- [93] NA60 collaboration, R. Arnaldi et al., *Evidence for the production of thermal-like muon pairs with masses above 1-GeV/c**2 in 158-A-GeV Indium-Indium Collisions*, *Eur. Phys. J.* **C59** (2009) 607–623, [0810.3204].
- [94] NA60 collaboration, H. J. Specht, *Thermal Dileptons from Hot and Dense Strongly Interacting Matter*, *AIP Conf. Proc.* **1322** (2010) 1–10, [1011.0615].
- [95] HADES COLLABORATION collaboration, S. Harabasz et al., *Multi-differential pattern of low-mass e^+e^- excess from $\sqrt{s_{NN}} = 2.4$ gev au-au collisions with hades, to be published in Quark Matter 2018 conference proceedings* .
- [96] C. Lourenco and H. K. Wohri, *Heavy flavour hadro-production from fixed-target to collider energies*, *Phys. Rept.* **433** (2006) 127–180, [hep-ph/0609101].
- [97] HARD PROBE collaboration, R. Vogt, *The A dependence of open charm and bottom production*, *Int. J. Mod. Phys.* **E12** (2003) 211–270, [hep-ph/0111271].
- [98] R. V. Gavai, S. Gupta, P. L. McGaughey, E. Quack, P. V. Ruuskanen, R. Vogt et al., *Heavy quark production in pp collisions*, *Int. J. Mod. Phys.* **A10** (1995) 2999–3042, [hep-ph/9411438].
- [99] P. Braun-Munzinger and J. Stachel, *(Non)thermal aspects of charmonium production and a new look at J / psi suppression*, *Phys. Lett.* **B490** (2000) 196–202, [nucl-th/0007059].
- [100] O. Linnyk, E. L. Bratkovskaya and W. Cassing, *Open and hidden charm in proton-nucleus and heavy-ion collisions*, *Int. J. Mod. Phys.* **E17** (2008) 1367–1439, [0808.1504].
- [101] P. Levai, T. S. Biro, P. Csizmadia, T. Csorgo and J. Zimanyi, *The Production of charm mesons from quark matter at CERN SPS and RHIC*, *J. Phys.* **G27** (2001) 703–706, [nucl-th/0011023].
- [102] A. P. Kostyuk, M. I. Gorenstein, H. Stoecker and W. Greiner, *Statistical coalescence model analysis of J / psi production in Pb + Pb collisions at 158-A-GeV*, *Phys. Lett.* **B531** (2002) 195–202, [hep-ph/0110269].
- [103] M. Gazdzicki and M. I. Gorenstein, *On the early stage of nucleus-nucleus collisions*, *Acta Phys. Polon.* **B30** (1999) 2705, [hep-ph/9803462].
- [104] NA50 collaboration, M. C. Abreu et al., *Evidence for deconfinement of quarks and gluons from the J/psi suppression pattern measured in Pb-Pb collisions at the CERN SPS*, *Phys. Lett.* **B477** (2000) 28–36.
- [105] M. Gazdzicki, *J/psi production in nuclear collisions*, *Phys. Rev.* **C60** (1999) 054903, [hep-ph/9809412].
- [106] DIRAC collaboration, B. Adeva et al., *Measurement of the πK atom lifetime and the πK scattering length*, *Phys. Rev.* **D96** (2017) 052002, [1707.02184].
- [107] O. E. Gorchakov and L. L. Nemenov, *The estimation of production rates of $\pi^+ K^-$, $\pi^- K^+$*

- and $\pi^+\pi^-$ atoms in proton–nucleus interactions at $450 \text{ GeV } c^{-1}$, *J. Phys.* **G43** (2016) 095004.
- [108] V. Yazkov, *Estimation of beam time needed for measurement of pion-kaon s-wave scattering length combination a_0^- with a statistical accuracy 5%*, Tech. Rep. **DIRAC-Note-2016-05**, Jun, 2016.
- [109] S. R. Beane, T. C. Luu, K. Orginos, A. Parreno, M. J. Savage, A. Torok et al., *Precise determination of the $I = 2\pi\pi$ scattering length from mixed-action lattice QCD*, *Phys. Rev.* **D77** (2008) 014505, [[0706.3026](#)].
- [110] X. Feng, K. Jansen and D. B. Renner, *The $\pi^+\pi^+$ scattering length from maximally twisted mass lattice QCD*, *Phys. Lett.* **B684** (2010) 268–274, [[0909.3255](#)].
- [111] Z. Fu, *Lattice QCD study of the s-wave $\pi\pi$ scattering lengths in the $I=0$ and 2 channels*, *Phys. Rev.* **D87** (2013) 074501, [[1303.0517](#)].
- [112] PACS-CS collaboration, K. Sasaki, N. Ishizuka, M. Oka and T. Yamazaki, *Scattering lengths for two pseudoscalar meson systems*, *Phys. Rev.* **D89** (2014) 054502, [[1311.7226](#)].
- [113] G. Colangelo, J. Gasser and H. Leutwyler, *$\pi\pi$ scattering*, *Nucl. Phys.* **B603** (2001) 125–179, [[hep-ph/0103088](#)].
- [114] J. R. Batley et al., *Determination of the S-wave $\pi\pi$ scattering lengths from a study of $K^\pm \rightarrow \pi^\pm\pi^0\pi^0$ decays*, *Eur. Phys. J.* **C64** (2009) 589–608, [[0912.2165](#)].
- [115] NA48-2 collaboration, J. R. Batley et al., *Precise tests of low energy QCD from K_{e4} decay properties*, *Eur. Phys. J.* **C70** (2010) 635–657.
- [116] B. Adeva et al., *Determination of $\pi\pi$ scattering lengths from measurement of $\pi^+\pi^-$ atom lifetime*, *Phys. Lett.* **B704** (2011) 24–29, [[1109.0569](#)].
- [117] DIRAC, PS212 collaboration, B. Adeva et al., *First observation of long-lived $\pi^+\pi^-$ atoms*, *Phys. Lett.* **B751** (2015) 12–18, [[1508.04712](#)].
- [118] DIRAC collaboration, B. Adeva et al., *First measurement of a long-lived $\pi^+\pi^-$ atom lifetime*, [1811.08659](#).
- [119] L. L. Nemenov, V. D. Ovsyannikov and E. V. Chaplygin, *Resonant enhancement of field-induced annihilation rate for $(\pi^+\pi^-)$ atom: a possibility to measure np–ns energy splitting*, *Nucl. Phys.* **A710** (2002) 303–328.
- [120] CBM collaboration, T. Ablyazimov et al., *Challenges in QCD matter physics –The scientific programme of the Compressed Baryonic Matter experiment at FAIR*, *Eur. Phys. J.* **A53** (2017) 60, [[1607.01487](#)].
- [121] AMS collaboration, M. Aguilar et al., *Antiproton Flux, Antiproton-to-Proton Flux Ratio, and Properties of Elementary Particle Fluxes in Primary Cosmic Rays Measured with the Alpha Magnetic Spectrometer on the International Space Station*, *Phys. Rev. Lett.* **117** (2016) 091103.
- [122] O. Adriani et al., *Measurement of the flux of primary cosmic ray antiprotons with energies of 60 MeV to 350 GeV in the PAMELA experiment*, *JETP Lett.* **96** (2013) 621–627.
- [123] M. Korsmeier, F. Donato and M. Di Mauro, *Production cross sections of cosmic antiprotons in the light of new data from the NA61 and LHCb experiments*, *Phys. Rev.* **D97** (2018) 103019, [[1802.03030](#)].
- [124] A. V. Giannini, V. P. Gonçalves and F. S. Navarra, *Intrinsic charm contribution to the*

- prompt atmospheric neutrino flux*, *Phys. Rev.* **D98** (2018) 014012, [[1803.01728](#)].
- [125] G. Giesen, M. Boudaud, Y. Génolini, V. Poulin, M. Cirelli, P. Salati et al., *AMS-02 antiprotons, at last! Secondary astrophysical component and immediate implications for Dark Matter*, *JCAP* **1509** (2015) 023, [[1504.04276](#)].
- [126] K2K collaboration, M. H. Ahn et al., *Measurement of Neutrino Oscillation by the K2K Experiment*, *Phys. Rev.* **D74** (2006) 072003, [[hep-ex/0606032](#)].
- [127] MINOS collaboration, P. Adamson et al., *A Study of Muon Neutrino Disappearance Using the Fermilab Main Injector Neutrino Beam*, *Phys. Rev.* **D77** (2008) 072002, [[0711.0769](#)].
- [128] T2K collaboration, K. Abe et al., *The T2K Experiment*, *Nucl. Instrum. Meth.* **A659** (2011) 106–135, [[1106.1238](#)].
- [129] DUNE collaboration, R. Acciarri et al., *Long-Baseline Neutrino Facility (LBNF) and Deep Underground Neutrino Experiment (DUNE)*, [1512.06148](#).
- [130] NA61/SHINE collaboration, N. Abgrall et al., *Measurements of Cross Sections and Charged Pion Spectra in Proton-Carbon Interactions at 31 GeV/c*, *Phys. Rev.* **C84** (2011) 034604, [[1102.0983](#)].
- [131] NA61/SHINE collaboration, N. Abgrall et al., *Measurement of Production Properties of Positively Charged Kaons in Proton-Carbon Interactions at 31 GeV/c*, *Phys. Rev.* **C85** (2012) 035210, [[1112.0150](#)].
- [132] NA61/SHINE collaboration, N. Abgrall et al., *Measurements of production properties of K_S^0 mesons and Λ hyperons in proton-carbon interactions at 31 GeV/c*, *Phys. Rev.* **C89** (2014) 025205, [[1309.1997](#)].
- [133] NA61/SHINE collaboration, N. Abgrall et al., *Measurements of π^\pm differential yields from the surface of the T2K replica target for incoming 31 GeV/c protons with the NA61/SHINE spectrometer at the CERN SPS*, *Eur. Phys. J.* **C76** (2016) 617, [[1603.06774](#)].
- [134] NA61/SHINE collaboration, A. Aduszkiewicz, *Report from the NA61/SHINE experiment at the CERN SPS*, Tech. Rep. [CERN-SPSC-2017-038](#). SPSC-SR-221, CERN, Geneva, Oct, 2017.
- [135] D.-M. Gomez-Coral, A. Menchaca Rocha, V. Grabski, A. Datta, P. von Doetinchem and A. Shukla, *Deuteron and Antideuteron Production Simulation in Cosmic-Ray Interactions*, *Phys. Rev.* **D98** (2018) 023012, [[1806.09303](#)].
- [136] J. Friedrich, O. Denisov and A. Vorobyev, *Addendum to the COMPASS-II Proposal (v1)*, Tech. Rep. [CERN-SPSC-2017-034](#) and [SPSC-P-340-ADD-1](#), CERN, Geneva, Apr, 2018.